POLITECNICO
MILANO 1863

SCUOLA DI INGEGNERIA INDUSTRIALE
E DELL'INFORMAZIONE

High Order Efficient Station Keeping Strategy for Low-Thrust Geostationary Satellites with Differential Algebra Techniques

Tesi di Laurea Magistrale in
Space Engineering - Ingegneria Spaziale

Author: **Stefano Carcano**

Student ID: 975976
Advisor: Prof. Pierluigi Di Lizia
Co-advisor: Michele Maestrini
Academic Year: 2021-22

Abstract

To allow a Geostationary Earth Orbit (GEO) satellite to precisely and safely achieve its goals preventing collisions with other spacecrafts located on the GEO, a set of periodic and scheduled manoeuvres, known as Station Keeping (SK) strategy, is required to maintain the vehicle inside an assigned slot. Moved by stringent requirements on accuracy and by the intention to find higher performance algorithms than standard numerical methods, a novel SK program is here proposed. It foresees the resolution of a feedback optimal control problem (OCP) for a low-thrust electric propulsion system by exploiting differential algebraic techniques. Unlike widespread linear solutions, leading to an accuracy drop when dealing with nonlinear dynamics, differential algebra (DA) enables to tackle nonlinearities by an arbitrary order Taylor series expansion of the OCP about a reference. The obtained polynomials allow to represent the dependency of the spacecraft state on eventual displacements of the initial conditions from the considered baseline. The feedback OCP can be reduced to a two-point boundary value problem (TPBVP) and then fixed by a high order polynomial approximation, whose manipulation permits to enforce eventual constraints and subsequently find the optimality commands. When perturbations in the nominal status occur, new optimal control laws are derived by the mere evaluation of polynomials in the perturbed state.

The SK strategy adopted in this thesis is based on a cyclic sequence made of a natural motion stage followed by a controlled section targeting a specific point inside the allowable region, tailored to maximize the free permanence within the permitted latitude-longitude bands until the next powered phase starts. A year evolution, affected by the geopotential perturbation, the Sun and Moon influence and the solar radiation pressure effects, is considered. DA is applied to compute the optimal, arbitrary order solution for each thrust arc.
The analysis is divided into two steps. The former consists in solving an Energy Optimal Problem (EOP) with continuous and non-saturated action. Its output can be directly achieved by considering the slot as a neighbourhood of the nominal state and by expanding the TPBVP about its centre, bypassing the need of a reference path. This also makes it possible to build up a control law evaluating, at every cycle, the same high order

polynomial approximating the time independent dynamics and then correcting it with the complete linear output, so that constant perturbations and time-variant ones can be treated separately. The latter takes the result of the first one as initial guess and solves a Fuel Optimal Problem (FOP) with a bang-bang control profile, with the help of a continuation method. This application involves a numerical baseline and consequently polynomials are exploited for a robust correction to any possible deviation from it.

Although a simplified problem is taken into account, its relevant findings suggest further investigations. The power of this method is demonstrated since it grants: an increased precision compared to linearized control; a low computational burden as against numerical techniques; the opportunity to build up a quick and robust controlling action from onboard DA maps; a low overall annual consumption.

Keywords: GEO, Station-Keeping, Differential Algebra, Optimal Control, Optimization

Abstract in lingua italiana

Affinché un satellite geostazionario possa conseguire con precisione e in sicurezza i propri obiettivi prevenendo la collisione con altri corpi localizzati in GEO, è necessario pianificare una sequenza periodica di manovre, nota come strategia di Station Keeping (SK), che consenta di mantenere il veicolo all'interno di una regione assegnata, delimitata longitudinalmente e latitudinalmente. In questo elaborato viene presentata una nuova programmazione dello SK, al fine di soddisfare stringenti requisiti di accuratezza e ottenere un algoritmo più performante rispetto ai metodi numerici largamente impiegati. Tale approccio prevede la risoluzione di un problema di controllo ottimo (OCP) a retroazione per un sistema propulsivo elettrico a bassa spinta mediante l'applicazione di tecniche di algebra differenziale (DA). Contrariamente ai diffusi criteri linearizzati, che risultano imprecisi nei casi di dinamiche non lineari, la DA permette di far fronte alle non linearità espandendo in serie di Taylor, ad un certo ordine, la soluzione dell'OCP rispetto a un riferimento. I polinomi così ottenuti consentono di esprimere la dipendenza dello stato del satellite dalle possibili variazioni delle condizioni iniziali rispetto ai valori nominali. Riducendo l'OCP retroattivo a un TPBVP, la soluzione è approssimabile con un polinomio di grado arbitrario, la cui manipolazione permette di fissare eventuali vincoli ed ottenere successivamente i comandi ottimali. Grazie alla semplice valutazione della suddetta mappa polinomiale, eventuali disturbi agenti sullo stato di riferimento sono contrastati e corretti variando la legge di controllo ottimo.

La strategia di SK adottata nel presente progetto si basa su una sequenza ciclica composta da una fase di moto naturale, affetto dalla perturbazione del campo gravitazionale, dall'influenza del Sole e della Luna e dagli effetti della pressione di radiazione solare, seguita da un periodo di spinta. L'obiettivo di quest'ultimo consiste nell'allineamento del satellite ad un punto target, scelto in modo da massimizzare lo stazionamento incontrollato nella regione permessa. L'analisi si estende su un arco temporale annuale e la DA viene applicata per calcolare la soluzione ottima a differenti ordini di espansione per ogni stadio di controllo. Lo studio si articola in due argomenti principali. Il primo risolve un EOP, caratterizzato da un'azione continua e non saturata. Il comando di SK, in questo caso, è ottenibile considerando lo slot ammissibile come un intorno dello stato nominale

ed espandendo il TPBVP rispetto al suo centro, evitando così il calcolo di una traiettoria di riferimento. Risulta in tal modo possibile generare una legge di controllo valutando, ad ogni ciclo, il medesimo polinomio che approssima la dinamica indipendente dal tempo, correggendola con la soluzione lineare del moto completo e separando quindi i contributi delle perturbazioni costanti da quelle tempo-varianti. Il secondo, ricorrendo all'utilizzo della soluzione ottenuta precedentemente come condizione iniziale, risolve un FOP con un profilo di spinta bang-bang tramite un metodo di continuazione. Poiché tale applicazione richiede un riferimento numerico, i polinomi sono utilizzati per una correzione robusta ad ogni possibile deviazione rispetto ad esso.

Nonostante si tratti di un problema semplificato, i rilevanti risultati ottenuti sono tali da giustificarne un'ulteriore e più approfondita analisi. Sono evidenti, infatti, le potenzialità di questo approccio in quanto esso garantisce: una maggior precisione rispetto al controllo lineare; un costo computazionale inferiore comparato a quello richiesto dai metodi numerici; la possibilità di ottenere un'azione di controllo rapida e robusta mediante la valutazione di mappe polinomiali disponibili direttamente a bordo; un modesto consumo annuale complessivo.

Parole chiave: GEO, Station-Keeping, Algebra Differenziale, Controllo Ottimo, Ottimizzazione

Contents

1 | Introduction

Placed on a circular orbit at an altitude of more than 35000 km and on the equatorial plane, a geostationary spacecraft is able to cover a large portion of the Earth's surface, remaining fixed above the same region during its whole life.

Weather satellites for real-time monitoring and data collection are usually located on the Geostationary Earth Orbit (GEO), as well as the majority of communications and navigation missions. Their motion, together with the Earth's rotation, allows ground stations to constantly point the vehicle, granting a permanent link with the spacecraft and avoiding iterative tracking procedures with movable antennas.

Thanks to these benefits, a lot of bodies crowd the GEO, sharing the same ring above the equator. According to [9], 425 satellites actually populate the zone within a latitude of $\pm 3°$. Each one is practically visible from a huge area extending $75°$ away from its position in both N-S and E-W directions.

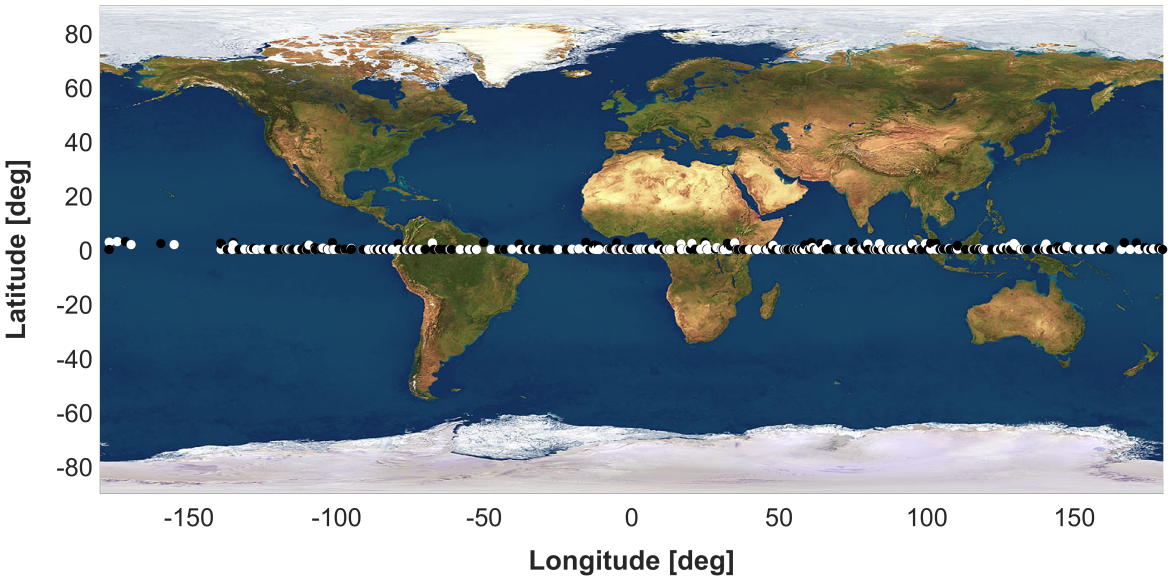

Figure 1.1: GEO Active Satellites in 2022

1.1. Geostationary Station Keeping

Active control is mandatory during a GEO mission. In order to maintain its nominal position and to ensure the cohabitation with other spacecrafts, a set of programmed manoeuvres shall be applied to a GEO satellite. This sequence of thrust actions is called *Station Keeping* (SK) strategy.

With the aim of preventing any possible collision and avoiding the body to freely drift from the prescribed location, SK provides the vehicle to stay within an assigned slot made of certain angular edges. Figure 1.2 shows a typical SK window, with its latitude $[-\phi_{max}, \phi_{max}]$ and longitude $[-\lambda_{max}, \lambda_{max}]$ bands, around the desired point $[l_s, 0°]$. In fact, due to some disturbances, a displacement in both geographical coordinates is expected to occur. The influence of the non-spherical Earth causes an important westward or eastward shift of the satellite, as well as the solar radiation pressure contribution which acts on the eccentricity; the impact of the Sun and Moon's gravity induces a change in the inclination instead.

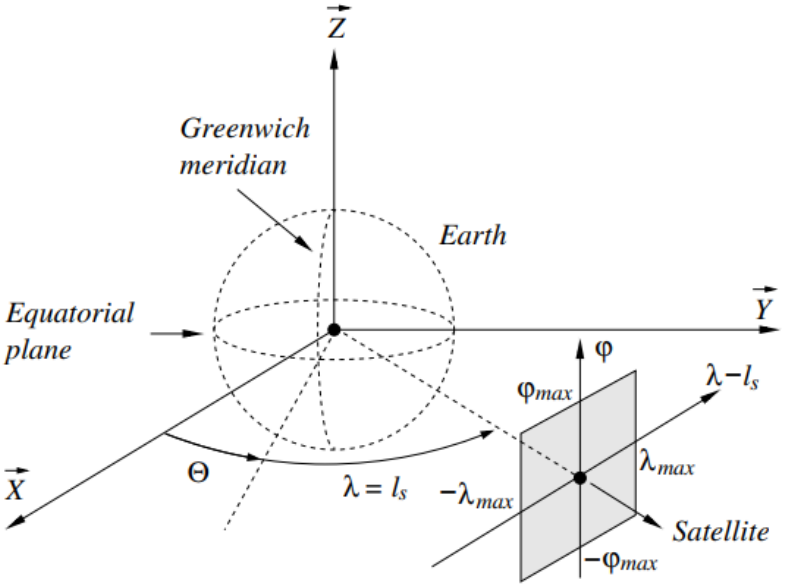

Figure 1.2: Station Keeping Window [14] in ECEF frame. Θ: Greenwich Hour Angle

Space trajectories and manoeuvres are usually designed in order to optimize the performances and improve the efficiency of the overall strategy adopted. Many technologies come to the aid of these objectives and the most important one is electric propulsion, whose motors have a specific impulse in the order of ten times higher than the one peculiar of chemical engines. This enables to save propellant mass extending the operational lifetime; however, it involves long working hours and precise and flexible control capacities.

As a consequence, actual geostationary SK is mostly achieved thanks to ion thrusters and so low-thrust systems permit an accurate N-S and E-W control with a series of continuous and optimized actions.

1.1.1. State of the Art

The SK optimal problem is an already existing and developed task, simply consisting of satisfying the satellite assigned box constraints (with reference to Figure 1.2, typically: $\phi_{max} = \lambda_{max} < 0.1°$) while minimizing a cost function.

Nowadays, the SK of GEO satellites is achieved by considering technological and operational features, such as electric propulsion, and optimal control strategies, taking various constraints into account (minimum elapsed time between two consecutive firings, on-off profile of the thrusters, thrust allocation). Optimal SK control problems may be solved according to several techniques.
When simplifying assumptions are used, analytical, albeit approximated, control laws may be obtained, as proved by Sukhanov and Prado [21] in 2012. They developed a mathematical procedure for the optimization of low-thrust SK manoeuvres based on a linearization of the satellite motion near a reference orbit.
Otherwise, it is in general necessary to resort to heavy numerical methods, such as direct collocation based methods. For this kind of approaches integrating the satellite dynamics, the state and the control variables are discretised to produce a non linear programming problem and get an optimal open loop control. In 2005 Losa [14] explored a direct method relying on a differential inclusion approach [22] for geostationary SK formulated as a constrained linear quadratic optimal control problem and built on a linear time-varying model for the dynamics of an electric spacecraft affected by perturbations. Gazzino resumes the real motion of a GEO body in a linearized state space representation in 2017 [4], deepening the formulation of the perturbing potentials in different reference frames. He than applied it to solve a minimum fuel geostationary SK introducing a switching system theory and imposing operational constraints on the duration of the firings. This issue is faced through a integer programming formulation in [5], consisting in a single step that foresees the linearization of the dynamics and the computation of the state transition matrix by the discretisation of the control variables. Another approach to implement the same optimal strategy can be found in [6], where the propellant minimization is achieved after three steps. The first one solves a problem without operational constraints on the thrusters thanks to an indirect method based on the Pontryagin Maximum Principle and initialized by a direct collocation procedure; then the propulsion requirements are enforced through an equivalent scheme and, at the end, the commutation times sequence

is optimized via a particular switching theory developed by Xu and Antsaklis [26]. This solution obtained an annual cost of $79.67\,m/s$ for a $4850\,kg$ satellite equipped with 4 engines, located in the North-East, North-West, South-East and South-West directions. A closed loop control was instead investigated by Guelman in 2013 [7]. He obtained an annual Δv of $70\,m/s$ for a $2000\,kg$ spacecraft, with a closed loop action that does not rely on previously computed reference trajectories.

With the aim of optimizing and simplifying the SK problem avoiding the numerical procedures and, in particular, the effort required by direct methods, this thesis proposes a further development of the strategy introduced by Di Lizia et al. in 2011 [11]. Here the SK optimal solution was obtained thanks to differential algebraic techniques, investigating and proving the strength of high order feedback control applied in this particular field. As previously done by Pasta [19] in 2010, a simplified problem is considered, excluding thrusters configurations and requirements. In his thesis work, Pasta applied the ASRE (Approximating Sequence of Riccati Equations) method to the geostationary SK optimization problem, developing a feedback EOP controller through the factorization of pseudo-linear dynamical equations and finding a quite high annual Δv of $79.69\,m/s$ for a $3000\,kg$ satellite characterized by a specific impulse of $3000\,s$, corresponding to $8.11\,kg$ of burnt propellant.

1.2. Notes on Differential Algebra

A high order optimal feedback indirect method based on differential algebraic techniques is proposed in this work.

Thanks to differential algebra (DA) it is possible to compute the derivatives of functions in a computer environment. The classical implementation of real algebra can be replaced by the new one of Taylor polynomials. Given any function f of m variables, it is approximated by its Taylor series up to an arbitrary order n. If it is possible to turn an Optimal Control Problem (OCP) into a Two-Point Boundary Value Problem (TPBVP), DA techniques can be applied to enable the expansion of the OCP solution about a reference state or trajectory with respect to either initial or terminal conditions. The computation of feedback control laws in relatively large neighborhoods of the nominal baseline is then reduced to the mere evaluation of high order polynomials.

DA was developed by Berz in 1999 [15] with the aim to solve analytical problems with an algebraic approach. Berz concentrates his study on the use of DA techniques for the solution of differential and partial differential equations, in particular for the efficient computation of Taylor expansions of the flow of differential equations with respect to the

initial conditions. While classical numerical algorithms are founded on function evaluations at specific points, causing inaccuracies due to cancellation, DA techniques rely on the idea that it is possible to have a better knowledge of the considered problem from its characteristic function rather than its values. This is made by creating a new computer environment where real numbers are substituted by Taylor expansions of the function.

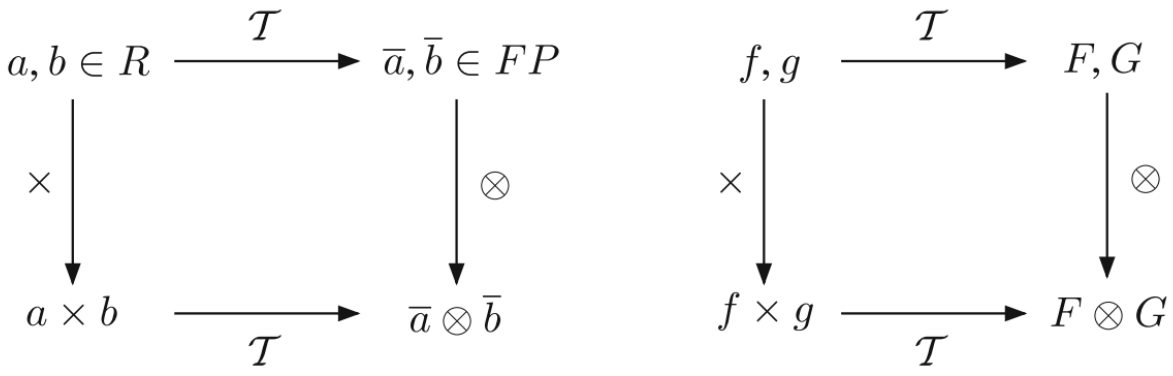

Figure 1.3: Analogy between floating point representation and differential algebraic framework

With reference to Figure 1.3, the classical transformation from real numbers (a, b) to their floating point (FP) representation $(\bar{a}, \bar{b})$ is applied to work on them in a numerical space. Defining a real operation '$\times$' between the two real terms, an adjoint one '$\otimes$' describes the same task in FP environment. Transforming the real numbers a and b in their FP representation and performing '$\otimes$' in the FP set is equivalent to carry out '$\times$' in the set of real numbers and then turning the result in its FP representation. Similarly, if two sufficiently regular functions f and g are of interest, the computer operates on them in DA framework using their Taylor series expansions, F and G respectively. Therefore, the analogy with the transformation of real numbers in their FP formulation is represented by the Taylor series of f and g. Indeed, extracting the Taylor expansions of f and g and operating on them in the space of Taylor polynomials returns the same result as operating on f and g in the real environment and then extracting the polynomial of the resulting function. The straightforward implementation of DA in a computer allows to compute the Taylor coefficients of a function up to a specified order n, along with the function evaluation, with a fixed amount of effort.

Berz and Makino implemented their version in the software COSY-Infinity, but in this thesis a Python interface [20] of the Differential Algebra Computational Toolbox (DACE) developed in a $C{+}{+}$ language by Massari and Wittig [16] is used.

With this algorithm, classical algebraic operations, methods to compose and invert functions, to solve nonlinear systems, differentiation and integration processes can be written and performed in a DA environment, dealing with n^{th} order polynomials.

1.2.1. High order Expansion of the Flow and Applications

According to [10], DA allows to compute the derivatives of any function f of m variables up to an arbitrary order n. Consequently, this has an important role when integrating an Ordinary Differential Equation (ODE) through a certain method. Explicit integration schemes rely on algebraic operations, evaluating the ODE right hand side at several integration points. Thus, working in a DA environment allows differential algebra to compute the arbitrary order expansion of the flow of a general ODE Initial Value Problem (IVP).

Given a generic IVP described by the dynamical flow $f(x,t)$:

$$\begin{cases} \dot{x} = f(x,t) \\ x(t_0) = x_0 \end{cases} \tag{1.1}$$

the initial condition x_0 can be initialized as a DA variable

$$[x_0] = \tilde{x}_0 + \delta x_0 \tag{1.2}$$

where $\tilde{x}_0$ is the reference expansion point. The Taylor expansion of the flow is obtained at each step of the considered integration scheme if all its operations are carried out in the DA space.

Working with a forward Euler's scheme:

$$x_i = x_{i-1} + f(x_{i-1}, t_{i-1})\,\Delta t \tag{1.3}$$

Considering the first step and the above DA starting condition, the DA representation at the first iteration is found:

$$[x_1] = [x_0] + f([x_0], t_0)\,\Delta t \tag{1.4}$$

Indeed, if f is evaluated in the DA framework, the output $[x_1]$ is the Taylor expansion of the solution x_1 at time t_1. The previous procedure can be inferred through the subsequent

steps until the last integration cycle is reached. The result at the final point is the n^{th} order polynomial of the flow of the IVP 1.1 at the final time t_f. Thus, the expansion of the flow of a dynamical system can be computed up to order n with a fixed amount of effort.

These techniques can be applied to more complex and precise schemes such as Runge-Kutta integration methods.

As detailed in the next chapters, DA is applicable to expand an optimal TPBVP and to solve control problems. According to this, many contributions investigate the benefits of DA high order optimization dealing with different cases.
In [10] two applications are proposed. The first one is about the identification of the family of halo orbits around the Lagrangian point L1 of the Earth–Moon system while the other concerns the design of an aerocapture maneuver for different values of entry velocity and drag coefficient.
Di Lizia et al. solved EOPs with DA techniques in 2014 [12] for rendezvous manoeuvres, lunar landing and low-thrust Eart-Mars transfer, showing the computational advantages and the accuracy of the high order approach. As a comparison, the same rendezvous problem was previously taken into account by Park et al. in 2006 [18], where the canonical optimal feedback control TPBVP is solved with generating functions.
The application of DA to a FOP is designed in [13], where saturating actuators, which are a critical aspect of nonlinear optimal feedback control, are managed with DA. The constraints have been included in the optimal control problem formulation and differential algebra have been used to expand the associated optimal bang-bang solution with respect to initial and terminal states.
Finally, in 2011, Armellin et al. [1] considered a DA method for the nonlinear propagation of uncertainties in celestial mechanics and to study the close encounter of asteroid Apophis with Earth in 2029. The arbitrary order Taylor expansion of the flow with respect to the initial conditions has been exploited to implement an accurate and computationally efficient Monte Carlo algorithm, in which thousands of pointwise integrations can be substituted by polynomial evaluations.

1.3. Thesis Outline

This thesis is divided into 5 chapters.

In chapter 2 the theoretical fundamentals are introduced, describing the GEO environment and dynamics, together with an insight on optimal control methods, focusing on the objective function formulation, on the linearized solution and on the high order approach

with DA.

Chapter 3 presents the adopted SK strategy and the procedure followed to choose the target states, tailored to reach a quasi global optimization. The energy optimal problem is then solved computing the controlled trajectory with respect to the nominal SK state; its outcomes are presented comparing various DA results with numerical techniques.

Chapter 4 applies the DA to a minimum fuel optimization. A precise, numerically calculated reference path gives the baseline of the commutation times sequence. The control arc is here about the nominal controlled structure, generating new thrust profiles. Various initial displacements are considered to validate the DA fuel optimal solution.

A summary of the conclusions and suggestions for further developments are finally presented in chapter 5.

1.3.1. Objectives and Assumptions

This research proposes a novel approach to optimal SK for low-thrust, electric, geostationary satellites. The project aims to prove the applicability of differential algebraic techniques and to highlight their computational benefits and the potential advantages in terms of accuracy, optimality and on board feasibility for future eventual developments. As a primary DA analysis, a simplified solution is proposed, based on the following assumptions.

- The DA optimal feedback control problem is solved with indirect methods by expanding a TPBVP.
- Only initial and final conditions are imposed. The thrust phases are not subject to path constraints. This means that during a controlled path the spacecraft is allowed to slightly violate the SK box.
- N-S and E-W station keeping are not considered separately. Thrust direction is unbounded.
- No particular engines configuration is considered.
- No operational restrictions are enforced concerning the duration of the firings, their sequence and the *OFF* periods.
- Satellite attitude is not taken into account.
- The GEO dynamics is written in Earth Centered Earth Fixed spherical coordinates. The SK is achieved by focusing on the two geographical coordinates only.

2 | Fundamentals

2.1. Orbital Dynamics and Environment

2.1.1. Generalities

The GEO is a particular geosynchronous orbit with zero inclination and zero eccentricity. From the definition of geosynchronous orbits, their period is equal to the one of the Earth's rotation. This enables to easily compute the semi-major axis of the GEO by the following relation:

$$a_{GEO} = \sqrt[3]{\frac{\mu_E T_E^2}{4\pi^2}} \tag{2.1}$$

with μ_E the geocentric standard gravitational parameter and T_E the sidereal Earth rotation period.

The motion of a GEO satellite can be beforehand approximated and described by the keplerian restricted Two Body Problem (TBP). Considering the Earth as a perfect sphere and neglecting any other possible perturbing action, according to the Newton gravitational law, the orbiting body undergoes the force

$$\mathbf{F} = -G\frac{m_E m_{body}}{r^3}\mathbf{r} \tag{2.2}$$

where m_E is the Earth's mass, m_{body} and $\mathbf{r}$ indicate the mass and the position vector of the satellite respectively, r is the GEO radius given by Equation 2.1 and G is the gravitational constant. The above main parameters are introduced by Table 2.1.

$\mathbf{m_E}[kg]$	$\mathbf{T_E}[s]$	$\mathbf{G}[km^3 \cdot kg^{-1} \cdot s^{-2}]$	$\mu_\mathbf{E}[km^3 \cdot s^{-2}]$	$\mathbf{a_{GEO}}[km]$
$5.972 \cdot 10^{24}$	86164	$6.674 \cdot 10^{-20}$	398600	42164.12

Table 2.1: General parameters and GEO semi-major axis

Under these assumptions and ignoring the mass of the vehicle with respect to the Earth's one, the dynamics is given by a 2^{nd} order Ordinary Differential Equation (ODE). Remembering that the variation of the spacecraft momentum is equal to the sum of the external forces, according to Newton's second law, the relation 2.3 gives the equations of motion for the TBP, where $\ddot{\mathbf{r}}$ is the acceleration transmitted to the satellite by the external force.

$$\ddot{\mathbf{r}} = -\frac{\mu_E}{r^3}\mathbf{r} \tag{2.3}$$

2.1.2. Reference Frames

In this section the adopted coordinate systems are presented, in particular:

1. Geocentric Equatorial Coordinate System (GECS);
2. Earth Centered Earth Fixed (ECEF) frame;

Geocentric Equatorial Coordinate System

The GECS system in Figure 2.1 has its origin in the center of the Earth, it is fixed and it is built as follows:

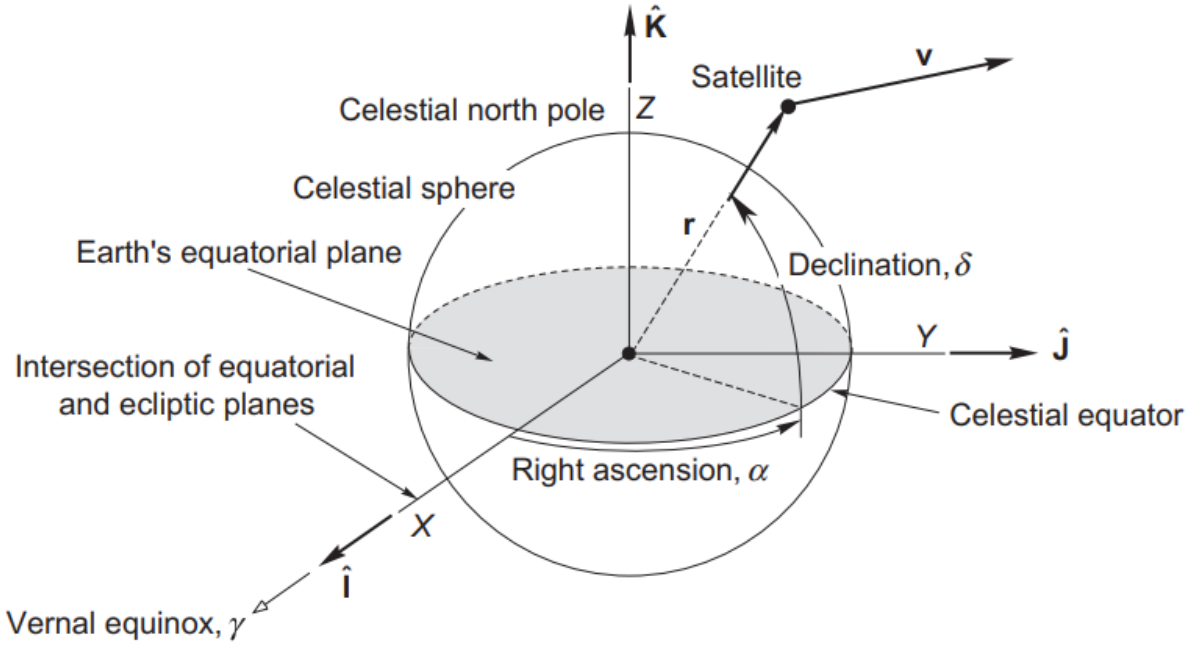

Figure 2.1: Geocentric Equatorial Reference System [3]

- X ($\hat{\mathbf{I}}$) axis points to the Vernal equinox γ;
- Z ($\hat{\mathbf{K}}$) axis is directed towards the North Pole;
- Y ($\hat{\mathbf{J}}$) axis completes the right orthogonal tern.

According to this reference, two different set of coordinates can be defined. The X, Y and Z cartesian ones, that are the $\hat{\mathbf{I}}$, $\hat{\mathbf{J}}$ and $\hat{\mathbf{K}}$ components of the position vector $\mathbf{r}$, and the spherical ρ, α and δ. The latter can be related to the former by the definition of *distance*, *right ascension* and *declination*, as described by the 2.4.

$$\begin{cases} \rho = \sqrt{X^2 + Y^2 + Z^2} \\ \alpha = \arctan \dfrac{Y}{X} \\ \delta = \arcsin \dfrac{Z}{\rho} \end{cases} \tag{2.4}$$

with the ambiguity on α solved by looking at the sign of the x-coordinate:

$$\begin{cases} -\pi/2 < \alpha < \pi/2 \quad if \quad X > 0 \\ \pi/2 < \alpha < 3\pi/2 \quad if \quad X < 0 \end{cases} \tag{2.5}$$

Similarly, the cartesian coordinates can be expressed as functions of the spherical ones thanks to the 2.6.

$$\begin{cases} X = \rho \cos\delta \cos\alpha \\ Y = \rho \cos\delta \sin\alpha \\ Z = \rho \sin\delta \end{cases} \tag{2.6}$$

Earth Centered Earth Fixed frame

The second system introduced is the ECEF. Shown in Figure 2.2, this reference is very similar to the GECS since it is Earth-centered and lies on the equatorial plane but it is not fixed. Its main peculiarity is its angular velocity equal to the Earth's one computed in Equation 2.7. This characteristic becomes a huge advantage when dealing with GEO satellites due to their motion integral with the Earth's rotation and to their zero inclination. An unperturbed GEO spacecraft, in fact, is constantly in its nominal position $(r_{GEO},\ \lambda_n,\ \phi_n)$ with respect to this frame.

It is built starting from the GECS as explained: the Z ($\hat{\mathbf{K}}$) axis remains fixed, pointing the North Pole; the X ($\hat{\mathbf{I}}$) and Y ($\hat{\mathbf{J}}$) axis rotates on the equatorial plane following the Greenwich Hour Angle (GHA). In this way, the GECS X axis now moves with the Greenwich Meridian and it is called x_G ($\hat{\mathbf{x}}$). From this new non-fixed axis $\hat{\mathbf{x}}, \hat{\mathbf{y}}, \hat{\mathbf{z}}$, a new set of spherical coordinates is defined:

- r is the distance of the satellite from the Earth center;
- λ $[-\pi, \pi]$ is the *longitude* of the satellite, defined as the angle between the spacecraft projection on the equatorial plane and x_G, positive towards East;
- ϕ $[-\pi/2, \pi/2]$ is the *latitude* of the body, comparable to the GECS δ and positive in the Northern Hemisphere.

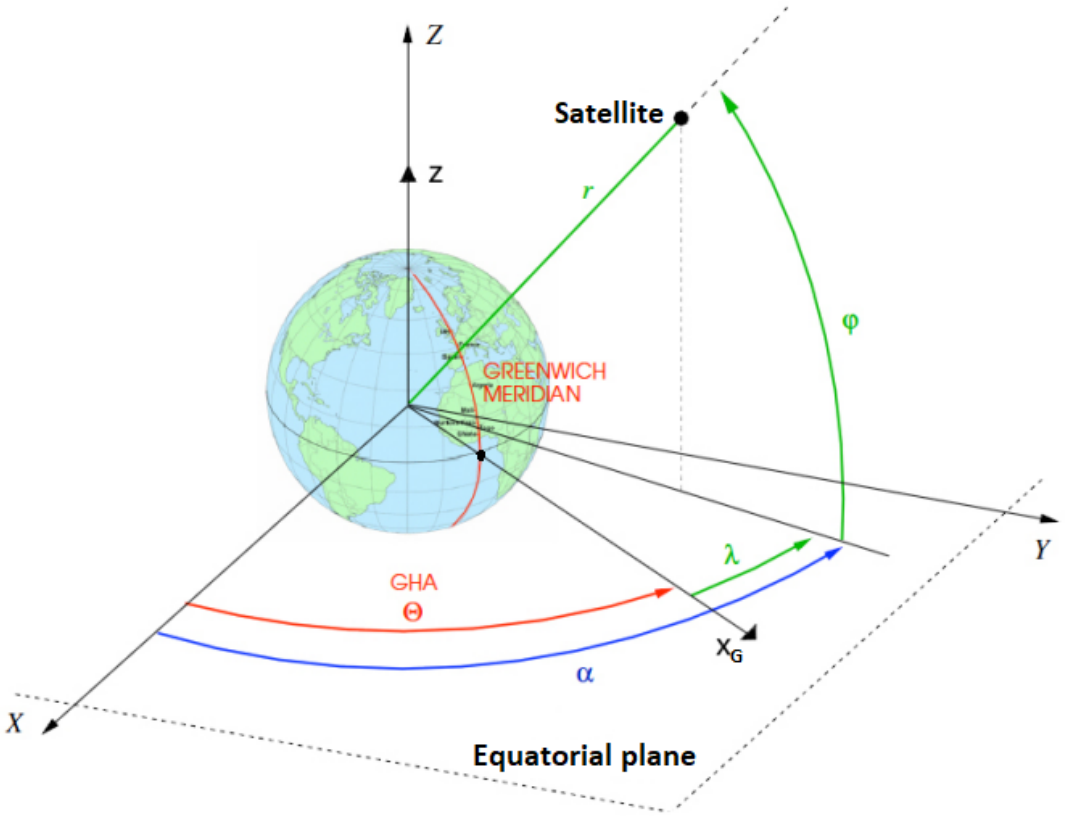

Figure 2.2: Earth Centered Earth Fixed frame [19]

As said, the motion of this frame follows the GHA (Θ), and so it depends on the considered initial epoch, as shown in Equation 2.7.

$$\Theta(t) = \Theta_0 + \omega_E(t - t_0), \quad \omega_e = \frac{2\pi}{T_E} \tag{2.7}$$

Knowing the right ascension α of the satellite, one can compute its longitude λ as:

$$\lambda = \alpha - \Theta(t) \tag{2.8}$$

The relations between ECEF cartesian and spherical coordinates are again the 2.4 and 2.6, while the transformation from GECS to ECEF can be achieved through a rotation around axis Z of an angle α:

$$\begin{pmatrix} x \\ y \\ z \end{pmatrix} = \mathbf{R_Z} \begin{pmatrix} X \\ Y \\ Z \end{pmatrix} \tag{2.9}$$

with $\mathbf{R_Z}$ the rotation matrix.

$$\mathbf{R_Z} = \begin{bmatrix} \cos\alpha & \sin\alpha & 0 \\ -\sin\alpha & \cos\alpha & 0 \\ 0 & 0 & 1 \end{bmatrix} \tag{2.10}$$

If the passage from the spherical to the cartesian is of interest, the following conversion shall be applied in the ECEF [25], from the definition of the radial, transversal and out-of-plane directions:

$$\begin{cases} \hat{\mathbf{r}} = \cos\phi\cos\lambda\,\hat{\mathbf{x}} + \cos\phi\sin\lambda\,\hat{\mathbf{y}} + \sin\phi\,\hat{\mathbf{z}} \\ \hat{\lambda} = \sin\phi\cos\lambda\,\hat{\mathbf{x}} + \sin\phi\sin\lambda\,\hat{\mathbf{y}} - \cos\phi\,\hat{\mathbf{z}} \\ \hat{\phi} = -\sin\lambda\,\hat{\mathbf{x}} + \cos\lambda\,\hat{\mathbf{y}} \end{cases} \tag{2.11}$$

Knowing the ECEF spherical components, the cartesian ones are obtained:

$$\begin{pmatrix} x \\ y \\ z \end{pmatrix} = \begin{bmatrix} \cos\phi\cos\lambda & \cos\phi\sin\lambda & \sin\phi \\ \sin\phi\cos\lambda & \sin\phi\sin\lambda & -\cos\phi \\ -\sin\lambda & \cos\lambda & 0 \end{bmatrix} \begin{pmatrix} r \\ \lambda \\ \phi \end{pmatrix} \tag{2.12}$$

2.1.3. Equations of Motion

Once the ECEF frame is selected as the best option to write the GEO dynamics, in this section the procedure that leads to the motion of a generic body of mass m is reported for the approximated keplerian problem and then extended to the real one.

Keplerian Dynamics

The TBP presented in 2.3 can be turned into r, λ and ϕ spherical coordinates.

This is obtained through the Lagrangian formulation. Defining $\mathbf{q}$ the vector of the free coordinates r, λ and ϕ, K the kinetic energy and V the potential energy of the gravity force only, the Lagrangian L is:

$$L = K(\mathbf{q}, \dot{\mathbf{q}}) - V(\mathbf{q}) \tag{2.13}$$

The generalized equations of motion are written in the shape of 2.14.

$$\frac{d}{dt}\left(\frac{\partial L}{\partial \dot{\mathbf{q}}}\right) - \frac{\partial L}{\partial \mathbf{q}} = \mathbf{Q} \tag{2.14}$$

$\mathbf{Q}$ indicates the contribution of the non conservative forces acting on the body and, in this case, this term is null.

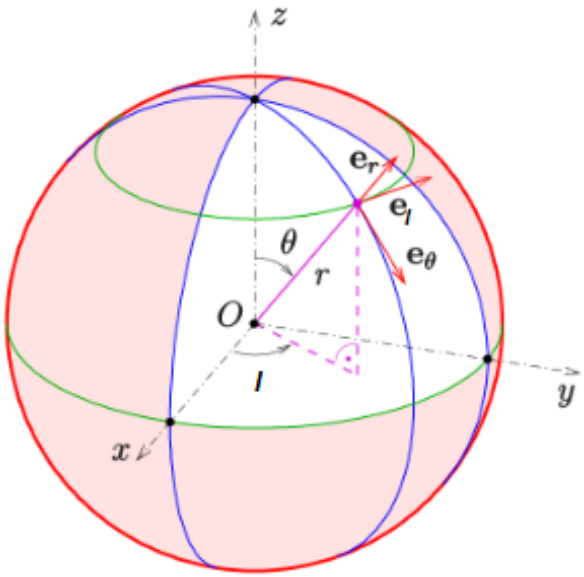

Figure 2.3: Spherical Coordinates [25]

According to [25] and to Figure 2.3, the position of a body in a spherical frame around Earth can be defined as $\mathbf{r} = r\mathbf{e_r}$.

Considering that the frame is not fixed, the expression for the velocity is then:

$$\mathbf{v} = \frac{d\mathbf{r}}{dt} = \dot{r}\mathbf{e_r} + r\dot{\theta}\mathbf{e}_\theta + r\dot{l}\sin\theta\mathbf{e_l} \tag{2.15}$$

Noticing that $\theta = 90° - \phi$ and $\dot{l} = \dot{\lambda} + \omega_E$, the kinetic energy can be computed, while the potential V is given by the dr integral of the opposite gravity force introduced in Equation 2.2.

$$K = \frac{1}{2}m\mathbf{v}\cdot\mathbf{v} = \frac{1}{2}m\left[\,\dot{r}^2 + r^2\dot{\phi}^2 + r^2(\dot{\lambda}+\omega_E)^2\cos\phi^2\,\right] \tag{2.16a}$$

$$V = -\frac{\mu_E m}{r} \tag{2.16b}$$

Defining $v = \dot{r}$, $\xi = \dot{\lambda}$, $\eta = \dot{\phi}$ and the state $\mathbf{x} = [r\ \lambda\ \phi\ v\ \xi\ \eta]$ as a six-elements vector with position and velocity spherical components, the dynamics 2.17 for the keplerian TBP is obtained in the form $\dot{\mathbf{x}} = f(\mathbf{x}, t)$ through the solution of the Lagrangian formulation.

$$\begin{cases} \dot{r} = v \\ \dot{\lambda} = \xi \\ \dot{\phi} = \eta \\ \dot{v} = -\dfrac{\mu_E}{r^2} + r\eta^2 + r(\xi+\omega_E)^2\cos\phi^2 \\ \dot{\xi} = 2\eta(\xi+\omega_E)\tan\phi - 2\dfrac{v}{r}(\xi+\omega_E) \\ \dot{\eta} = -2\dfrac{v}{r}\eta - (\xi+\omega_E)^2\sin\phi\cos\phi \end{cases} \tag{2.17}$$

Complete Dynamics

According to [2], in the presence of perturbing forces, as in the case of GEO real motion, a new contribution is added to Equation 2.14. The expression of the complete dynamics is obtained by appending the conservative, disturbing actions potential $W^p(r, \lambda, \phi)$ to the Lagrangian L:

$$L = \frac{1}{2}m\left[\,\dot{r}^2 + r^2\dot{\phi}^2 + r^2(\dot{\lambda}+\omega_E)^2\cos\phi^2\,\right] + \frac{\mu_E m}{r} + W^p(r,\lambda,\phi) \tag{2.18}$$

Solving the Equation 2.14, the accelerations are then represented by a new set of spherical equations:

$$\begin{cases} \dot{v} + \dfrac{\mu_E}{r^2} - r\eta^2 - r(\xi + \omega_E)^2 \cos\phi^2 = F(r, \lambda, \phi) \\ \dot{\xi} - 2\eta(\xi + \omega_E)\tan\phi + 2\dfrac{v}{r}(\xi + \omega_E) = G(r, \lambda, \phi) \\ \dot{\eta} + 2\dfrac{v}{r}\eta + (\xi + \omega_E)^2 \sin\phi\cos\phi = H(r, \lambda, \phi) \end{cases} \tag{2.19}$$

F, G, H are the disturbing actions to the motion of the body. If $W^p(r, \lambda, \phi)$ is the perturbing potential, they are written as follows:

$$F = \frac{1}{m}\frac{\partial W^p}{\partial r}, \quad G = \frac{1}{m}\frac{\partial W^p}{\partial \lambda}, \quad H = \frac{1}{m}\frac{\partial W^p}{\partial \phi}, \tag{2.20}$$

Since the gradient of a generic quantity can be computed in spherical coordinates as

$$\nabla(\cdot) = \frac{\partial(\cdot)}{\partial r} + \frac{1}{r\cos\phi}\frac{\partial(\cdot)}{\partial \lambda} + \frac{1}{r}\frac{\partial(\cdot)}{\partial \phi} \tag{2.21}$$

and knowing that F, G, H represent the perturbing accelerations $a_r^p, a_\lambda^p, a_\phi^p$, the right-hand side of 2.19 is finally given and the final dynamics $\dot{\mathbf{x}} = f(\mathbf{x}, t)$ is:

$$\begin{cases} \dot{r} = v \\ \dot{\lambda} = \xi \\ \dot{\phi} = \eta \\ \dot{v} = -\dfrac{\mu_E}{r^2} + r\eta^2 + r(\xi + \omega_E)^2 \cos\phi^2 + a_r^p(r, \lambda, \phi) \\ \dot{\xi} = 2\eta(\xi + \omega_E)\tan\phi - 2\dfrac{v}{r}(\xi + \omega_E) + \dfrac{1}{r\cos\phi}a_\lambda^p(r, \lambda, \phi) \\ \dot{\eta} = -2\dfrac{v}{r}\eta - (\xi + \omega_E)^2 \sin\phi\cos\phi + \dfrac{1}{r}a_\phi^p(r, \lambda, \phi) \end{cases} \tag{2.22}$$

Since the GEO motion occurs in a real environment, a non spherical attractor must be taken into account, as well as the typical high altitude perturbations, such as the Sun and Moon gravity effects and the solar radiation pressure (SRP).
All these disturbances are detailed in the next section.

2.1.4. Perturbations

As mentioned in 2.1.1, many disturbances must be taken into account when dealing with a GEO real problem. The three main contributions affecting an high altitude orbit such as the geostationary one can be seen in Figure 2.4 and are:

- non-uniformity of the gravity field;
- *third bodies* gravity influence (Sun and Moon specifically);
- solar radiation pressure (SRP).

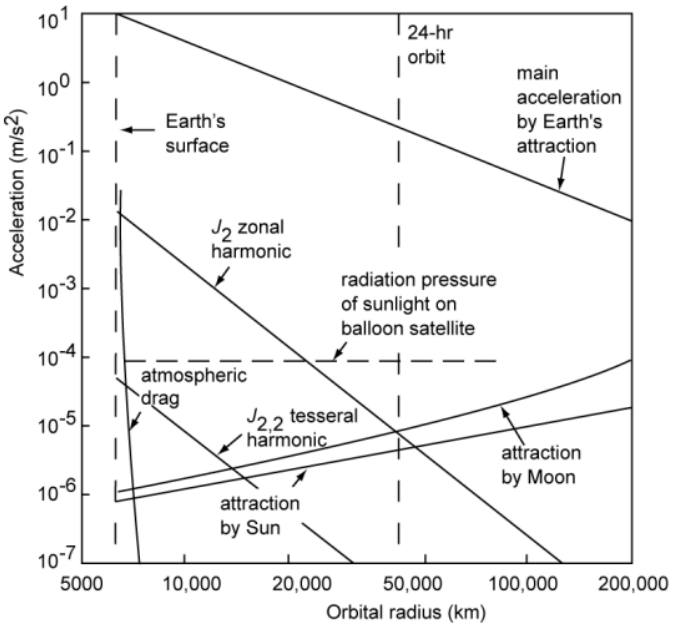

Figure 2.4: Relevant perturbations and magnitude [23]

These perturbations constitute the accelerations collected in the term $\mathbf{a^P}$ in Equation 2.22.

Earth's Oblateness

Due to the fact that the Earth is not a perfect sphere, according to [4] and [24], the gravity potential can be expressed like a series of harmonics:

$$V_{grav}(r,\lambda,\phi) = \frac{\mu_E}{r}\left[1 + \sum_{l=2}^{\infty}\sum_{m=0}^{l}\left(\frac{R_E}{r}\right)^l P_{l,m}[\sin\phi]\{C_{l,m}\cos m\lambda + S_{l,m}\sin m\lambda\}\right] \quad (2.23)$$

The first term represents the spherical potential, which has been already considered in the dynamics 2.22.

Figure 2.5: zonal, sectorial and tesseral harmonics [23]

As shown in Figure 2.5, the terms with $m = 0$ indicate the *zonal* harmonics; the ones with $l = m \neq 0$ are the *sectorial* harmonics and the cases with $l \neq m \neq 0$ corresponds to the *tesseral* harmonics. The perturbing term is then:

$$V^p_{grav}(r, \lambda, \phi) = \frac{\mu_E}{r} \sum_{l=2}^{\infty} \sum_{m=0}^{l} \left(\frac{R_E}{r} \right)^l P_{l,m}[\sin \phi]\{C_{l,m} \cos m\lambda + S_{l,m} \sin m\lambda\} \tag{2.24}$$

It is important to notice that, for a GEO body orbiting with a nominal longitude and latitude λ_n, ϕ_n, the perturbation caused by the Earth's gravity field is almost constant in time, since the satellite is located above the same bulge. The most important effect caused by this additional acceleration is a longitude drift, whose intensity and direction depend on λ_n (see Appendix A). The geopotential has four equilibrium points: two of them are stable and are located at $\lambda = 75.1°\ E$ and $\lambda = 104.7°\ W$; the others are unstable and correspond to $\lambda = 165.3°\ E$ and $\lambda = 14.7°\ W$, as shown in Figure 2.6.

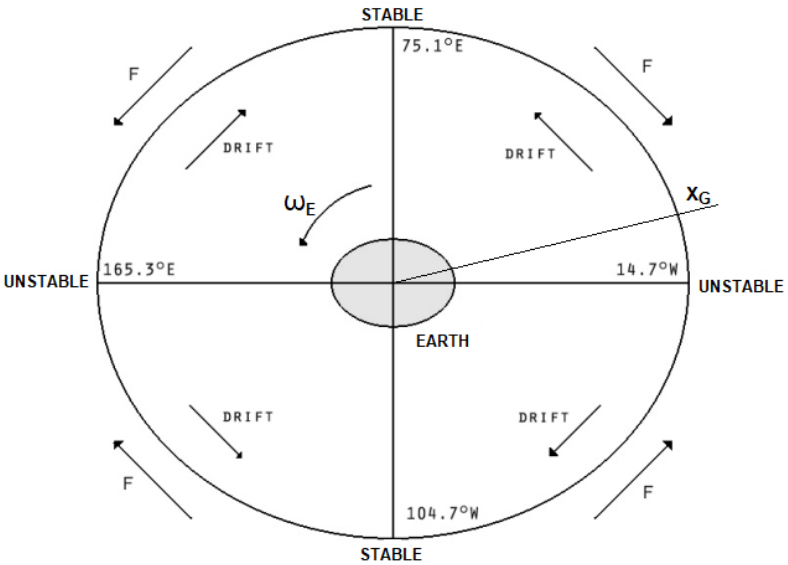

Figure 2.6: Stable and Unstable points [24]

The Legendre polynomials $P_{l,m}[\sin\phi]$ assume the form provided by the Rodrigues' generalized formula 2.25, where the argument $[\sin\phi]$ is replaced by x.

$$P_{l,m}[x] = \frac{1}{2^l l!}(1-x^2)^{m/2}\frac{d^{l+m}}{dx^{l+m}}(x^2-1)^l \tag{2.25}$$

The gravity model up to order $3,3$ is finally completed with the geopotential coefficients of l^{th} degree and m^{th} order $C_{l,m}$ and $S_{l,m}$ in Table 2.2. Higher orders are not considered due to their negligible effects.

l	m	$\mathbf{C_{l,m}}$	$\mathbf{S_{l,m}}$
2	0	$-1.083 \cdot 10^{-3}$	–
3	0	$2.532 \cdot 10^{-6}$	–
2	2	$1.574 \cdot 10^{-6}$	$-9.038 \cdot 10^{-7}$
3	3	$1.006 \cdot 10^{-7}$	$1.972 \cdot 10^{-7}$
2	1	$-2.414 \cdot 10^{-10}$	$1.543 \cdot 10^{-9}$
3	1	$2.191 \cdot 10^{-6}$	$2.687 \cdot 10^{-7}$
3	2	$3.089 \cdot 10^{-7}$	$-2.115 \cdot 10^{-7}$

Table 2.2: Harmonics coefficients [24]

Once the potential is introduced, the perturbing accelerations can be found by performing its spherical gradient:

$$\mathbf{a^p_{grav}}(r,\lambda,\phi) = \frac{\partial V^p_{grav}(r,\lambda,\phi)}{\partial r}\hat{\mathbf{r}} + \frac{1}{r\cos\phi}\frac{\partial V^p_{grav}(r,\lambda,\phi)}{\partial \lambda}\hat{\lambda} + \frac{1}{r}\frac{\partial V^p_{grav}(r,\lambda,\phi)}{\partial \phi}\hat{\phi} \tag{2.26}$$

Sun and Moon Disturbances

Another relevant disturbance is the one associated to the influence of both the Sun and the Moon on a geostationary satellite. The higher the orbit, the stronger the effect of these *third bodies* on the stability of the spacecraft. Their impact is very critical in the latitude drift and it is time dependent, since the position of the attractors changes with time.

A potential formulation is again the most suitable option to analyse and compute the

perturbing accelerations:

$$V_{3B}^{p}(r,\lambda,\phi) = \mu_3\left(\frac{1}{r_{s-3}} - \frac{\mathbf{r}\cdot\mathbf{r_3}}{r_3^3}\right) \tag{2.27}$$

With reference to Figure 2.7 and thanks to the cosine law it is found that

$$\frac{1}{r_{3-sat}} = \frac{1}{|\mathbf{r_3}-\mathbf{r_{sat}}|} = \frac{1}{r_3\left(1+\frac{r_{sat}^2}{r_3^2} - 2\frac{r_{sat}}{r_3}\cos\psi_3\right)^{1/2}} \tag{2.28}$$

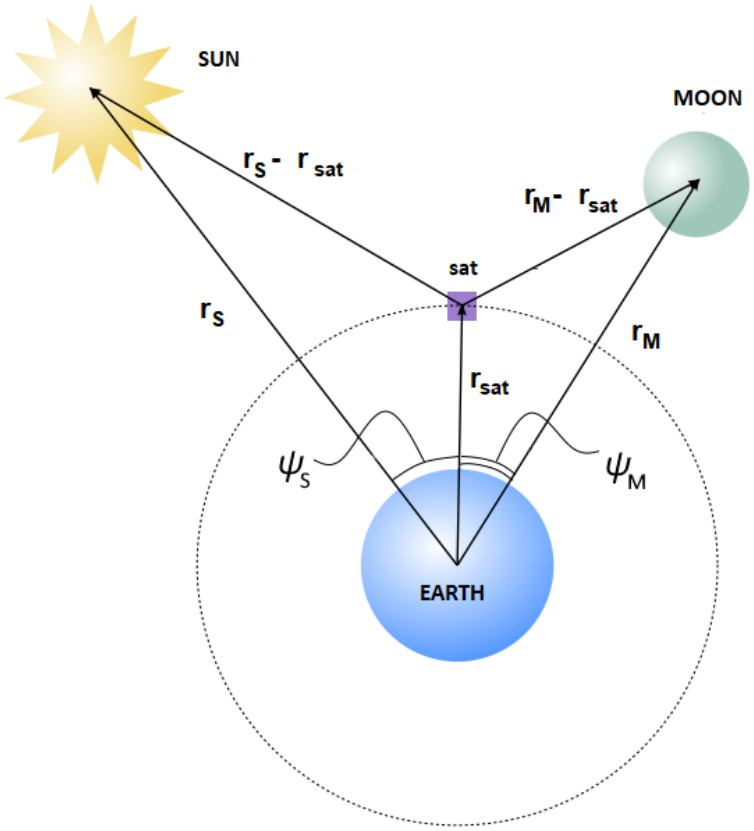

Figure 2.7: Third body perturbation. Reference geometry [4]

Noticing that $r_{sat}/r_3 << 1$, the expression above can be approximated as a Legendre polynomial $P_k[x]$, with $x = \cos\psi_3$, as in [19]. The expression of the polynomial is given again by the Rodrigues' formula 2.25 with $l = k$ and $m = 0$.

$$\frac{1}{|\mathbf{r_3}-\mathbf{r_{sat}}|} = \frac{1}{r_3}\sum_{k=0}^{\infty}\left(\frac{r_{sat}}{r_3}\right)^k P_k[\cos\psi_3] \tag{2.29}$$

In this way, the potential V_{3B} can be firstly separated into Sun and Moon contributions and then rewritten considering an expansion up to order $k = 2$:

$$V_{3B}^{p}(r,\lambda,\phi) = \frac{\mu_S}{r_S}\left[1 + \left(\frac{r_{sat}}{r_S}\right)^2 \frac{3\cos\psi_S - 1}{2}\right] + \frac{\mu_M}{r_M}\left[1 + \left(\frac{r_{sat}}{r_M}\right)^2 \frac{3\cos\psi_M - 1}{2}\right] \quad (2.30)$$

The dependence on r, λ, ϕ is achieved through spherical geometry:

$$\cos\psi_3 = \sin\phi\sin\delta_3 - \cos\phi\cos\delta_3\cos\left(\Theta(t) + \lambda - \alpha_3\right) \quad (2.31)$$

where δ_3 and α_3 are respectively the declination and the right ascension of the Sun/Moon, given by the ephemeris at the current epoch. The perturbing accelerations are finally computed:

$$\mathbf{a_{3B}^{p}}(r,\lambda,\phi) = \frac{\partial V_{3B}^{p}(r,\lambda,\phi)}{\partial r}\hat{\mathbf{r}} + \frac{1}{r\cos\phi}\frac{\partial V_{3B}^{p}(r,\lambda,\phi)}{\partial\lambda}\hat{\lambda} + \frac{1}{r}\frac{\partial V_{3B}^{p}(r,\lambda,\phi)}{\partial\phi}\hat{\phi} \quad (2.32)$$

Solar Radiation Pressure

The last significant, perturbing force coming from the high altitude environment is the solar pressure disturbance (SRP). It acts on the eccentricity of the orbit and so its main effect is an E-W drift. According to quantum physics, the radiation emitted by the Sun contains photons. They are massless elementary particles travelling at the speed of light c and carrying energy and momentum, which values can be computed through the Planck constant h. Knowing the frequency $f[Hz]$ of the electromagnetic wave associated to a photon, its energy can be written as $E = hf$, while its momentum is given by $p = hf/c$. In this analysis the Sun is considered as a black body emitting photons from its visible surface (the photosphere) on the whole electromagnetic spectrum and at a temperature T. Thanks to the Stefan-Boltzmann law, the intensity of the emitted radiation is $S_0 = \sigma T^4$, where σ is the Stefan-Boltzmann constant.

Indicating R_p and R_{E-S} the radius of the photosphere and the mean Earth-to-Sun distance, referring to Table 2.3, the radiation intensity S_E at the Earth's orbit is rescaled as:

$$S_E = S_0\left(\frac{R_p}{R_{E-S}}\right)^2 = 1367\ W/m^2 \quad (2.33)$$

that is the energy flux transported by the photons across a surface normal to the direction

of the radiation. Dividing S_E by c, the momentum flux at Earth's distance, which is equal to a pressure (the SRP), is found:

$$P_{SR} = \frac{S_E}{c} = 4.56\ \mu Pa \tag{2.34}$$

The force transmitted to a satellite of mass m, with a reflectivity area A_s, characterized by a reflection coefficient C_r lying between 1 (total absorption) and 2 (total reflection) is:

$$\mathbf{F^p_{SRP}} = \nu C_r P_{SR} A_s \hat{\mathbf{u}} \tag{2.35}$$

where $\hat{\mathbf{u}}$ is the direction from the Sun to the spacecraft and ν assumes the value of 1, except during eclipse time when it is 0. The SRP main parameters are summarized in Table 2.3.

$\mathbf{h}[J \cdot s]$	$\mathbf{c}[m/s]$	$\mathbf{T}[K]$	$\sigma[W \cdot m^{-2} \cdot K^{-4}]$	$\mathbf{R_p}[km]$	$\mathbf{R_{E-S}}[km]$
$6.626 \cdot 10^{-34}$	$2.998 \cdot 10^{8}$	5777	$5.670 \cdot 10^{-8}$	696000	$149.6 \cdot 10^{6}$

Table 2.3: Solar Radiation Pressure parameters [3]

Consequently, the perturbing acceleration is:

$$\mathbf{a^p_{SRP}} = \nu C_r \frac{P_{SR} A_s}{m} \hat{\mathbf{u}} \tag{2.36}$$

Looking again at Figure 2.7 and approximating the Sun-to-satellite direction to the Sun-to-Earth one, the acceleration $\mathbf{a^p_{SRP}}$ can be computed from a pseudo-potential written in the ECEF spherical coordinates $V_{SRP}(r, \lambda, \phi)$:

$$V^p_{SRP}(r, \lambda, \phi) = -\nu P_{SR} \frac{C_r A_s}{m} r \cos \psi_S \tag{2.37}$$

The angle ψ_S is function of r, λ and ϕ thanks to Equation 2.31 and so the perturbing accelerations due to the SRP in the ECEF spherical coordinates are found:

$$\mathbf{a^p_{SRP}}(r, \lambda, \phi) = \frac{\partial V^p_{SRP}(r, \lambda, \phi)}{\partial r} \hat{\mathbf{r}} + \frac{1}{r \cos \phi} \frac{\partial V^p_{SRP}(r, \lambda, \phi)}{\partial \lambda} \hat{\lambda} + \frac{1}{r} \frac{\partial V^p_{SRP}(r, \lambda, \phi)}{\partial \phi} \hat{\phi} \tag{2.38}$$

2.1.5. Free-Drift Dynamics

All in all, the uncontrolled dynamics can be written as a TBP perturbed by various accelerations coming from the environment, in the form $\dot{\mathbf{x}} = f(\mathbf{x}, \mathbf{a^P}(r, \lambda, \phi), t) = f(\mathbf{x}, t)$, as in 2.22, with $\mathbf{a^P}$ expressing the disturbances as function of the state $\mathbf{x}$ (see Appendix A). Without control, the perturbations in Equation 2.39 will let a test spacecraft characterized by a generic nominal state $\mathbf{x_n} = [a_{GEO}, 60° E, 0°, 0, 0, 0]$, of mass $m = 3000\,kg$ and reflectivity area $A_s = 100\,m^2$, to drift from the assigned initial conditions, as shown in Figure 2.8.

$$\mathbf{a^P}(r, \lambda, \phi) = \mathbf{a^P_{grav}}(r, \lambda, \phi) + \mathbf{a^P_{3B}}(r, \lambda, \phi) + \mathbf{a^P_{SRP}}(r, \lambda, \phi) \tag{2.39}$$

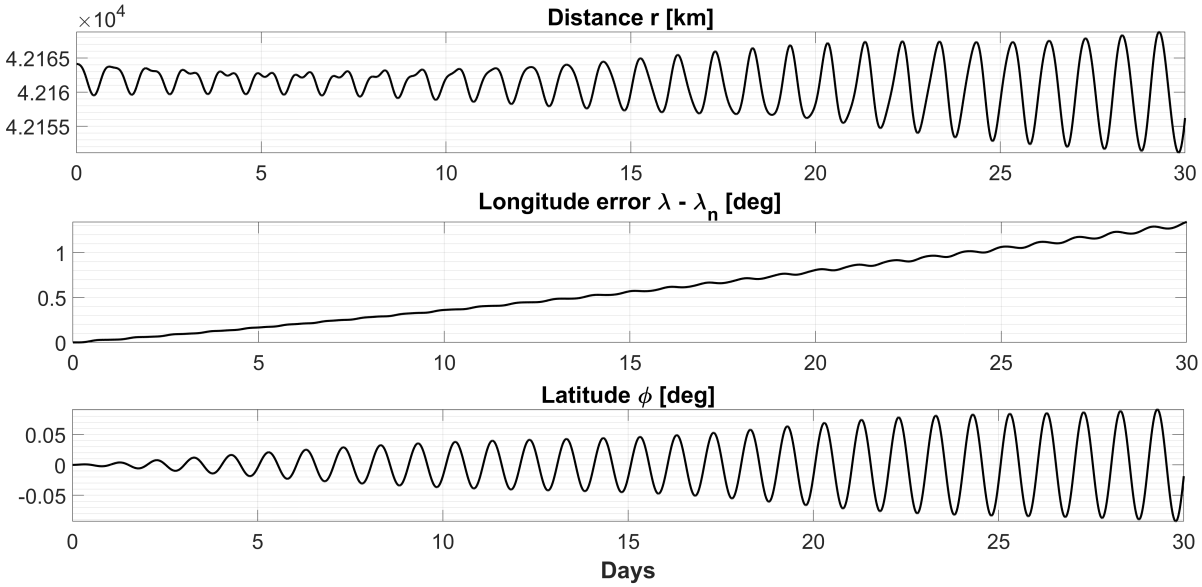

Figure 2.8: One month free-drift from $\lambda = 60° E$

Long time oscillations can be noticed for r and λ in a longer period, as can be seen in Figure 2.9. Secular periodicity for r is mainly due to the motion of the Sun, while the ones on λ are caused by the fact that, even if $\lambda_n = 60° E$ is not a stable point, as presented in Figure 2.6, the longitude drift towards East will bring the body above the stable longitude at $75.1° E$. This will cause an oscillation taking the spacecraft back to nominal longitude after two years. It is possible to highlight that, for this specific case, unless a control action, the vehicle will drift about $30°/year$ in longitude and about $0.85°/year$ in latitude, which is clearly unacceptable for a GEO satellite. The nearer to an unstable point, the higher the λ displacement is. The latitude drift, mainly due to the influence of the third bodies, is totally and always divergent in time.

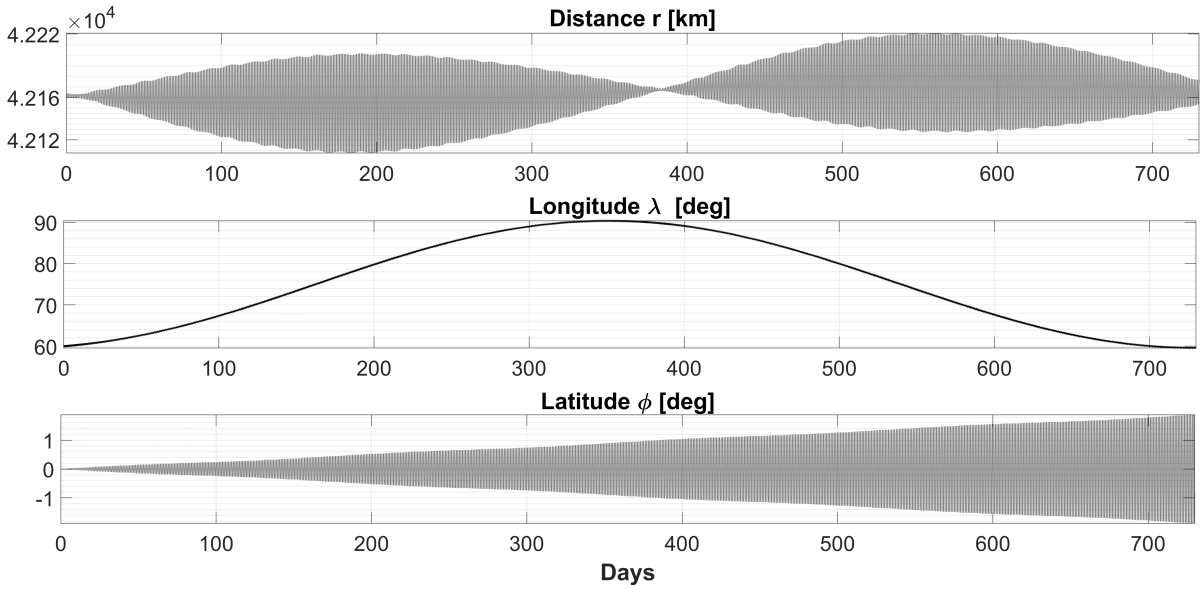

Figure 2.9: Two years free-drift from $\lambda = 60°$ E

The same spacecraft above a stable gravity condition at $\lambda_n = 75.1°$ E will remain confined in a quite small East-West region $[-2.5°, 2.5°]$. However, this still does not satisfy the longitude band requirements for a typical GEO station keeping problem.

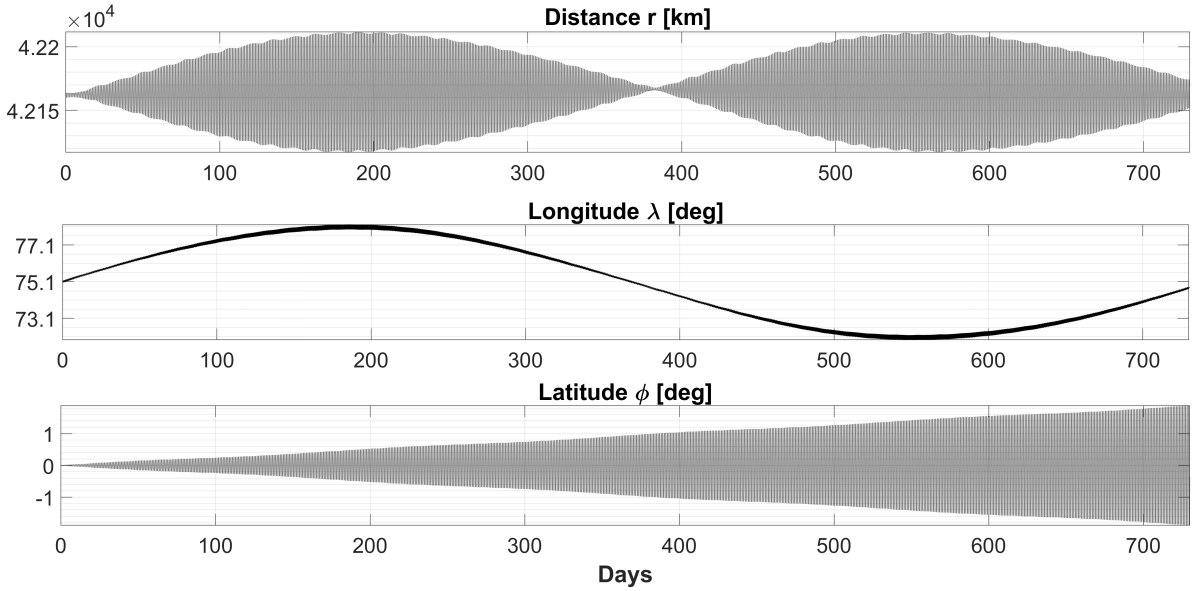

Figure 2.10: One year free-drift around stable point at $\lambda = 75.1°$ E

Further details can be found in Appendix A.

2.2. Control Fundamentals

An optimal control problem implies the determination of the control law (thrust magnitude and direction) while minimizing a certain performance index, such as the mass consumption, the transfer time or the energy and satisfying boundary constraints, path constraints or mid-point conditions. Since an analytic approach can not be selected for this kind of problems, numerical methods are usually adopted to find the optimal solution. Two main categories can be introduced: direct methods and indirect methods. The former rely on direct transcription method, through which the optimization is written as a non-linear programming problem. They are generally robust and can fulfill path constraints, but they require high computational burden. The latter have a small convergence radius and they are very sensitive to initial costates, but their convergence is much quicker with a good initial guess. Thanks to the calculus of variations the problem can be transformed and then solved as a Two-Point Boundary Value Problem (TPBVP). Indirect methods are used in this project.

2.2.1. Optimal Control

According to [17] and [22], defining a set of n first-order differential equations in the form

$$\dot{\mathbf{x}} = f(\mathbf{x}, \mathbf{u}, t) \tag{2.40}$$

where f is the dynamical flow, $\mathbf{x}(t)$ is a set of state variables, $\mathbf{u}(t)$ is the vector of control actions and $t = [t_0, t_f]$ represents the independent time variable, it is possible to define the performance index J as:

$$J = \phi(\mathbf{x}(t_f), t_f) + \int_{t_0}^{t_f} L(\mathbf{x}, \mathbf{u}, t)\, dt \tag{2.41}$$

satisfying the final boundary conditions as a q-dimensional vector:

$$\psi(\mathbf{x}(t_f), \mathbf{u}(t_f), t_f) = 0 \tag{2.42}$$

If ν is a q-dimensional vector of constant multipliers of the terminal constraints and $\mathbf{l}$ is a $\{n \times 1\}$ array of the costate variables multiplying the dynamics, the objective function can be augmented as:

$$\hat{J} = \phi(\mathbf{x}(t_f), t_f) + \nu^{\mathbf{T}}(\psi(\mathbf{x}(t_f), \mathbf{u}(t_f), t_f)) + \int_{t_0}^{t_f} [L(\mathbf{x}, \mathbf{u}, t) + \mathbf{l}^{\mathbf{T}}(f(\mathbf{x}, \mathbf{u}, t) - \dot{\mathbf{x}})]\, dt \quad (2.43)$$

The minimization of $\hat{J}$ is reached with the help of the calculus of variations by performing its gradient with respect to $\mathbf{x}, \mathbf{l}, \mathbf{u}$ and equating it to zero. A simplified notation is achieved introducing the Hamiltonian

$$H(\mathbf{x}, \mathbf{l}, \mathbf{u}, t) = L(\mathbf{x}, \mathbf{u}, t) + \mathbf{l}^{\mathbf{T}} f(\mathbf{x}, \mathbf{u}, t) \quad (2.44)$$

and imposing the first variation of the functional:

$$\begin{cases} \dfrac{\partial H}{\partial \mathbf{l}} = \dot{\mathbf{x}}, & \mathbf{x}(t_0) = \mathbf{x_0} \\ \dfrac{\partial H}{\partial \mathbf{x}} = -\dot{\mathbf{l}}^{\mathbf{T}}, & \mathbf{l}(t_f) = [\phi + \nu^{\mathbf{T}}\psi]_{t=t_f} \\ \dfrac{\partial H}{\partial \mathbf{u}} = 0 \end{cases} \quad (2.45)$$

The solution of the differential-algebraic systems representing the state and costate dynamics in the so called Euler-Lagrange equations 2.45 can be found through the solution of a TPBVP with $\mathbf{x}(t_0) = \mathbf{x_0}$ the assigned initial conditions. The derivative of H with respect to $\mathbf{u}$ is an application of the Pontryagin maximum principle thanks to which the control $u \in U$ is chosen to be an extreme of H at every instant of time. In this way the feasible control u belonging to a set of feasible actions U optimizes the Hamiltonian along the whole time span.

Analysing the case where the final state is also imposed, the set of Euler-Lagrange equations becomes:

$$\begin{cases} \dfrac{\partial H}{\partial \mathbf{l}} = \dot{\mathbf{x}}, & \mathbf{x}(t_0) = \mathbf{x_0} \ \cup \ \mathbf{x}(t_f) = \mathbf{x_f} \\ \dfrac{\partial H}{\partial \mathbf{x}} = -\dot{\mathbf{l}}^{\mathbf{T}} \\ \dfrac{\partial H}{\partial \mathbf{u}} = 0 \end{cases} \quad (2.46)$$

The solution of this set of equations is usually achieved using numerical iterative techniques such as a single shooting method, whose aim is to find the initial values of the costate in order to both find the optimal control laws and accomodate all the constraints.

This project requires the solution of two optimal control problems:

- an Energy Optimal Problem (EOP);
- a Fuel Optimal Problem (FOP).

As specifically shown in chapter 3 and chapter 4, the control laws assume different shapes, due to the distinct nature of constraints, objective functions and, as a consequence, of the Hamiltonians.

Once the control vector $\mathbf{u}$ is found, its contribution arises in the complete dynamics 2.22, that can be rewritten as:

$$\begin{cases} \dot{r} = v \\ \dot{\lambda} = \xi \\ \dot{\phi} = \eta \\ \dot{v} = -\dfrac{\mu_E}{r^2} + r\eta^2 + r(\xi + \omega_E)^2 \cos\phi^2 + a_r^p(r, \lambda, \phi) + u_r(t) \\ \dot{\xi} = 2\eta(\xi + \omega_E)\tan\phi - 2\dfrac{v}{r}(\xi + \omega_E) + \dfrac{1}{r\cos\phi} a_\lambda^p(r, \lambda, \phi) + \dfrac{1}{r\cos\phi} u_\lambda(t) \\ \dot{\eta} = -2\dfrac{v}{r}\eta - (\xi + \omega_E)^2 \sin\phi\cos\phi + \dfrac{1}{r} u_\phi(t) \end{cases} \tag{2.47}$$

2.2.2. Linear Control and State Transition Matrix

If a dynamical problem in the form 2.40 can be considered or approximated as a linear system, the control can be easily achieved. A linearized system in the neighborhood of an equilibrium point is obtained from a series expansion of the dynamics about that point, neglecting all the nonlinear terms. Through this method, a very immediate solution can be found with the application of the State Transition Matrix (STM). On the other hand, a linearized solution is very imprecise and its accuracy drops when dealing with high nonlinearities.

Defining the augmented state as a $\{2n \times 1\}$ vector $\mathbf{z} = [\mathbf{x}; \mathbf{l}]$, the evolution of $\mathbf{z}$ is provided by the dynamical flow as: $\dot{\mathbf{z}}(t) = f(\mathbf{z}, t)$. If a generic perturbation $\delta\mathbf{z}$ occurs, the dynamics is now indicated by:

$$\dot{\mathbf{z}}(t) + \dot{\delta}\mathbf{z}(t) = f(\mathbf{z} + \delta\mathbf{z}, t) \tag{2.48}$$

Supposing to have a reference $\tilde{\mathbf{z}}$, in the case of a displaced trajectory flying close to the baseline, a linearization of the perturbed ODEs 2.48 can be performed as a Taylor 1^{st}

order expansion of the flow about the target:

$$\dot{\tilde{\mathbf{z}}}(t) + \dot{\delta}\mathbf{z} = f(\tilde{\mathbf{z}} + \delta\mathbf{z}, t) \simeq f(\tilde{\mathbf{z}}, t) + \left.\frac{\partial f(\mathbf{z}, t)}{\partial \mathbf{z}}\right|_{z=\tilde{z}} \delta\mathbf{z} \tag{2.49}$$

and so it is possible to express the evolution of the deviation, introducing $\hat{\mathbf{A}}(t)$:

$$\dot{\delta}\mathbf{z}(t) = \hat{\mathbf{A}}(t)\delta\mathbf{z}(t) \tag{2.50}$$

The derivative of f with respect to $\mathbf{z}$ is the Jacobian of the flow itself consisting of a $\{2n \times 2n\}$ array called *augmented state matrix* $\hat{\mathbf{A}}(t)$. The STM is defined by:

$$STM = \mathbf{\Phi}(t_0, t) \tag{2.51}$$

such that the generic perturbation of $\mathbf{z}$ at time t can be expressed as a function of the initial one $\delta\mathbf{z_0}(t_0)$:

$$\delta\mathbf{z} = \mathbf{\Phi}(t_0, t)\delta\mathbf{z_0} \tag{2.52}$$

Thanks to the variational approach, the evolution of the STM (see Appendix B) is achieved by integrating the following initial value problem (IVP), made of $2n(2n+1)$ equations:

$$\begin{cases} \dot{\mathbf{z}}(t) = f(\mathbf{z}, t), & \mathbf{z}(t_0) = \mathbf{z_0} \\ \dot{\mathbf{\Phi}}(t_0, t) = \hat{\mathbf{A}}(t)\mathbf{\Phi}(t_0, t), & \mathbf{\Phi}(t_0, t_0) = \mathbf{I} \end{cases} \tag{2.53}$$

The application of the STM to the optimal control problem is straightforward. The solution of a TPBVP like 2.46 can be obtained by considering a linearization about a reference solution and a perturbation of the state $\mathbf{x_0}$. The optimal control problem consists in finding the variation, caused by the starting disturbance, of the initial costates with respect to the reference ones, in order to match all the constraints. The linearized control law is then attained expanding the IVP 2.53 from t_0 to t_f and then imposing the desired final displacement $\delta\mathbf{x_f}$ compared to the reference. This is achieved writing the final STM in partitioned form (see Appendix B) and inverting it as:

$$\begin{Bmatrix} \delta\mathbf{x_f} \\ \delta\mathbf{l_f} \end{Bmatrix} = \begin{bmatrix} \mathbf{\Phi_{xx}} & \mathbf{\Phi_{xl}} \\ \mathbf{\Phi_{lx}} & \mathbf{\Phi_{ll}} \end{bmatrix}_{t=t_f} \begin{Bmatrix} \delta\mathbf{x_0} \\ \delta\mathbf{l_0} \end{Bmatrix} \tag{2.54}$$

$$\delta \mathbf{l_0} = \mathbf{\Phi_{xl}^{-1}}[\delta \mathbf{x_f} - \mathbf{\Phi_{xx}} \delta \mathbf{x_0}] \tag{2.55}$$

2.2.3. High Order Control with DA

With the aim of tackling nonlinearities and increase the accuracy with respect to the linearized case, high order methods are taken into account in this thesis work. Differential algebraic techniques introduced in section 1.2 are useful to build up this kind of control problems. As an extension of the STM solution, suppose to deal with a dynamical TPBVP of this kind:

$$\begin{cases} \dot{\mathbf{x}} = f(\mathbf{x}, \mathbf{l}, t) \\ \dot{\mathbf{l}} = g(\mathbf{x}, \mathbf{l}, t) \end{cases} \tag{2.56}$$

subject to initial conditions $\mathbf{x}(t_0) = \bar{\mathbf{x}}_\mathbf{0}$ and imposed final state $\mathbf{x}(t_f) = \bar{\mathbf{x}}_\mathbf{f}$. As presented before, the control problem objective is to find the initial value of the costates $\mathbf{l_0}$ solving the TPBVP and matching all the constraints. If a reference $\bar{\mathbf{l}}_\mathbf{0}$ is available, the procedure is similar to the STM. Thanks to DA, an arbitrary order k Taylor series expansion of the solution of the optimal control problem with respect to initial and final state can be performed. The first step consists in initializing the state and the costate at time t_0 as DA variables:

$$\mathbf{x_0} = \bar{\mathbf{x}}_\mathbf{0} + \delta \mathbf{x_0} \tag{2.57a}$$

$$\mathbf{l_0} = \bar{\mathbf{l}}_\mathbf{0} + \delta \mathbf{l_0} \tag{2.57b}$$

Unlike the STM case, where the dependence of the final conditions on the initial state and costate values is expressed through the matrix Φ, now it is obtained in terms of high order polynomial maps (M). Using the techniques described in section 1.2, the solution at t_f is expanded as a k order polynomial with respect to the starting conditions, as in [12].

$$\begin{pmatrix} [\mathbf{x_f}] \\ [\mathbf{l_f}] \end{pmatrix} = \begin{pmatrix} \bar{\mathbf{x}}_\mathbf{f} + \delta \mathbf{x_f} \\ \bar{\mathbf{l}}_\mathbf{f} + \delta \mathbf{l_f} \end{pmatrix} = \begin{pmatrix} M_{\mathbf{x_f}} \\ M_{\mathbf{l_f}} \end{pmatrix} \begin{pmatrix} \delta \mathbf{x_0} \\ \delta \mathbf{l_0} \end{pmatrix} \tag{2.58}$$

Subtracting the constant parts:

$$\begin{pmatrix} \delta \mathbf{x_f} \\ \delta \mathbf{l_f} \end{pmatrix} = \begin{pmatrix} M_{\mathbf{x_f}} \\ M_{\mathbf{l_f}} \end{pmatrix} \begin{pmatrix} \delta \mathbf{x_0} \\ \delta \mathbf{l_0} \end{pmatrix} \tag{2.59}$$

and extracting the map for the final state, the following new relation can be built concatenating $M_{\mathbf{x_f}}$ with the identity map $I_{\mathbf{x_0}}$ related to the initial state variation:

$$\begin{pmatrix} \delta\mathbf{x_f} \\ \delta\mathbf{x_0} \end{pmatrix} = \begin{pmatrix} M_{\mathbf{x_f}} \\ I_{\mathbf{x_0}} \end{pmatrix} \begin{pmatrix} \delta\mathbf{x_0} \\ \delta\mathbf{l_0} \end{pmatrix} \tag{2.60}$$

By virtue of the polynomial inversion techniques:

$$\begin{pmatrix} \delta\mathbf{x_0} \\ \delta\mathbf{l_0} \end{pmatrix} = \begin{pmatrix} M_{\mathbf{x_f}} \\ I_{\mathbf{x_0}} \end{pmatrix}^{-1} \begin{pmatrix} \delta\mathbf{x_f} \\ \delta\mathbf{x_0} \end{pmatrix} \tag{2.61}$$

the initial costate displacement with respect to the reference, representing the optimal control law, can be finally found similarly to Equation 2.55, where the STM coincides with a 1^{st} order polynomial map:

$$\begin{aligned} \delta\mathbf{l_0} &= M_{\mathbf{l_0}}(\delta\mathbf{x_f}, \delta\mathbf{x_0}) \\ \mathbf{l_0} &= \overline{\mathbf{l}}_\mathbf{0} + \delta\mathbf{l_0} \end{aligned} \tag{2.62}$$

3 | Energy Optimal Station Keeping Design

This chapter goes deeply into the SK formulation and it covers the approach to find the solution of the energy optimal control problem. It is organized into three main topics: one concerns the overall strategy adopted and introduces the algorithm needed for the control targets search; the second one is about the EOP formulation and the implemented solutions; finally relevant results are shown at the end of the analysis.

3.1. SK Strategy and Target Selection

The station keeping problem formulation presented in this thesis work is made of a sequence of uncontrolled-controlled phases with the aim of maintaining a test spacecraft, whose parameters are collected in Table 3.1, within a certain longitude-latitude assigned box around its nominal state. The Free-Drift (FD) stage (see 2.1.5) starts from a specific point called $\mathbf{x_T} = [r_T, \lambda_T, \phi_T, v_T, \xi_T, \eta_T]$ and lasts as much as the vehicle remains inside the selected slot. Then the satellite is taken by the control action to a new target point $\mathbf{x'_T}$, from which it will be subject to the natural motion once again as long as it stays in the allowable λ and ϕ bands.

$\mathbf{m}\,[kg]$	$\mathbf{A_s}\,[m^2]$	$\mathbf{C_r}$	$\lambda_\mathbf{n}\,[deg]$	$\phi_\mathbf{n}\,[deg]$	$\mathbf{r_n}\,[km]$
3000	100	1.5	$60E$	0	42165.8

Table 3.1: Test satellite properties

In light of this approach, a procedure to determine the target states shall be individuated. Two main possibilities are taken into account, one is analytical, while the other is a numerical procedure.

3.1.1. Analytical Targets

Following [8], the objective states of the controlled tracks might be selected by exploiting the longitude drift caused by the geopotential perturbation. This E-W or W-E displacement mainly due to the zonal $J_{2,2}$ is tabulated (see Appendix A) for the values of possible nominal longitude. The λ evolution can be approximated as a ballistic motion:

$$\begin{cases} \ddot{\lambda}(t) = C = const \\ \lambda(t) = \frac{1}{2}Ct^2 + \dot{\lambda}(0)t + \lambda(0) \end{cases} \tag{3.1}$$

Acting on the distance r it is possible to control the longitude drift rate as:

$$\dot{\lambda} = -\frac{3}{2}\frac{\omega_E}{a_{GEO}}\Delta r \tag{3.2}$$

Calling δ the amplitude of the E-W band, the target longitude can be easily determined like:

$$\begin{cases} \lambda(0) = \lambda_n + \frac{\delta}{2} & C > 0 \\ \lambda(0) = \lambda_n - \frac{\delta}{2} & C < 0 \end{cases} \tag{3.3}$$

From Equation 3.1, $\dot{\lambda}(0)$ is given and, consequently, the target Δr. The complete procedure and analysis can be found in [8].

$$\dot{\lambda}(0) = -2sign(C)\sqrt{2C\delta} \quad \longrightarrow \quad \Delta r = -\frac{2}{3}\frac{a_{GEO}}{\omega_E}\dot{\lambda}(0) \tag{3.4}$$

Basically this strategy foresees the collocation of the spacecraft on the eastern extreme of the box if the geopotential main effect is a westward drift or on the western boundary in the other case. The target state of such a kind is typically: $\mathbf{x_T^{an}} = [r_{GEO} + \Delta r,\ \lambda(0),\ 0,\ 0, 0, 0]$.

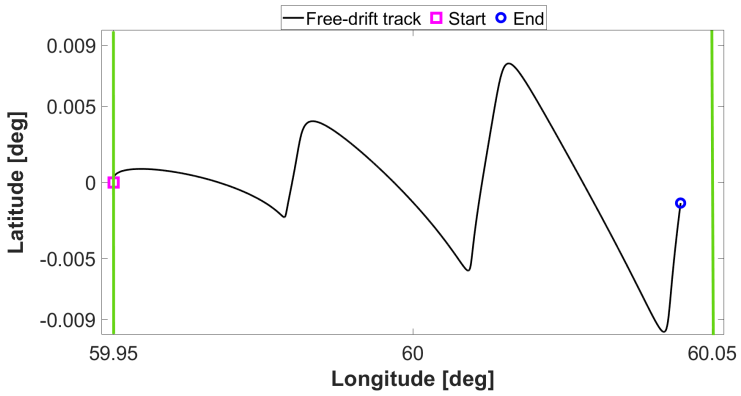

Figure 3.1: 3-days FD λ, ϕ trajectory from analytical target with all perturbations

It is a very intuitive, quick solution and provides the same time-independent target for every control cycle but, on the other hand it can not be considered a good approach. In fact, as previously introduced, many other perturbations affect the motion in addition to the 2,2 order zonal harmonics. These are time dependent and can possibly cause also an opposite drift, so they must be taken into account. Another reason which leads to search for another solution is founded on the fact that, as shown in Figure 3.1, in a E-W band of 0.1° around a nominal longitude of 60°E it takes the test satellite in Table 3.1 only about three days to drift freely from the western limit to the eastern one. This implies, during a longer time span, to have very frequent controlled phases and thus an increasing consumption.

3.1.2. Numerical Optimized Targets

With the purpose of building up a quasi-global optimization and reduce the control cycles to a minimum, a numerical procedure is implemented.

Exploiting the MATLAB® local optimizer *fmincon* and its nonlinear constraints, one can find a target state such that the uncontrolled phase starting from it will last a certain selected time and will be bound within the SK slot. Initializing $fmincon$ with the analytical target $\mathbf{x_T^{an}}$, passing an arbitrary FD duration to the optimizer and defining the objective function as the inverse of it, the output is the state that grants the residence of the satellite inside the allowed λ and ϕ bands for that period. The input time is the variable on which convergence depends: if it is too high, finding a target satisfying all the constraints will be very complicated.

A sort of *bisection* can be developed as follows:

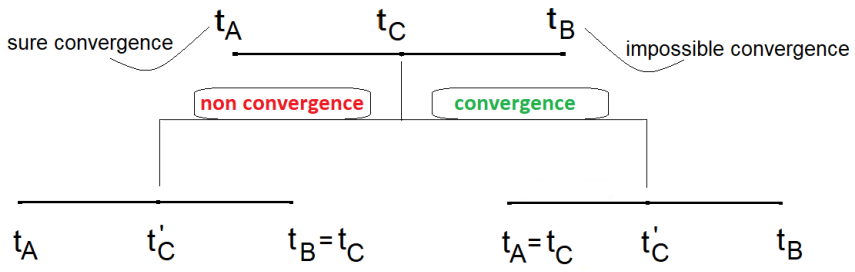

Figure 3.2: Bisection method on FD duration

1. after a trial and error phase, a long drift t_B is selected in order to avoid $fmincon$'s convergence to a feasible target. On the other hand, a short time t_A grants a quick solution;

2. t_c is defined as $(t_A + t_B)/2$;

3. $fmincon$ is performed in t_c;
4. a new interval is defined as in Figure 3.2, updating the extremes by looking at the $fmincon$ convergence in t_c and a new half time is defined as t_c';
5. the procedure is repeated until $t_B - t_A < 10'$

Since an *fmincon* optimization is performed at every time limit until *bisection* ends, the computational burden involved in this strategy is very high. However, at the end, the maximum FD term t_{FD}^{max} is found according to this procedure.
For a long time span analysis, the presented *bisection* shall be initialized at the epoch when the $k-$cycle is expected to begin, as shown in Algorithm 3.1. In fact, since the majority of the disturbances are time-dependent, the target $\mathbf{x_T}$ will be different at every loop, generating a $\{6 \times k\}$ matrix, as well as the t_{FD}^{max}, collected in $\{1 \times k\}$ vector.

Algorithm 3.1 Numerical Targets over a long period

Compute the $fmincon$ initial guess analytically: $\mathbf{x_0} = \mathbf{x_T^{an}}$;
Define t_A and t_B;
Set a fixed control duration $t_{CONTROL}$;
Initialize time at initial epoch: $time = t_0$;
Set an ending epoch: $t_{max} = t_0 + tspan$;
Initialize the index $k = 1$;
while $time < t_{max}$ **do**
    $[\mathbf{x_T}(:, \mathbf{k}), t_{FD}^{max}(k)] = bisection(time, t_A, t_B, \mathbf{x_0})$;
    $time = time + t_{FD}^{max}(k) + t_{CONTROL}$; $k = k + 1$;
end while

Through this approach, fixing *one*−day long control phases and considering *one*−year time span starting on January 1^{st}, 2023 at 00 : 00 : 00, fourteen control cycles only are needed to maintain the test spacecraft within a 0.1° E-W, 0.1° N-S bands. On the contrary, 104 control days shall be planned according to the analytical case and to the approximated dynamics just affected by the geopotential. The duration of the numerical FD stages are reported in Table 3.2, while the first two uncontrolled tracks are reported in Figure 3.3.

Cycle	0	1	2	3	4	5	6
FD [days]	20.689	26.296	26.012	25.979	25.942	25.131	25.673
Cycle	**7**	**8**	**9**	**10**	**11**	**12**	**13**
FD [days]	19.131	24.159	25.034	26.022	26.887	26.012	25.996

Table 3.2: FD phases duration in a year with optimized targets

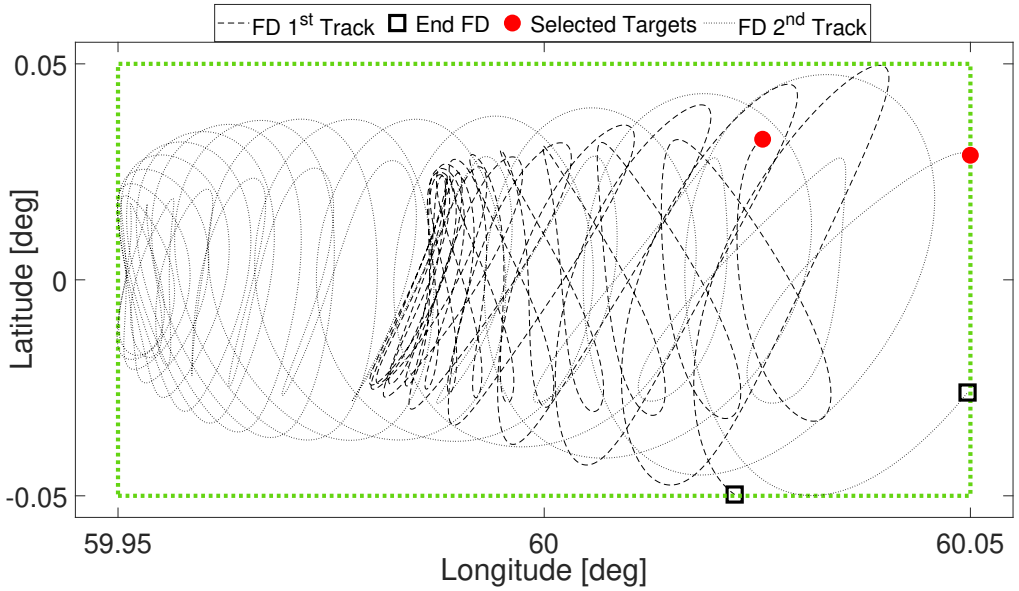

Figure 3.3: First two FD phases starting from the optimized targets ($\mathbf{x_T}$)

This sequence is run on ground and then its results can be loaded onboard, avoiding the optimization procedure in real time. After that, a control strategy able to quickly counteract any possible deviation with respect to this reference is needed, as presented later in this chapter. As an example of the typical numerical target state $\mathbf{x_T}$, the first one is reported:

$r_T^0\,[km]$	$\lambda_T^0\,[deg]$	$\phi_T^0\,[deg]$	$v_T^0\,[m\cdot s^{-1}]$	$\xi_T^0\,[deg\cdot s^{-1}]$	$\eta_T^0\,[deg\cdot s^{-1}]$
42168.50279	60.02562	0.03255	-0.13708	$-3.80160\cdot 10^{-7}$	$-4.17393\cdot 10^{-7}$

Table 3.3: First optimized target

3.2. Problem Formulation

The energy optimal control problem is defined in this section, according to 2.2.1. Given the dynamical system described by Equations 2.47, it can be rewritten introducing the matrix $\mathbf{B}(\mathbf{x})$, being $\mathbf{x} = [r, \lambda, \phi, v, \xi, \nu]$ the state and $\mathbf{u} = [0, 0, 0, u_r, u_\lambda, u_\phi]$ the control accelerations vector:

$$\dot{\mathbf{x}} = f(\mathbf{x}, \mathbf{u}, t) = \tilde{f}(\mathbf{x}, t) + \mathbf{B}(\mathbf{x})\mathbf{u} \tag{3.5}$$

where $\tilde{f}(\mathbf{x}, t)$ expresses the dynamics that does not depend on external commands. If $f(\mathbf{x}, \mathbf{u}, t)$ is the complete dynamical flow, it follows that (2.2.2):

$$\mathbf{A}(\mathbf{x}, \mathbf{u}, t) = \frac{\partial f(\mathbf{x}, \mathbf{u}, t)}{\partial \mathbf{x}} = \mathbf{A} \tag{3.6}$$

is the Jacobian of the state motion (see Appendix B).

The matrix $\mathbf{B}(\mathbf{x})$, in this case, is a $\{6 \times 1\}$ vector built from the Equations 2.47 as follows:

$$\mathbf{B}(\mathbf{x}) = \begin{bmatrix} 0 \\ 0 \\ 0 \\ 1 \\ \frac{1}{r\cos\phi} \\ \frac{1}{r} \end{bmatrix} = \mathbf{B} \tag{3.7}$$

Once selected the objective function that minimizes the energy:

$$J = \frac{1}{2}\int_{t_0}^{t_f} \mathbf{u}^\mathbf{T}\mathbf{u}\, dt \tag{3.8}$$

the TPBVP that solves the EOP is obtained through the gradient of the Hamiltonian

$$H = \frac{1}{2}\mathbf{u}^\mathbf{T}\mathbf{u} + \mathbf{l}^\mathbf{T}[\tilde{f}(\mathbf{x}, t) + \mathbf{B}(\mathbf{x})\mathbf{u}] \tag{3.9}$$

and the costate definition: $\mathbf{l} = [\mathbf{l_r}, \mathbf{l_v}] = [l_r, l_\lambda, l_\phi,\ l_v, l_\xi, l_\eta]$. It consists of the augmented dynamics of both the state $\mathbf{x}$ and the adjoint variables $\mathbf{l}$, subject to the initial reference $\mathbf{x_0}$ and the final target $\mathbf{x_T}$, as summarized in the Euler-Lagrange Equations 3.10.

$$\begin{cases} \dfrac{\partial H}{\partial \mathbf{l}} = \tilde{f}(\mathbf{x},t) + \mathbf{B}\mathbf{u} = \dot{\mathbf{x}} \\ \dfrac{\partial H}{\partial \mathbf{u}} = \mathbf{u}^{\mathbf{T}} + \mathbf{l}^{\mathbf{T}}\mathbf{B} \Rightarrow \mathbf{u}(\mathbf{l}) = -\mathbf{B}^{\mathbf{T}}\mathbf{l} \\ \dfrac{\partial H}{\partial \mathbf{x}} = -\dot{\mathbf{l}}^{\mathbf{T}} \Rightarrow \dot{\mathbf{l}} = -\left(\dfrac{\partial H}{\partial \mathbf{x}}\right)^{T} = -\left(\dfrac{\partial f(\mathbf{x},\mathbf{l},t)}{\partial \mathbf{x}}\right)^{T}\mathbf{l} = -\mathbf{A}^{\mathbf{T}}(\mathbf{x},\mathbf{l},t)\,\mathbf{l} = -\mathbf{A}^{\mathbf{T}}\mathbf{l} \\ \mathbf{x}(t_0) = \mathbf{x_0} \\ \mathbf{x}(t_f) = \mathbf{x_T} \end{cases} \tag{3.10}$$

The dynamical problem can be redefined introducing the augmented variable $\mathbf{z} = [\mathbf{x}, \mathbf{l}]$ and expressing the control $\mathbf{u}$ as function of $\mathbf{l}$:

$$\dot{\mathbf{z}} = \begin{Bmatrix} \dot{\mathbf{x}} \\ \dot{\mathbf{l}} \end{Bmatrix} = \begin{Bmatrix} \tilde{f}(\mathbf{x},t) - \mathbf{B}\mathbf{B}^{\mathbf{T}}\mathbf{l} \\ -\mathbf{A}^{\mathbf{T}}\mathbf{l} \end{Bmatrix} \tag{3.11}$$

Finally, the explicit TPBVP associated to an EOP in ECEF spherical coordinates and with boundary constraints only, is represented by the Equations 3.12.

$$\begin{cases} \dot{r} = v \\ \dot{\lambda} = \xi \\ \dot{\phi} = \eta \\ \dot{v} = -\dfrac{\mu_E}{r^2} + r\eta^2 + r(\xi+\omega_E)^2\cos\phi^2 + a_r^p(r,\lambda,\phi) + l_v \\ \dot{\xi} = 2\eta(\xi+\omega_E)\tan\phi - 2\dfrac{v}{r}(\xi+\omega_E) + \dfrac{1}{r\cos\phi}\,a_\lambda^p(r,\lambda,\phi) + \dfrac{1}{(r\cos\phi)^2}\,l_\xi \\ \dot{\eta} = -2\dfrac{v}{r}\eta - (\xi+\omega_E)^2\sin\phi\cos\phi + \dfrac{1}{r^2}\,a_\phi^p(r,\lambda,\phi) + \dfrac{1}{r^2}\,l_\eta \\ \dot{\mathbf{l}} = -\left(\dfrac{\partial f}{\partial \mathbf{x}}\right)^{T}\mathbf{l} \end{cases} \tag{3.12}$$

subject to $\mathbf{x}(t_0) = \mathbf{x_0}$ and $\mathbf{x}(t_f) = \mathbf{x_T}$.

3.3. EOP Solution

The solution of the energy optimal feedback control problem is achieved through different approaches. The first one is a numerical method that, in the case of the EOP, is used only as the *exact* controlled trajectory to be referred for comparison and validation. The DA techniques are then exploited to achieve the control law with a 2^{nd} order expansion. Last but not least, a splitted autonomous (time-independent) and non-autonomous problem is faced using both a DA expansion and the linear approximation with the STM.

All the methods rely on the same general idea: the SK assigned slot is viewed as a neighbourhood of the nominal state $\mathbf{x_n} = [r_{GEO}, \lambda_n, \phi_n, 0, 0, 0]$. Any sufficiently contained deviation from this reference can be considered as a perturbation $\delta\mathbf{x}$. Starting from the ballistic solution characterized by the initial costate $\mathbf{l_0}^{bal} = [0, 0, 0, 0, 0, 0]$, the flow can be expanded from the epoch t_{Ci}, when the control begins, to t_{Cf}, when it is switched off.

Then the boundary constraints on the final state are applied, together with an initial perturbation defined as $\delta\mathbf{x_0} = \mathbf{x_{Ci}} - \mathbf{x_n}$, where $\mathbf{x_{Ci}}$ contains the actual satellite position and velocity when the engines are turned on. The control law $\delta\mathbf{l_0}$ is given finding the optimal TPBVP 3.12 solution, with $\mathbf{x_0} = \mathbf{x_{Ci}} = \mathbf{x_n} + \delta\mathbf{x_0}$.

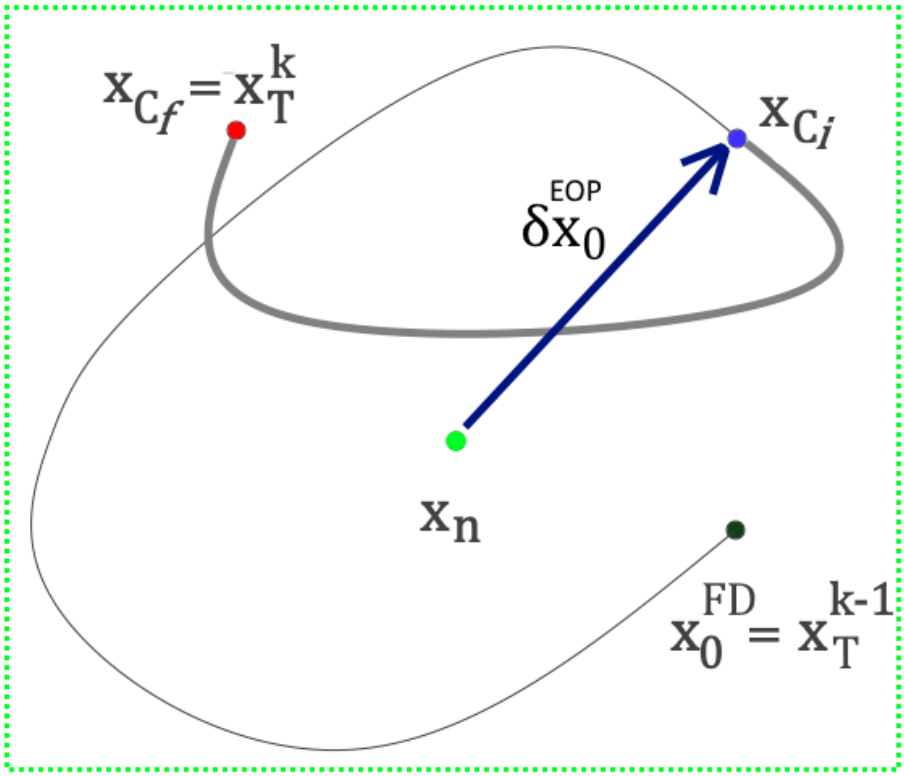

Figure 3.4: General EOP solution design in the neighbourhood of $\mathbf{x_n}$

In the specific case of the SK strategy adopted and presented in section 3.1, the procedure is the one shown in Figure 3.4. With reference to the k numerical targets previously determined in 3.1.2, the solution of a generic k cycle is obtained as follows:

1. compute the FD trajectory starting from the target point of the previous loop $\mathbf{x_T^{k-1}}$ and expanding the uncontrolled dynamics for t_{FD}^k;
2. integrate the TPBVP 3.10 from t_{Ci} to t_{Cf} with $\mathbf{z_0} = [\mathbf{x_n}; \mathbf{l_0}^{bal}]$;
3. impose the k target as final constraint: $\mathbf{x}(t_{Cf}) = \mathbf{x_T^k}$;
4. apply the initial perturbation $\delta\mathbf{x_0}$ and find the control law $\delta\mathbf{l_0}$.

3.3.1. Shooting Method

The numerical *exact* solution is achieved thanks to a single shooting method implemented in Python. Through the built-in solver of nonlinear equations systems $fsolve$, the required control is found by integrating the EOP TPBVP 3.12 as described and minimizing the displacement between the final expansion point and the current control target. The result is obtained iteratively by updating $\delta\mathbf{l_0}$ until the EOP is solved and the final constraints are met with a certain tolerance.

Since some loops are needed, this method is expected to be very precise but also quite computationally expensive. Moreover, the shooting technique must be performed every cycle and for every possible uncertainties of the initial or final coordinates. The shooting trajectory is used only for comparison with the approaches below.

3.3.2. High Order Solution with DA

By virtue of the Differential Algebra Computational Toolbox [16] (DACE) developed in a $C++$ language and its Python interface DACEyPy [20], the EOP is turned into the algebra of Taylor series and its solution is obtained through the mere evaluation of arbitrary order polynomials.
To do this, the next procedure has to be followed, referring to 2.2.3:

1. initialize DACE with the selected expansion order and the number of DA variables involved; in the EOP case they are 12 (6 describing the state and 6 for the costate);
2. erase the starting augmented state as a DA object $\mathbf{z_0} + \delta\mathbf{z_0}$, with $\mathbf{z_0} = [\mathbf{x_n}, \mathbf{l_0}^{bal}]$, thus the initial polynomial is defined;

3. expand the map from t_{Ci} to t_{Cf} with the DACE $RK78$ provided Python function and extract the last component, which expresses the final state dependence on the initial perturbations $\delta\mathbf{x_0} = \mathbf{x_{Ci}} - \mathbf{x_n}$ and $\delta\mathbf{l_0}$ (see Appendix B):

$$\begin{pmatrix} [\mathbf{x_f}] \\ [\mathbf{l_f}] \end{pmatrix} = \begin{pmatrix} \bar{\mathbf{x}}_\mathbf{f} + \delta\mathbf{x_f} \\ \bar{\mathbf{l}}_\mathbf{f} + \delta\mathbf{l_f} \end{pmatrix} = \begin{pmatrix} M_{\mathbf{x_f}} \\ M_{\mathbf{l_f}} \end{pmatrix} \begin{pmatrix} \delta\mathbf{x_0} \\ \delta\mathbf{l_0} \end{pmatrix} \tag{3.13}$$

4. build up the polynomial that imposes the final target constraint as:

$$C = [\mathbf{x_f}] - \mathbf{x_T} \tag{3.14}$$

5. take the Equation 2.61:

$$\begin{pmatrix} \delta\mathbf{x_0} \\ \delta\mathbf{l_0} \end{pmatrix} = \begin{pmatrix} M_{\mathbf{x_f}} \\ I_{\mathbf{x_0}} \end{pmatrix}^{-1} \begin{pmatrix} \delta\mathbf{x_f} \\ \delta\mathbf{x_0} \end{pmatrix} \tag{3.15}$$

evaluate it in $\delta\mathbf{x_0}$ and impose $\delta\mathbf{x_f}$ equal to the opposite of the constant part of C to enforce the final target and find the control law $\delta\mathbf{l_0}$.

This sequence has to be replicated for every control cycle, due to the time-dependence of the maps. The epoch shall be updated every loop and new polynomials are computed. However, in case of initial or final uncertainty, the solution is simply obtained by evaluating the current map with the new $\delta\mathbf{x_0}$, avoiding the repetition of the aforementioned workflow.

3.3.3. DA and STM Combination

As already introduced in [11], it is possible to separate the time-varying perturbations from the others and consider their motion effects individually. As presented in 2.1.4, the dynamics subject to the disturbance accelerations coming from the geopotential is called *autonomous* and it does not change with the epoch, while the one affected by the SRP, the Sun and the Moon influence is called *non-autonomous*.

The EOP can be solved taking advantage from this fact and combining the DA expansion with the STM. The first component consists in a 4^{th} order map of the autonomous problem expanded from t_{Ci} to t_{Cf} and then manipulated as detailed above; the other one is the solution of the complete motion thanks to the STM and can be interpreted as a linear correction to the former result.

The method is summarized below and developed for a year SK in Algorithm 3.2.

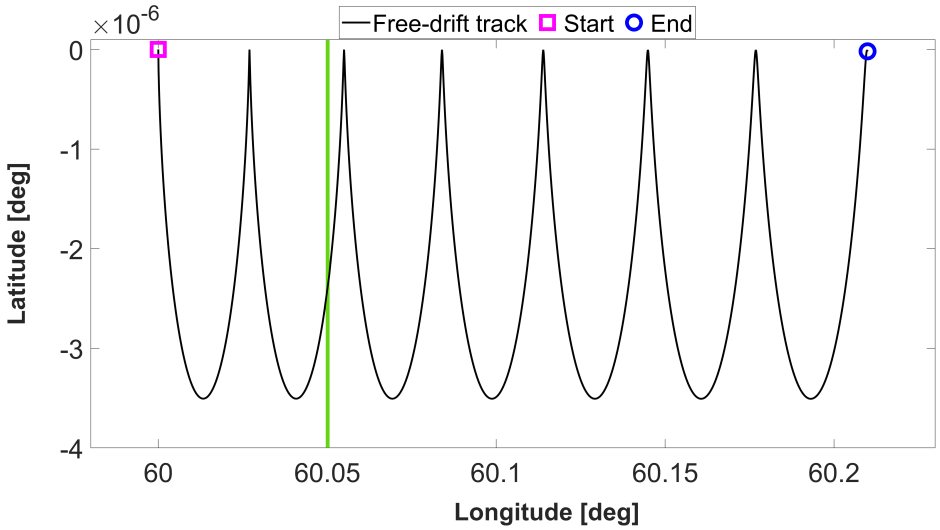

Figure 3.5: Autonomous one-week Free-Drift starting from $\mathbf{x_n}$

From the time-invariant polynomial describing the dynamics affected by the geopotential (GG):

$$\begin{pmatrix} \delta \mathbf{x_0} \\ \delta \mathbf{l_0}^{GG} \end{pmatrix} = \begin{pmatrix} M_{\mathbf{x_f}}^{GG} \\ I_{\mathbf{x_0}} \end{pmatrix}^{-1} \begin{pmatrix} \delta \mathbf{x_f} \\ \delta \mathbf{x_0} \end{pmatrix} \tag{3.16}$$

the autonomous control law $\delta \mathbf{l_0}^{GG}$ is found, applying the initial displacement $\delta \mathbf{x_0} = \mathbf{x_{Ci}} - \mathbf{x_n}$ and the final one as in 3.15.

$$\mathbf{l_0}^{GG} = \mathbf{l_0}^{bal} + \delta \mathbf{l_0}^{GG} = \mathbf{0} + \delta \mathbf{l_0}^{GG} = \delta \mathbf{l_0}^{GG} \tag{3.17}$$

Then, the STM must be integrated together with the flow from t_{Ci} to t_{Cf} to obtain the linear (L) final state $\mathbf{x_f}^L$ as (see Appendix B):

$$\begin{cases} \dot{\mathbf{z}}(t) = f(\mathbf{z}, t), & \mathbf{z}(t_0) = [\mathbf{x_n}, \mathbf{l_0}^{GG}] \\ \dot{\mathbf{\Phi}}(t_0, t) = \hat{\mathbf{A}}(t)\mathbf{\Phi}(t_0, t), & \mathbf{\Phi}(t_0, t_0) = \mathbf{I} \end{cases} \tag{3.18}$$

Consequently, the 1^{st} order feedback of the overall (autonomous and non-autonomous) motion is given by:

$$\begin{Bmatrix} \delta\mathbf{x_f}^L \\ \delta\mathbf{l_f}^L \end{Bmatrix} = \begin{bmatrix} \mathbf{\Phi_{xx}} & \mathbf{\Phi_{xl}} \\ \mathbf{\Phi_{lx}} & \mathbf{\Phi_{ll}} \end{bmatrix}_{t=t_{Cf}} \begin{Bmatrix} \delta\mathbf{x_0}^L \\ \delta\mathbf{l_0}^L \end{Bmatrix} \tag{3.19}$$

$$\delta\mathbf{l_0}^L = \mathbf{\Phi_{xl}^{-1}}[\delta\mathbf{x_f}^L - \mathbf{\Phi_{xx}}\delta\mathbf{x_0}^L] \tag{3.20}$$

with $\delta\mathbf{x_f}^L = \mathbf{x_T} - \mathbf{x_f}^L$ and $\delta\mathbf{x_0}^L = \delta\mathbf{x_0}$.

Summing up the two contributions, the final control action is:

$$\mathbf{l_0} = \mathbf{l_0}^{GG} + \delta\mathbf{l_0}^L \tag{3.21}$$

The main benefit of this strategy is the low computational burden. In fact, the GG 4^{th} order map is fixed in time and so the autonomous control law is generated by the simple and immediate evaluation of it at the current SK cycle. The STM shall be integrated every loop, but this process is expected to be very quick. The drawback is the lack of precision with respect to high order complete expansions or numerical methods. The longer is the $[t_{Ci}, t_{Cf}]$ span, the higher is the influence of the linear term and the so the target matching error.

Algorithm 3.2 DA and STM combination strategy over a year. Part 1

1: **Setup**
2: Initialize DACE: $(4^{th} order, 12\, variables)$;
3: Initialize time at initial epoch: $time = t_0$;
4: Set a fixed control duration: t_C;
5: Extract the number of numerical targets (3.1.2) in a year: k_{max} ;
6: Initialize FD augmented state: $\mathbf{z_0}^{FD} = [\mathbf{x_T}^0, \mathbf{0}]$;
7: Initialize control augmented state: $\mathbf{z_0}^C = [\mathbf{x_n}, \mathbf{l_0}^{bal}]$;
8: **Expand Autonomous Map**
9: Obtain final time-invariant map with DACE $RK78$ propagator:
$[\mathbf{z_f}^{GG}] = RK78(\mathbf{z_0}^C, 0, t_C, @AutonomousDynamics)$

Algorithm 3.3 DA and STM combination strategy over a year. Part 2

for $i = 1 : k_{max}$ **do**
  Expand FD flow with an ODE propagator:
  $\mathbf{x_{Ci}} = FreeDriftPropag(\mathbf{z_0}^{FD}, t_{FD}^{i-1})$;
  Autonomous Control Law
  Extract the map: $[\mathbf{x_f}^{GG}] = [\mathbf{z_f}^{GG}][:6]$;
  Compute the map for the final constraint: $C^{GG} = [\mathbf{x_f}^{GG}] - \mathbf{x_T}^{i}$;
  Define: $\delta\mathbf{x_0}^{GG} = \mathbf{x_{Ci}} - \mathbf{x_n}$;
  Extract the constant part of C^{GG} with DACE function *cons* and define: $\delta\mathbf{x_f}^{GG} = -C^{GG}.cons()$;
  Define the 6 *variables* identity map: $[I]$;
  Concatenate the final map with DACE function *concat*:
  $M = [\mathbf{x_f}^{GG}].concat([I])$;
  Invert it with DACE function *invert*:
  $M_{inv} = M.invert()$;
  Evaluate it with DACE function *eval* and compute:
  $\mathbf{l_0}^{GG} = M_{inv}.eval(\delta\mathbf{x_f}^{GG}, \delta\mathbf{x_0}^{GG})$;
  STM Linear Correction
  Initialize STM: $\mathbf{z_0}^{STM} = [\mathbf{x_n}, \mathbf{l_0}^{GG}]$; $\mathbf{\Phi_0} = \mathbf{I}$;
  Expand STM with an ODE propagator:
  $[\mathbf{x_f}^{L}, \mathbf{\Phi}(t_0, t_{Cf})] = STMpropag(\mathbf{z_0}^{STM}, \mathbf{\Phi_0}, t_C)$;
  Define: $\delta\mathbf{x_0}^{L} = \mathbf{x_{Ci}} - \mathbf{x_n}$;
  Define: $\delta\mathbf{x_f}^{L} = \mathbf{x_T}^{i} - \mathbf{x_f}^{L}$;
  Invert the final STM and find:
  $\delta\mathbf{l_0}^{L} = STMinversion(\mathbf{\Phi}(t_0, t_{Cf}), \delta\mathbf{x_f}^{L}, \delta\mathbf{x_0}^{L})$
  Overall control law: $\mathbf{l_0} = \mathbf{l_0}^{GG} + \delta\mathbf{l_0}^{L}$;
  Update for next Loop
  Propagate the controlled trajectory with an ODE propagator:
  $\mathbf{x_{Cf}} = ControlPropag([\mathbf{x_{Ci}}, \mathbf{l_0}], t_C)$;
  Update inital FD augmented state: $\mathbf{z_0}^{FD} = [\mathbf{x_{Cf}}, \mathbf{0}]$;
  Update epoch: $time = time + t_{FD}^{i-1} + t_C$;
end for

3.4. EOP Results and Analysis

The findings of the EOP strategies introduced are here reported. The simulations are about the test spacecraft already described in Table 3.1 and rely on the SK solution presented in section 3.1. The main analysis uses the numerical optimized targets searched within a λ and ϕ bands of $0.1°$ as in section 3.1.2, starting on January 1^{st}, 2023 at $00:00:00$, with the associated maximum FD duration and the fixed *one*-day long control phases.

In order to highlight the benefits and the drawbacks of DA techniques applied in this field, the results are presented as a comparison of the three approaches adopted:

- single shooting numerical method;
- 1^{st} (linear) and 2^{nd} order expansion with DA;
- 4^{th} order autonomous solution with complete linear corrections.

Great accuracy in target matching by the control actions means being sure to stay in the assigned SK slot for the next uncontrolled planned time. The larger the final error, the lower is the probability to meet the latitude and longitude requirements during the natural motion.
In the next figure the position and velocity deviations at each objective $\mathbf{x_T}$ are presented showing their order of magnitude in a logarithmic scale.

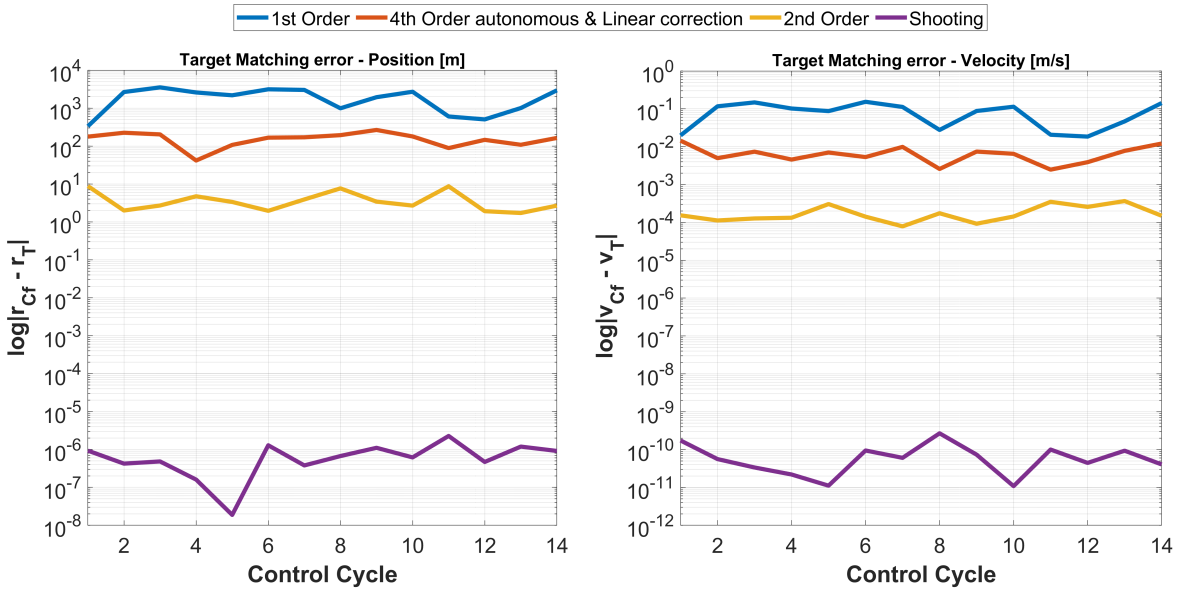

Figure 3.6: State error on target matching during every control cycle

Shooting Reference Solution

The most precise method is the numerical one. The single shooting grants important final bonds accomodation and so the SK conditions are well satisfied as represented in Figure 3.7.

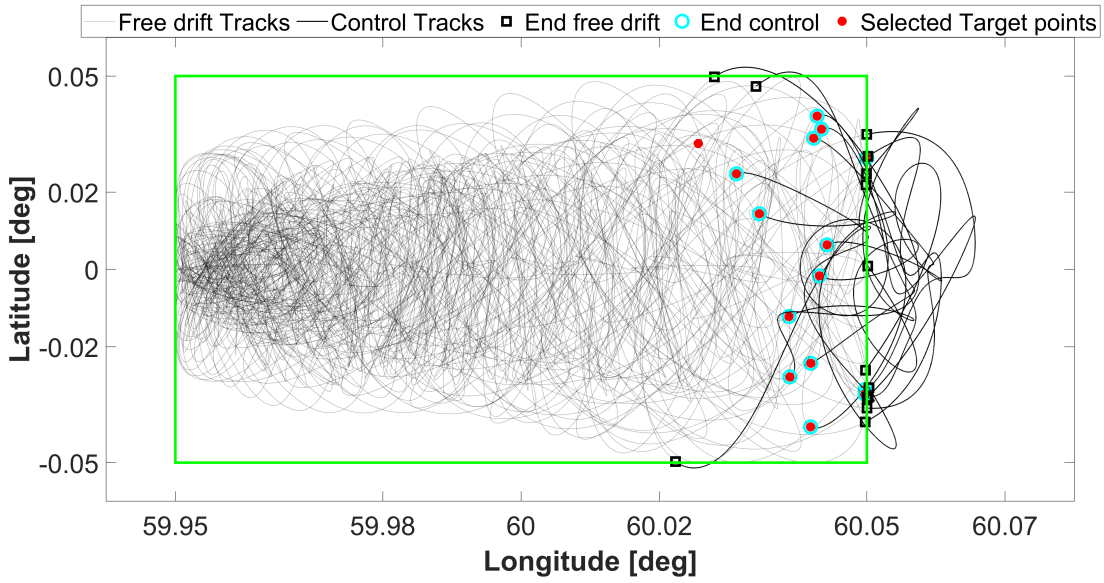

Figure 3.7: SK Box in a Year. Shooting Solution

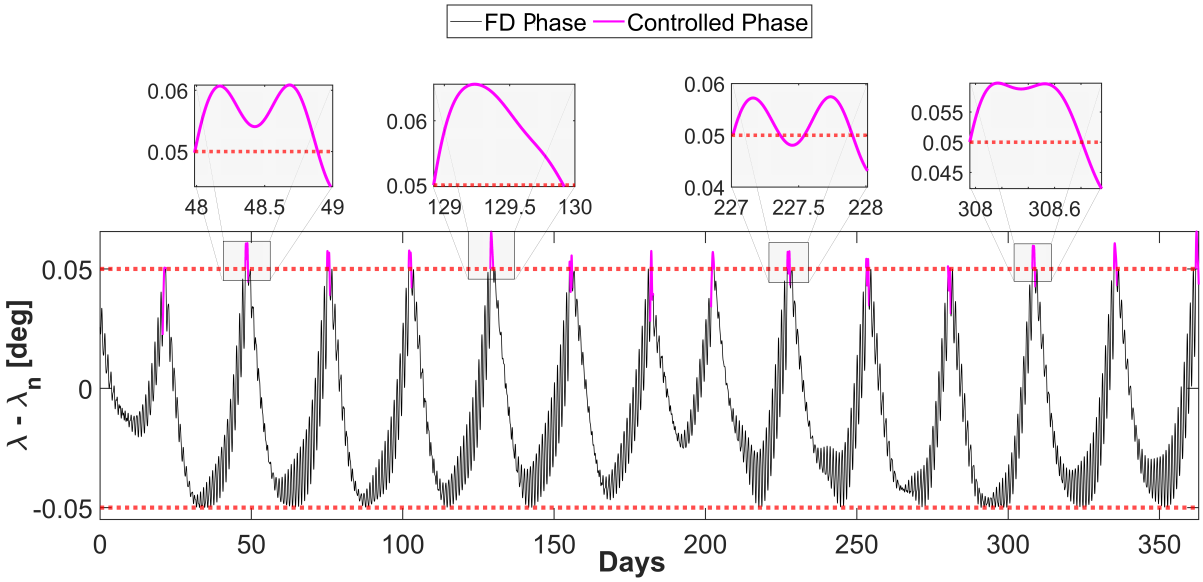

Figure 3.8: λ evolution over a Year. Shooting Solution

The box is slightly violated at the eastern border during the thrust arcs and this is due to the fact that no path constraints are imposed along these phases. However the time spent by the satellite outside its allowable region is very small and can be easily predicted by looking at the longitude evolution in Figure 3.8.

Figure 3.9 and Figure 3.10 complete the dynamics of the state for the whole time span. In particular, the first one shows the oscillations of the distance r around its nominal value of 42165.8 km and the admissible latitude fluctuations, while the other is about the barely undetectable velocity variations along the three directions.

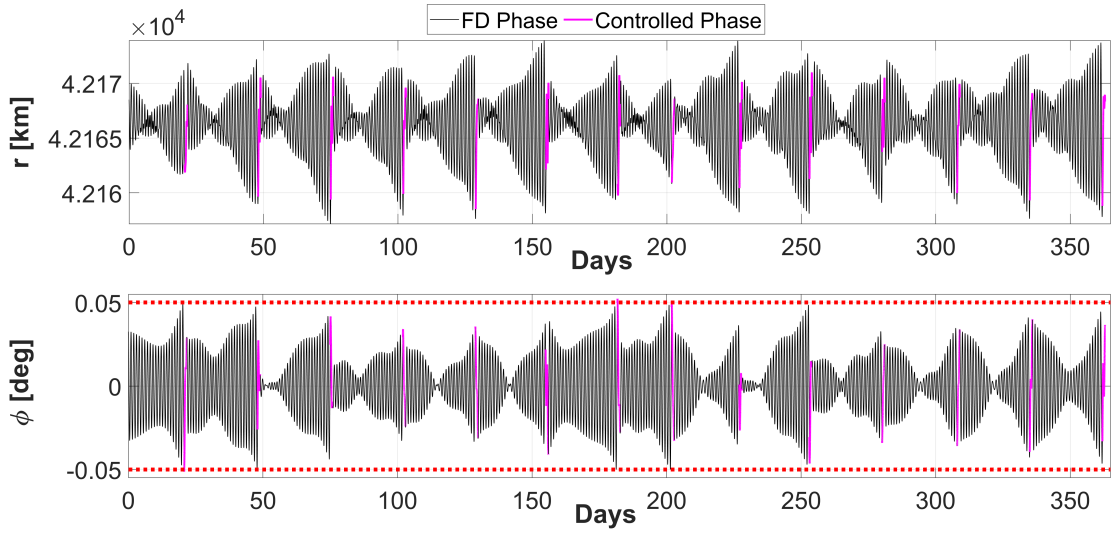

Figure 3.9: r and ϕ evolution over a Year. Shooting Solution

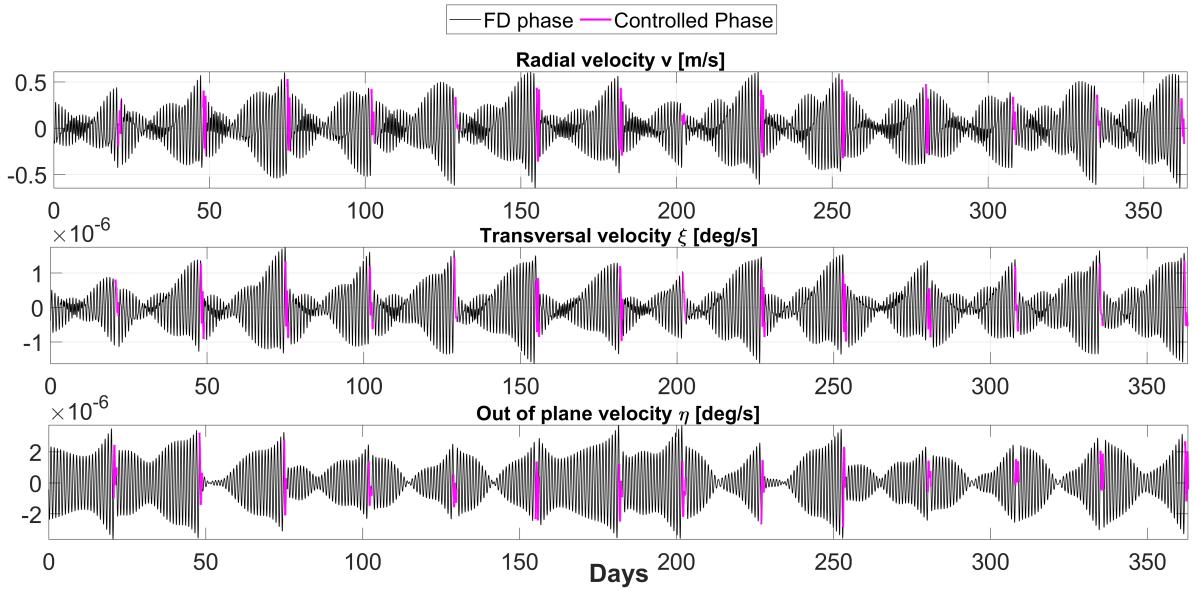

Figure 3.10: Velocities evolution over a Year. Shooting Solution

1 st Order Solution

The less accurate result is provided by the linear approach. It can be obtained by expanding the initial polynomial using DACE or through the integration of the actual STM. The second way avoids data allocation in the memory and it is computationally faster, providing the same result. All in all, what is found is clearly unacceptable for this strategy. As clearly explained by the next two charts, the SK requirements can not be satisfied.

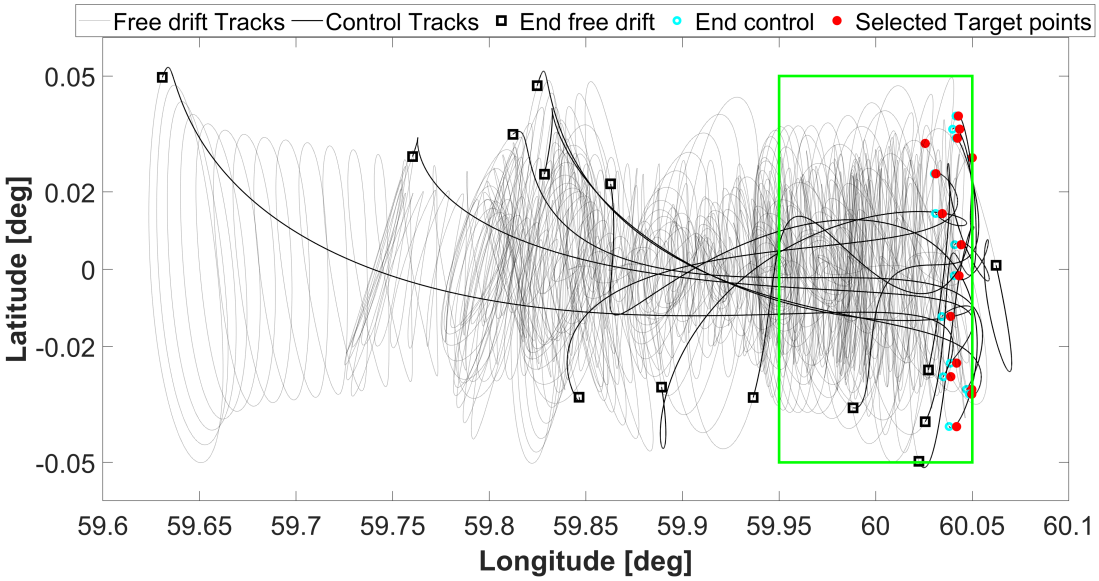

Figure 3.11: SK Box in a Year. Linear Solution

Since the targets are selected in order to maximize the permanence inside certain longitude and latitude bands, very few FD initial states are acceptable and, consequently, the final constraints matching tolerance is very low. With reference to Figure 3.6 the target error generated by a 1^{st} order control is too high, both in position and, mainly, in velocity. As a consequence, the FD trajectories that begin when the engines are shut down do not correspond to the ones expected by the optimization procedure in section 3.1.2. Figure 3.11 shows what happens: even if the feedback takes the satellite back inside the slot, the time spent outside is larger than the resident one. When nonlinearities grow, there is no possibility to keep the spacecraft inside its box with this solution.

The overall evolution of position coordinates is presented in Figure 3.12. Despite the acceptable behaviour of the latitude, the semi-major axis oscillations are too big, pushing the body $50\,km$ far from the geostationary orbit mean distance.

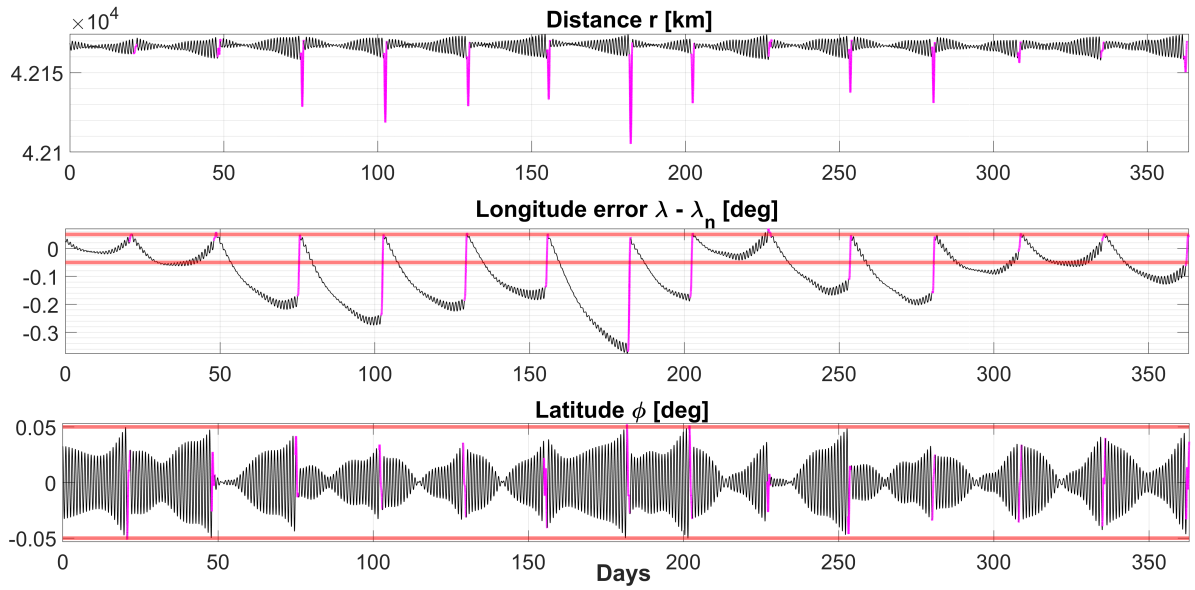

Figure 3.12: r, λ and ϕ evolution over a Year. Linear Solution

2 nd Order Solution

Thanks to DA it is possible to solve this issue. As presented before, differential algebraic techniques enables to expand the dynamics at higher orders. Since the GEO problem is affected by small perturbations that do not vary too much in time, the nonlinearities are not cumbersome to counteract. According to this, a 2^{nd} order solution is enough to obtain the same SK provided by the single shooting method. The DA quadratic expansion result can be seen in the next two plots. One can easily notice that Figure 3.13 and Figure 3.14 represent the same dynamics set by the numerical method.

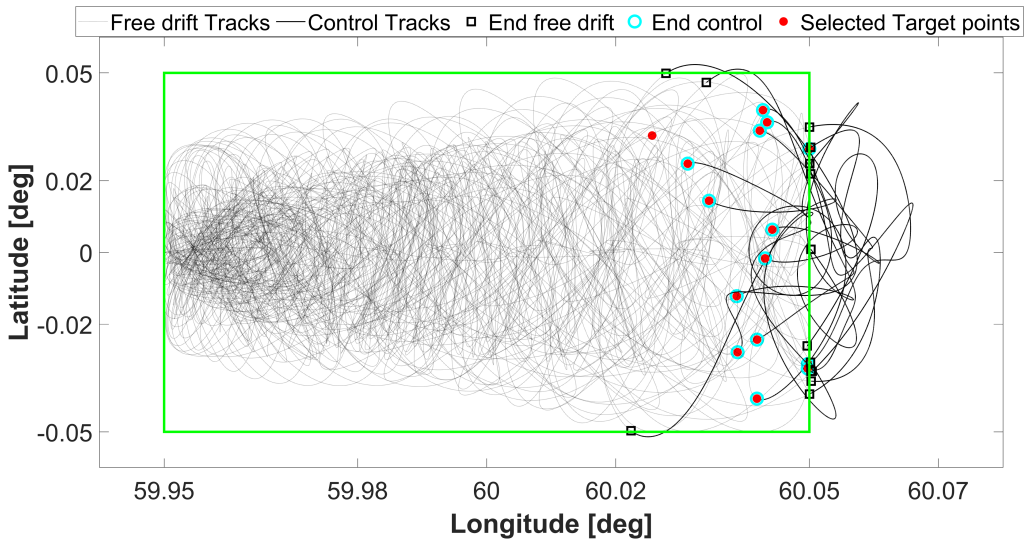

Figure 3.13: SK Box in a Year. 2^{nd} order Solution

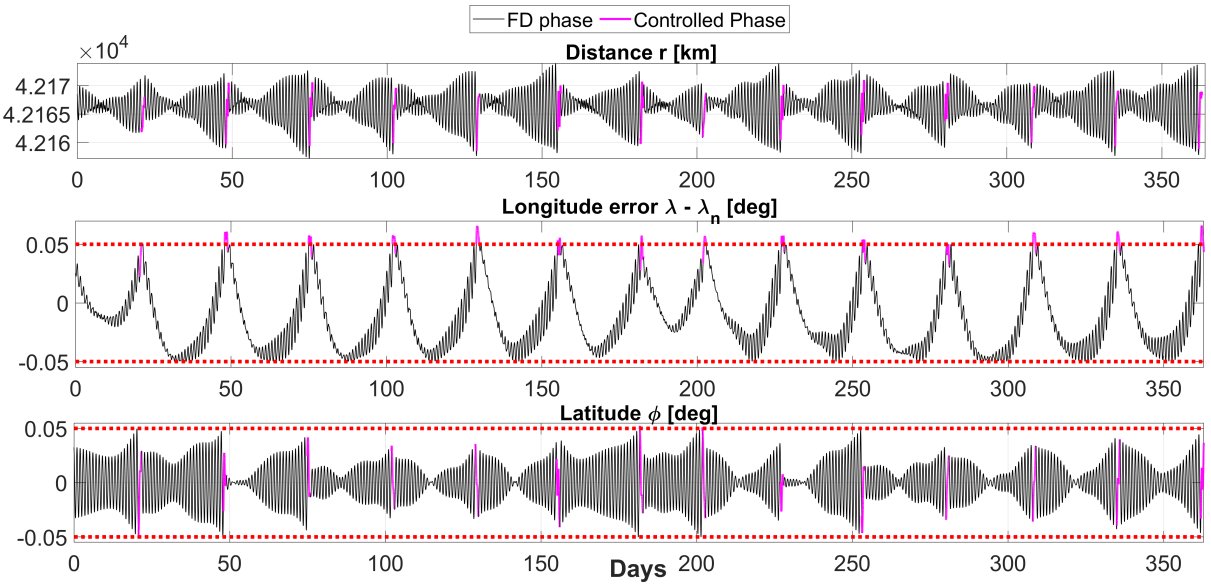

Figure 3.14: r, λ and ϕ evolution over a Year. 2^{nd} order Solution

DA and STM Combination Solution

The intermediate case corresponds to the splitted strategy in which autonomous and non-autonomous dynamics are treated separately. As said, a 4^{th} order DA expansion solves the first part and, then, it is corrected by the linear complete motion. The outcome is the one provided by Figure 3.15. It is clear how the 1^{st} order component influences the evolution. In fact, in addition to the lack of path constraints during the control phases on the eastern side, the slot is infringed by approximately 0.025° also on the western edge.

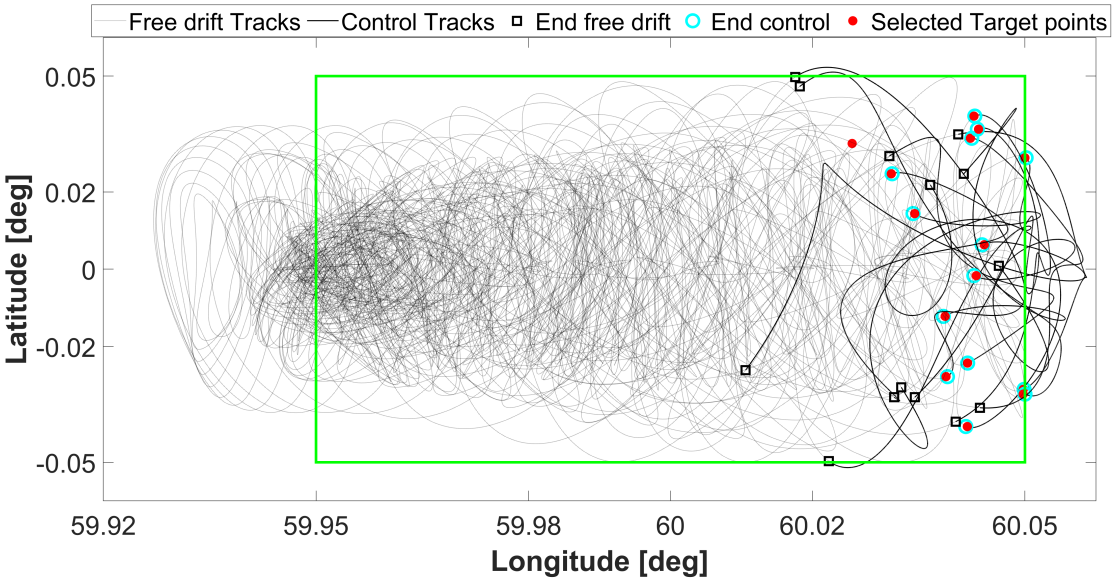

Figure 3.15: SK Box in a Year. 4^{th} order Autonomous expansion and Linear Correction

Anyway, this can be considered a good solution for five main reasons:

1. the error is contained and, as shown in Figure 3.16, characterizes only few cycles and for a short, predictable, period of time;
2. the other two position coordinates remain well bounded around their nominal values, as in Figure 3.17;
3. One can think to rely on the 2^{nd} order expansion when nonlinearities are big and on this approach when it is acceptable;
4. it involves the advantages of the DA approach, since the autonomous map loaded onboard and the STM can be evaluated whenever it is needed in order to counteract possible uncertainties, and the very low computational burden typical of 1^{st} order techniques.
5. since the failure is small compared to the linear issues, this problem can be faced by reducing the control duration or giving a different interpretation, as detailed later.

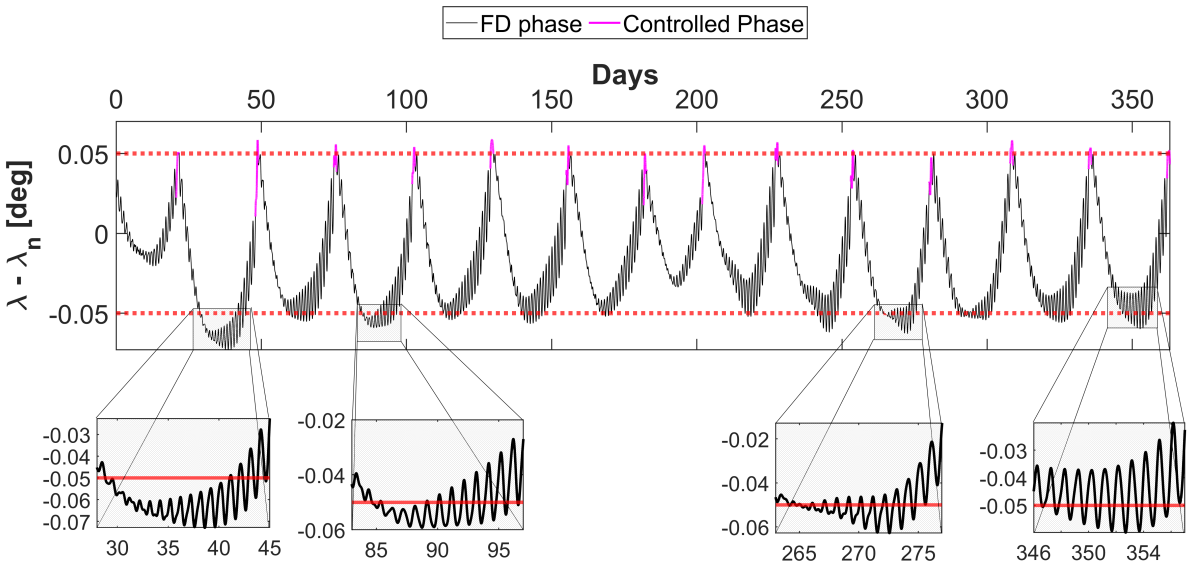

Figure 3.16: λ in a Year. 4^{th} order Autonomous expansion and Linear Correction

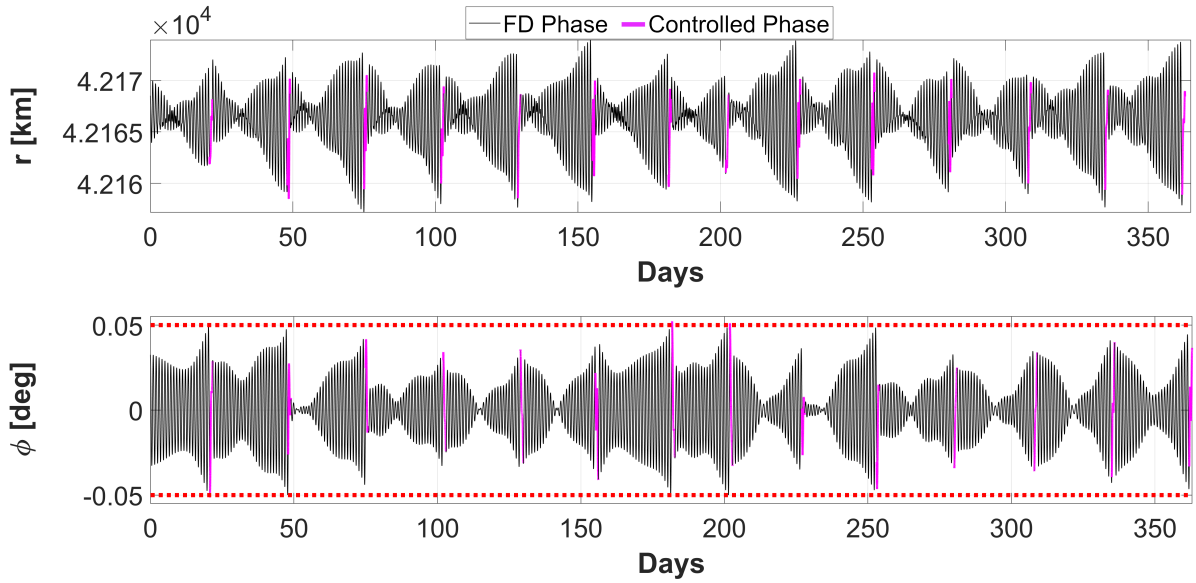

Figure 3.17: r and ϕ in a Year. 4^{th} order Autonomous expansion and Linear Correction

3.4.1. Computational Cost

Figure 3.18 indicates the onboard burden required every cycle by the three different solutions: the single shooting reference, the 2^{nd} order DA expansion and the one obtained combining DA and STM.

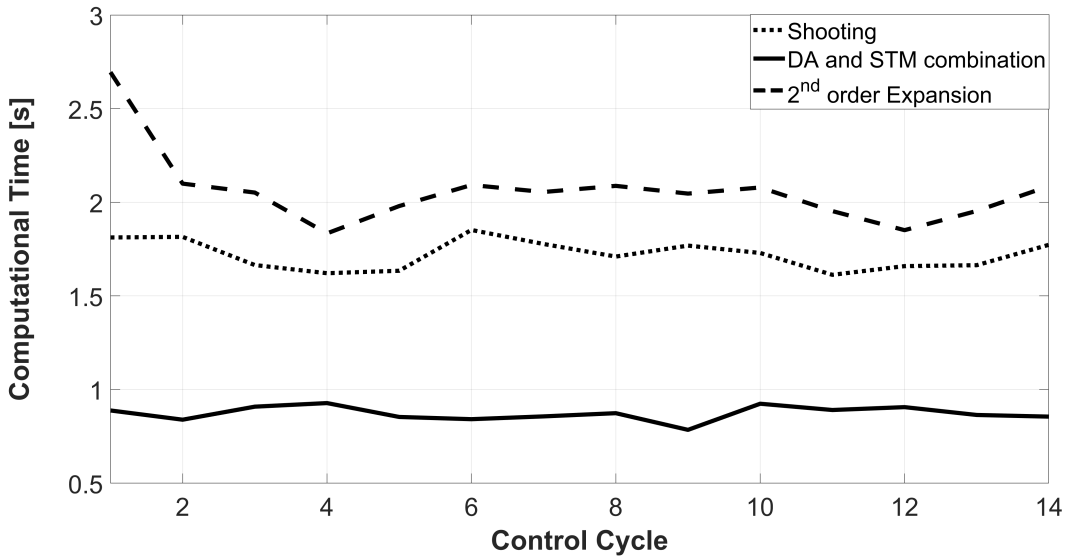

Figure 3.18: Computational Times for the adopted methods

This analysis is performed using Python on an Intel Core i7-1065G7 1.50 GHz, running Windows 11 Home 64 bit, 16 GB RAM.

To deal with acceptable run periods, the problem is adimensionalized. Times and distances are scaled such that the mean motion of the satellite on the orbit becomes unitary. In order to have:

$$\omega_{sat} = \frac{2\pi}{T_E} = \sqrt{\frac{\mu_E}{a_{GEO}^3}} = 1 \tag{3.22}$$

the adimensional units L and T must be, respectively:

$$L = a_{GEO}, \qquad T = \sqrt{\frac{L^3}{\mu_E}} \tag{3.23}$$

This gives the dimensionless dynamics (ad). To return back at the dimensional (d) problem, the following rescaling has to be taken into account:

$$\mathbf{z^{(d)}} = [\mathbf{x^{(d)}}, \mathbf{l^{(d)}}] = \mathbf{z^{(ad)}} \left[L,\ 1,\ 1,\ \frac{L}{T}, \frac{1}{T}, \frac{1}{T},\quad \frac{L}{T^3}, \frac{L^2}{T^3}, \frac{L^2}{T^3},\ \frac{L}{T^2}, \frac{L^2}{T^2}, \frac{L^2}{T^2} \right]^T \tag{3.24}$$

The most expensive approach is the 2^{nd} order polynomial expansion. Unfortunately, the map shall be computed every cycle since it is time dependent, but, on the other hand, if any further disturbance occurs, it is still valid and only an immediate evaluation is needed to update the control law for that SK loop. The combination between autonomous and non-autonomous dynamics is the fastest strategy. In fact, the time independent map is loaded onboard and remains the same, while its application, together with the STM integration and evaluation, takes less than one second by bit. Despite the lack of precision, this method shares the benefits of the DA polynomials and it is computationally cheap.

	Shooting	**2nd Order**	**DA and STM**
Cost$[s]$	24.0939	28.8635	12.2172

Table 3.4: Overall Computational Effort in a Year simulation

3.4.2. Control Profiles and Consumption

Once the dynamics is integrated on the whole time span, from the evolution of the costate $\mathbf{l}$, it is possible to obtain the control accelerations along the radial $\hat{r}$, transversal $\hat{\lambda}$ and out-of-plane $\hat{\phi}$ directions, thanks to the relation between $\mathbf{u}$ and $\mathbf{l}$ in Equation 3.10.

For the first SK cycle with *one*-day thrust duration, the shape of u_r, u_λ and u_ϕ is reported in Figure 3.19.

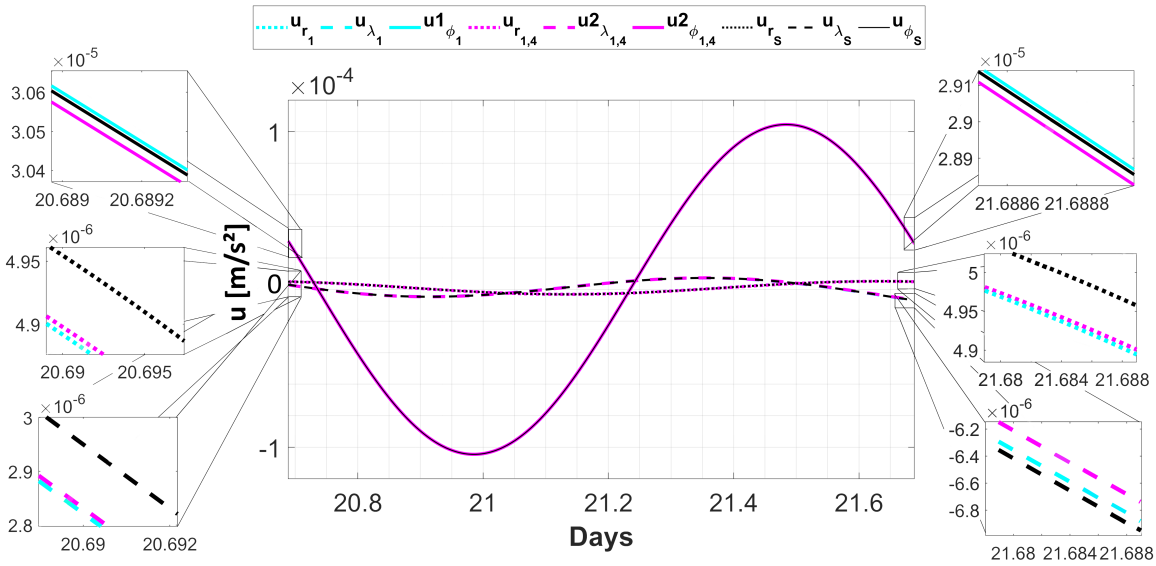

Figure 3.19: u_r, u_λ, u_ϕ evolution in a Cycle. Solution Comparison

The acceleration profiles characterizing the linear solution (1), the DA and STM combination one $(1,4)$ and the shooting method (s) are compared. Highlighting very small differences in the actions, they still cause relevant errors on the SK requirements, as described above.

The control acts mainly on the out-of-plane component and does not change too much from cycle to cycle. As shown in Figure 3.20, the intensity of the accelerations repeats similarly.

If the impulses are known, it is possible to compute the effective thrust as:

$$T = m|\mathbf{u}| \tag{3.25}$$

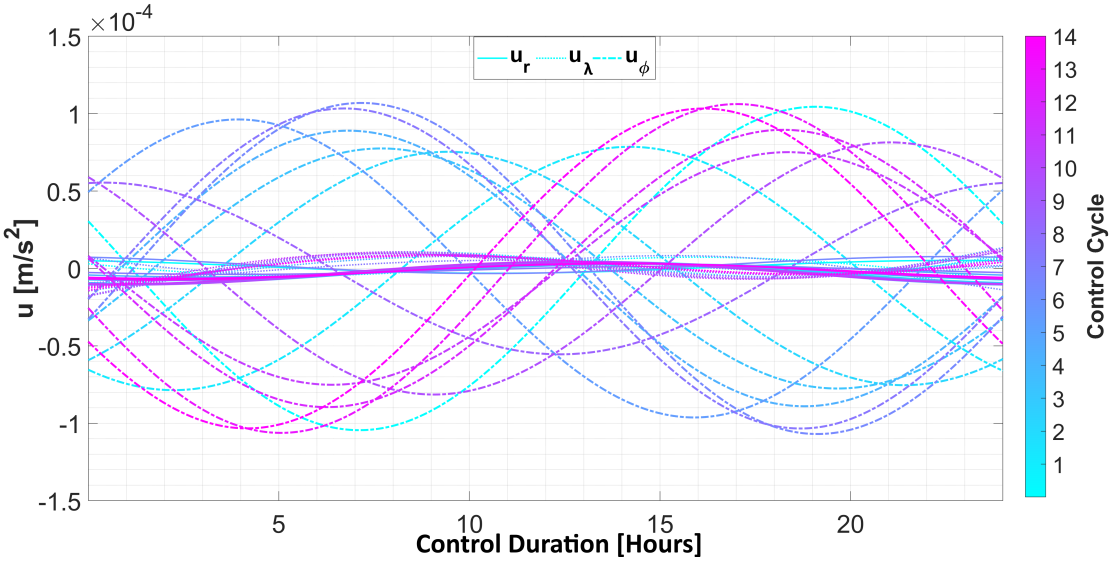

Figure 3.20: u_r, u_λ, u_ϕ evolution in a Year. Numerical Solution

The actual mass of the satellite m is obtained by integrating the linear ODE:

$$\dot{m} = -\frac{T_{max}}{I_{sp} g_0} |\mathbf{u}| \tag{3.26}$$

where I_{sp} is the specific impulse and g_0 the surface gravity. Considering an initial spacecraft mass of $3000\,kg$ and a specific impulse of $3800\,s$, the thrust profile is given by Figure 3.21, in which the force required during every *one*-day long powered phase is reported.

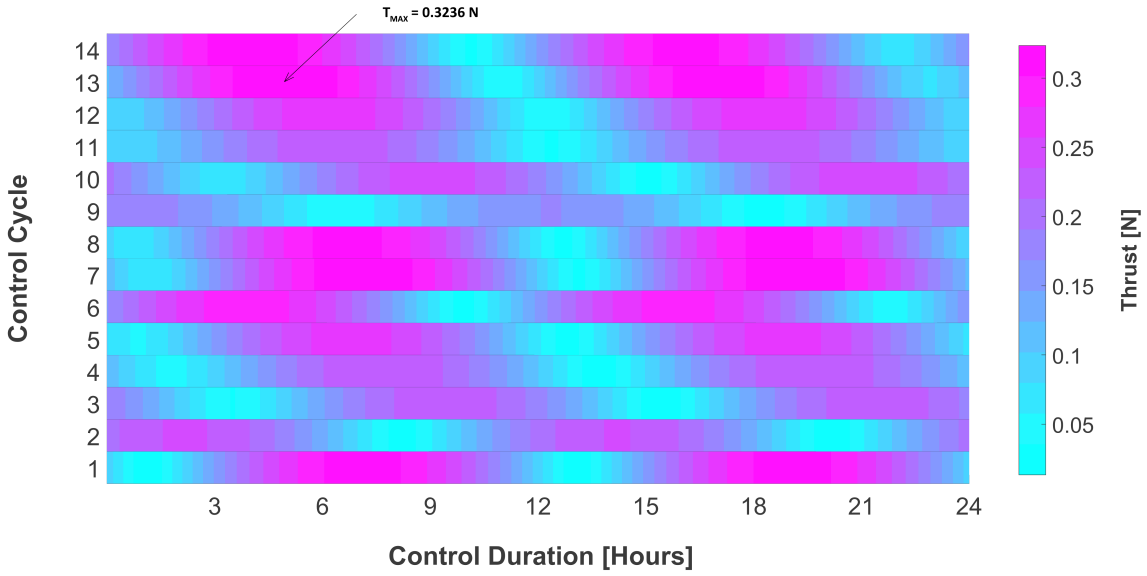

Figure 3.21: Continuous Thrust in a Year SK. *One*-day control duration. EOP

According to these parameters, the maximum value is $0.3236\,N$. Every further analysis shall deal with at least the same propulsion system characteristics.

The consumption is then calculated in terms of mass and velocity variation imposed to the spacecraft for each significant EOP solution.

The fuel burnt M_b is obtained by integrating Equation 3.26 from t_{Ci} to t_{Cf}, while the Δv is given by the Tsiolkovsky law:

$$\Delta v = -I_{sp}\, g_0\, \ln \frac{M_0 - M_b}{M_0} \tag{3.27}$$

Table 3.5 clearly shows that the higher the precision of the adopted method, the higher the optimality is. However, the difference in terms of propellant needed is very contained. The total amount is here reported, other detailed considerations are made in chapter 4.

	Shooting	**2nd Order**	**DA and STM**
$\mathbf{M_b}\,[kg]$	5.585843	5.759367	5.85788
$\mathbf{\Delta v}\,[m/s]$	69.403582	71.561659	72.786910

Table 3.5: Overall Consumption in a Year simulation. EOP

3.4.3. Dependence on Control Duration

An additional analysis is performed by changing the duration of the controlled trajectories. The longer these tracks, the higher is the error increment between a precise approach and a less accurate one. In the case of the splitted autonomous and non-autonomous solution, the target matching error causes a violation of the slot at the western side (Figure 3.15). It is immediate to notice in Figure 3.22 that for less prolonged thrusts, with respect to the *one*-day reference, the westward offset is very limited.

This leads to a different, reversed interpretation of the problem. The new aim is not about fulfilling specified SK requirements, rather find the realistic ones that can potentially be met through a particular strategy:

1. certain E-W and N-S bands are selected for the target optimization procedure;
2. a specific control solution and duration is choosen;

3. with the selected above parameters, the satisfied SK box is finally determined.

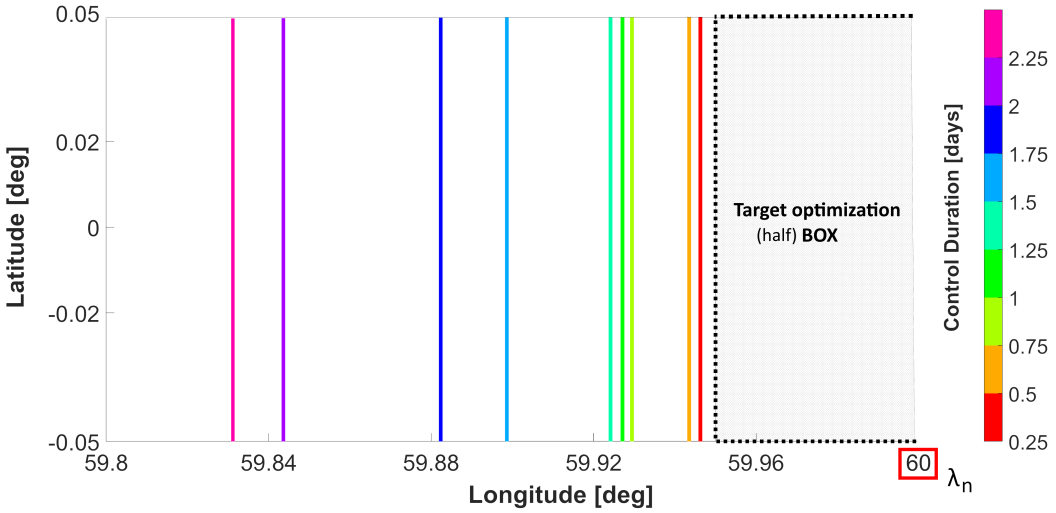

Figure 3.22: Westward Edge Shift depending on Control phases duration

In this specific case, for example, if the targets are searched in a 0.1° longitude and latitude bands, thanks to the autonomous 4^{th} order map linearly corrected approach and a 1.5 days powered phase, the prospective SK slot has a western bond at approximately 0.1° from the nominal longitude λ_n. If this shift wants to be reduced, three ways are available:

- choose a numerical method or at least a 2^{nd} order DA expansion;
- reduce the control length;
- shrink the E-W and N-S limits during the target optimization procedure by adopting a sort of *safety factor* and, consequently, reduce the free-drift times. The higher this margin, the less globally optimized the final solution is.

4 | Fuel Optimal Problem

The transformation from the energy optimal problem to the fuel optimal (FOP) one is proposed in this chapter. Due to its high sensitivity to initial conditions, it is solved sequentially after the EOP, whose results are taken as starting guesses for the FOP. The discussion of four main topics is included. First of all the problem is introduced and formulated, then its solution is designed with the aim of computing a numerical reference; afterward, DA techniques are developed for this particular case and are finally used to build up a robust control trajectory capable of counteracting potential uncertainties or additional perturbations. Relevant achievements are presented too.

4.1. Problem Formulation

The minimum fuel control problem is defined in this section, according to section 2.2.1.

Once the propulsion system has been characterized with I_{sp} the specific impulse and T_{max} the overall maximum available thrust as its two main parameters, the propellant consumption and, thus, the spacecraft mass variation, is expressed by the following 1^{st} order ODE:

$$\dot{m} = -\frac{T_{max}}{I_{sp} g_0} u \tag{4.1}$$

where u is a scalar representing the intensity of the control action and behaves as a throttle ranging from 0 to 1.

Following the EOP formulation in section 3.2, being the state $\hat{\mathbf{x}} = [\mathbf{x}, m] = [\mathbf{r},\ \mathbf{v}, m] = [r,\ \lambda,\ \phi,\ v,\ \xi,\ \eta,\ m]$, the thrust direction $\hat{\alpha} = [0, 0, 0,\ \alpha_r, \alpha_\lambda, \alpha_\phi]$, the FD perturbed motion $\tilde{f}(\mathbf{x}, t)$ and $\mathbf{B}$ the matrix 3.7, a typical low-thrust propulsion dynamical system is:

$$\begin{cases} \dot{\mathbf{x}} = f(\mathbf{x}, \hat{\alpha}, u, t) = \tilde{f}(\mathbf{x}, t) + \dfrac{T_{max}}{m} u\, \mathbf{B}\, \hat{\alpha} \\ \dot{m} = -\dfrac{T_{max}}{I_{sp} g_0} u \end{cases} \tag{4.2}$$

Integrating the 4.1 between initial and final powered conditions, the consumed fuel is found:

$$m_{prop} = M_b = \int_{m_i}^{m_f} dm = -\frac{T_{max}}{I_{sp} g_0} \int_{t_{Ci}}^{t_{Cf}} u \, dt \tag{4.3}$$

The FOP objective functional is consequently imposed in order to reduce that consumption to a minimum:

$$J = \frac{T_{max}}{I_{sp} g_0} \int_{t_{Ci}}^{t_{Cf}} u \, dt \tag{4.4}$$

If the costate is $\hat{\mathbf{l}} = [\mathbf{l}, l_m] = [\mathbf{l_r}, \mathbf{l_v}, l_m] = [l_r, l_\lambda, l_\phi, l_v, l_\xi, l_\eta, l_m]$, J can be augmented as:

$$J = \int_{t_{Ci}}^{t_{Cf}} \left[\frac{T_{max}}{I_{sp} g_0} u + \mathbf{l_r^T} \, \mathbf{v} + \mathbf{l_v^T} \left(\tilde{f}(\mathbf{x}, t) + \frac{T_{max}}{m} u \, \mathbf{B} \, \hat{\alpha} \right) - l_m \frac{T_{max}}{I_{sp} g_0} u \right] dt \tag{4.5}$$

and so the Hamiltonian H to be minimized is:

$$H = \frac{T_{max}}{I_{sp} g_0} u + \mathbf{l_r^T} \, \mathbf{v} + \mathbf{l_v^T} \left(\tilde{f}(\mathbf{x}, t) + \frac{T_{max}}{m} u \, \mathbf{B} \, \hat{\alpha} \right) - l_m \frac{T_{max}}{I_{sp} g_0} u \tag{4.6}$$

Performing its gradient and equating it to zero, what is obtained is a TPBVP consisting of the Euler-Lagrange equations describing a FOP subject to initial and final constraints:

$$\begin{cases} \dfrac{\partial H}{\partial \mathbf{l}} = 0 & \text{(4.7a)} \\ \dfrac{\partial H}{\partial \mathbf{u}} = 0 & \text{(4.7b)} \\ \dfrac{\partial H}{\partial \hat{\mathbf{x}}} = 0 & \text{(4.7c)} \end{cases}$$

subject to $\mathbf{x}(t_0) = \mathbf{x_0}$ and $\mathbf{x}(t_f) = \mathbf{x_T}$.
In particular:

- Equation 4.7a gives the state dynamics 4.2, which is always satisfied;
- the derivative of H with respect to $\mathbf{u}(u, \alpha)$ introduces two optimality conditions on thrust direction and its magnitude, that assumes the 4.1 rectangular profile. These are:

$$\hat{\alpha} = -\mathbf{B^T} \frac{\mathbf{l_v}}{|\mathbf{l_v}|} \tag{4.8}$$

and

$$\begin{cases} u = 0 & if \quad \rho > 0 \\ u = 1 & if \quad \rho < 0 \end{cases} \tag{4.9}$$

with

$$\rho = 1 - \frac{I_{sp} g_0}{m} |\mathbf{l_v}| - l_m \tag{4.10}$$

the switching function generating the so called *bang-bang* control 4.9.

- the last component, Equation 4.7c, leads to the costate dynamics as in 3.10:

$$\begin{cases} \dot{\mathbf{l}} = [\dot{\mathbf{l}}_\mathbf{r}, \dot{\mathbf{l}}_\mathbf{v}] = -\left(\dfrac{\partial f(\mathbf{x}, \mathbf{l}, t)}{\partial \mathbf{x}}\right)^T \mathbf{l} = -\mathbf{A^T}(\mathbf{x}, \mathbf{l}, t)\, \mathbf{l} = -\mathbf{A^T} \mathbf{l} \\ \dot{l}_m = -\dfrac{T_{max}\, u}{m^2} |\mathbf{l_v}| \end{cases} \tag{4.11}$$

Finally, the explicit TPBVP associated to the FOP in ECEF spherical coordinates and with boundary constraints only, is represented by the Equations 4.12.

$$\begin{cases} \dot{r} = v \\ \dot{\lambda} = \xi \\ \dot{\phi} = \eta \\ \dot{v} = -\dfrac{\mu_E}{r^2} + r\eta^2 + r(\xi + \omega_E)^2 \cos\phi^2 + a_r^p - \dfrac{T_{max}}{m}\, u\, \dfrac{l_v}{|\mathbf{l_v}|} \\ \dot{\xi} = 2\eta(\xi + \omega_E) \tan\phi - 2\dfrac{v}{r}(\xi + \omega_E) + \dfrac{1}{r\cos\phi}\, a_\lambda^p - \dfrac{1}{(r\cos\phi)^2}\, \dfrac{T_{max}}{m}\, u\, \dfrac{l_\xi}{|\mathbf{l_v}|} \\ \dot{\eta} = -2\dfrac{v}{r}\eta - (\xi + \omega_E)^2 \sin\phi\cos\phi + \dfrac{1}{r^2}\, a_\phi^p - \dfrac{1}{r^2}\, \dfrac{T_{max}}{m}\, u\, \dfrac{l_\eta}{|\mathbf{l_v}|} \\ \dot{m} = -\dfrac{T_{max}}{I_{sp} g_0}\, u \\ \dot{\mathbf{l}} = -\left(\dfrac{\partial f}{\partial \mathbf{x}}\right)^T \mathbf{l} \\ \dot{l}_m = -\dfrac{T_{max}\, u}{m^2} |\mathbf{l_v}| \end{cases} \tag{4.12}$$

subject to $\mathbf{x}(t_0) = \mathbf{x_0}$ and $\mathbf{x}(t_f) = \mathbf{x_T}$, together with the transversality condition $l_m(t_f) = 0$.

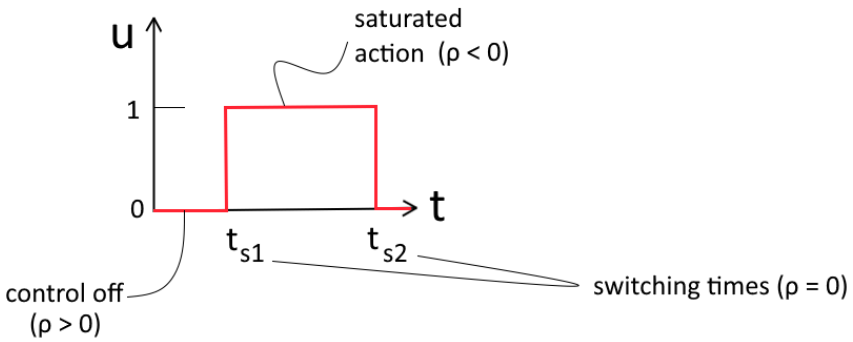

Figure 4.1: Bang-Bang control action

4.2. Numerical Reference

In the case of the fuel optimal control problem, it is very cumbersome to build up a bang-bang action through DA techniques like in the EOP. The FOP trajectory is characterized by a sequence of commutations between 'ON' and 'OFF' mode at certain switching times t_s. In this thesis, this pattern is computed numerically. Consequently, the FOP control region is shifted from being a neighbourhood of the nominal state, as in the continuous and non-saturated action of the EOP, to be about the numerical reference (Figure 4.2).

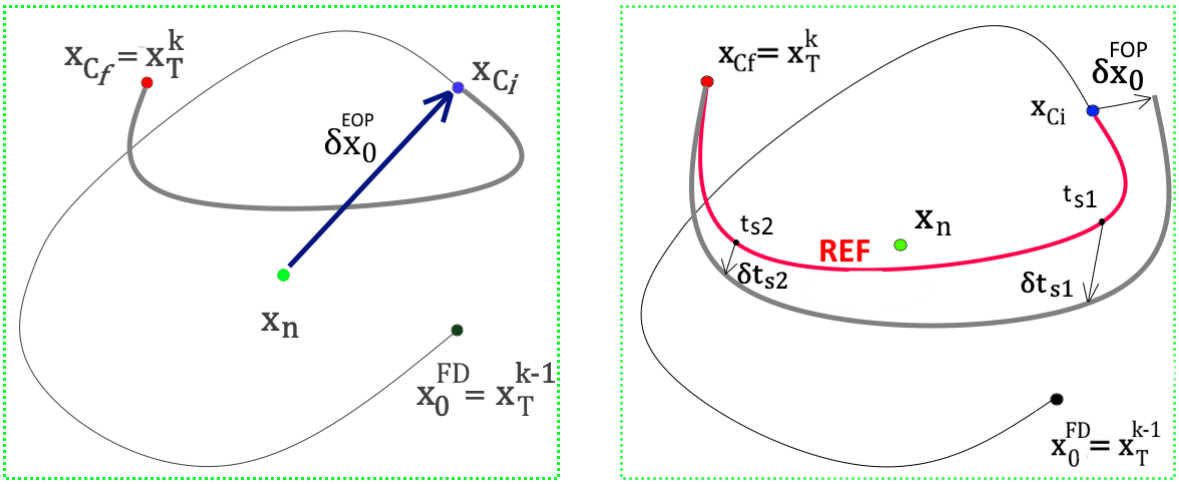

(a) EOP solution.

(b) FOP solution.

Figure 4.2: FOP control Approach

Any displacement from the baseline is corrected and a new optimal bang-bang profile, marked by new switching times $t_s + \delta t_s$, can be found through differential algebra, as detailed in the next sections.

Here the computation of the reference control is of interest. With this aim, a single shooting method with Python *fsolve* is implemented to solve the TPBVP 4.12. Due to its high sensitivity to initial conditions, the EOP solutions are taken as first guesses. The transformation to the bang-bang control is achieved thanks to the continuation method adopted by [13].

The discontinuous law 4.9 is reached by firstly defining u as a C^∞ function:

$$u = \frac{1}{1 + e^{p\rho}} \tag{4.13}$$

where ρ is the switching function 4.10 and p is a continuation parameter. Starting from $p = 1$, the shooting solution of the TPBVP is iteratively computed by increasing its value until the bang-bang shape appears.
This result is finally used to initialize the last propagation where u is imposed to be 0 or 1 according to the sign of ρ (4.9.)

Considering the propulsion properties in Table 4.1, and applying the described continuation method developed in Algorithm 4.1, the results are shown hereafter.

$\mathbf{I_{sp}}\,[s]$	$\mathbf{T_{max}}\,[N]$	$\mathbf{Mass}\,[kg]$
3800	0.33	3000

Table 4.1: Electric Propulsion test data and Satellite initial Mass

Algorithm 4.1 Continuation Method. FOP Reference Solution. One control cycle. Part 1

1: Find: $\mathbf{l_0}^{EOP}$ from EOP solution;
2: Initialize: $\mathbf{l_0}^{guess} = \mathbf{l_0}^{EOP}$;
3: Initialize: $l_{m0} = 1$ and m_0;
4: Define the constraints: $\mathbf{x}(t_f) = \mathbf{x_T}$; $l_{mf} = 0$;
5: Set a fixed control duration t_C;
6: Initialize time at initial epoch: $time = t_0$;
7: Initialize the continuation parameter: $p = 1$;
8: Initialize an arbitrary variable to enter the loop: $k = 1$;

Algorithm 4.2 Continuation Method. FOP Reference Solution. One control cycle. Part 2

while $k = 1$ **do**
  Solve the TPBVP: $\mathbf{l_0}^{FOP} = fsolve(@shootingFOP, \mathbf{l_0}^{guess}, constraints, p)$;
  Initialize the augmented state: $\mathbf{z_0} = [\mathbf{x_n}, m_0, \mathbf{l_0}^{FOP}, l_{m0}]$;
  Propagate: $ControlState = ContinuationPropag([\mathbf{z_0}, t_C, p)$
  Compute: ρ at every instant from 4.10;
  Compute switching times: t_s such that $\rho = 0$;
  if bang-bang profile = yes **then**
    k = 0;
  else
    p = p + 1;
  end if
end while
Find real bang-bang solution: $\mathbf{l_0}^{BB} = fsolve(@shootingBB, \mathbf{l_0}^{FOP}, constraints)$;
Initialize the augmented state: $\mathbf{z_0} = [\mathbf{x_n}, m_0, \mathbf{l_0}^{FOP}, l_{m0}]$;
Propagate the bang-bang trajectory: $BBState = ContinuationPropag(\mathbf{z_0}, t_C)$

4.2.1. Numerical Reference Results

The numerical transformation from the EOP to the FOP is here proposed. Considering the EOP target points found in 3.1.2 with *one*-day long powered phases and the DA 2^{nd} order EOP solution as initial guess, the following control baseline is obtained with the single shooting technique and the continuation method previously introduced.
Only the first SK cycle is initially treated, then the whole year span SK problem is turned into a FOP.

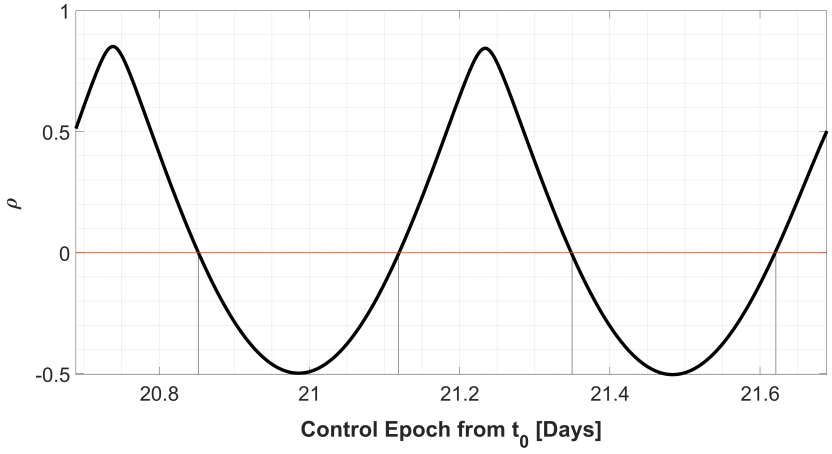

Figure 4.3: Switching Function ρ. First Cycle

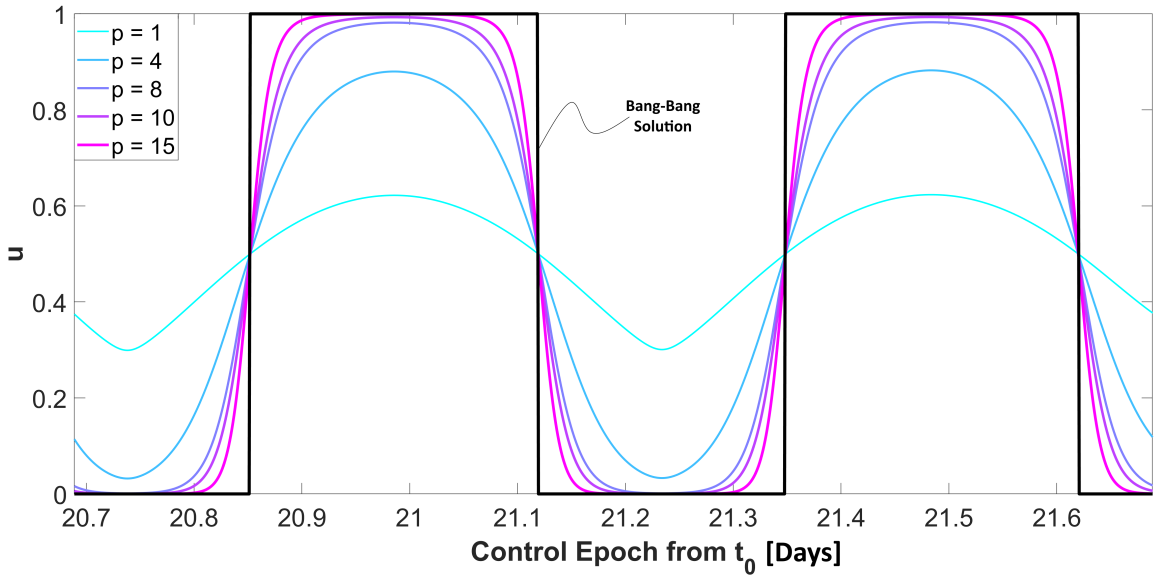

Figure 4.4: From C^{∞} solution to Bang-Bang. First Cycle

Figure 4.4 represents the bang-bang thrust profile arising by incrementing the continuation parameter p and according to the switching function ρ in Figure 4.3.

Switch	**Switching Time**$[Days]$	**Sign**(ρ)	**Control Mode**
1	20.85203721	$> 0 \Rightarrow < 0$	OFF $\Rightarrow$ ON
2	21.11924697	$< 0 \Rightarrow > 0$	ON $\Rightarrow$ OFF
3	21.34850475	$> 0 \Rightarrow < 0$	OFF $\Rightarrow$ ON
4	21.61997056	$< 0 \Rightarrow > 0$	ON $\Rightarrow$ OFF

Table 4.2: First SK cycle Switching Sequence from Initial Epoch t_0

Changing the control law means also obtaining a different trajectory pointing to the final target. In particular, in Figure 4.5 and 4.6 three thrust arcs are shown: one is given by the DA 2^{nd} order EOP solution, the second is generated by the continuous law with $p = 1$ and the last one represents the fuel optimal track.

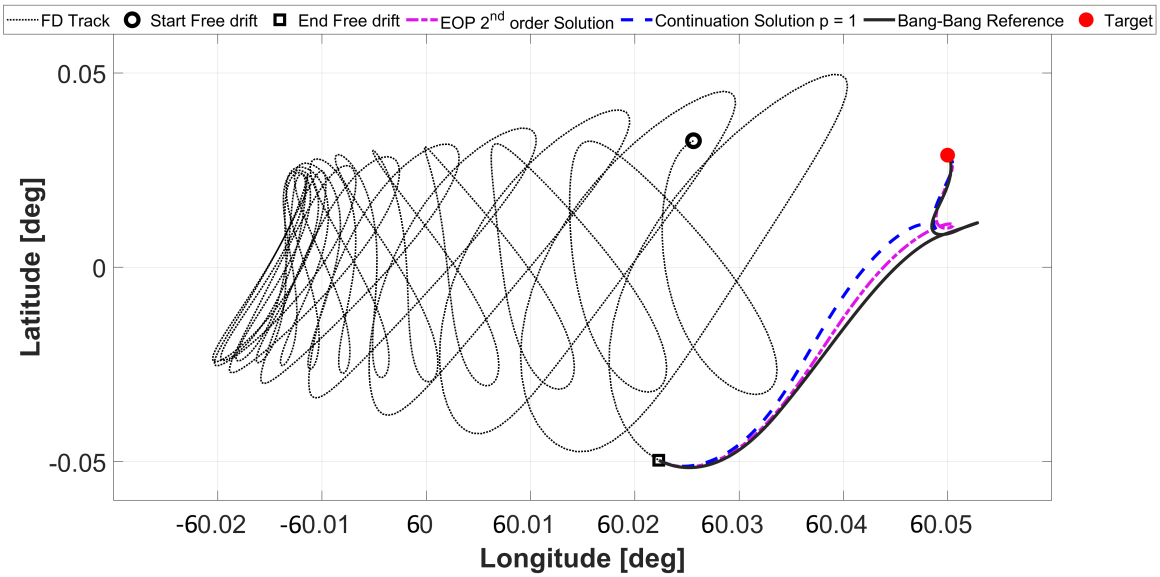

Figure 4.5: First SK cycle FD and following Powered Trajectories

The paths are clearly different due to the distinct nature of the optimal control law, but they precisely point to the final objective, as expected.

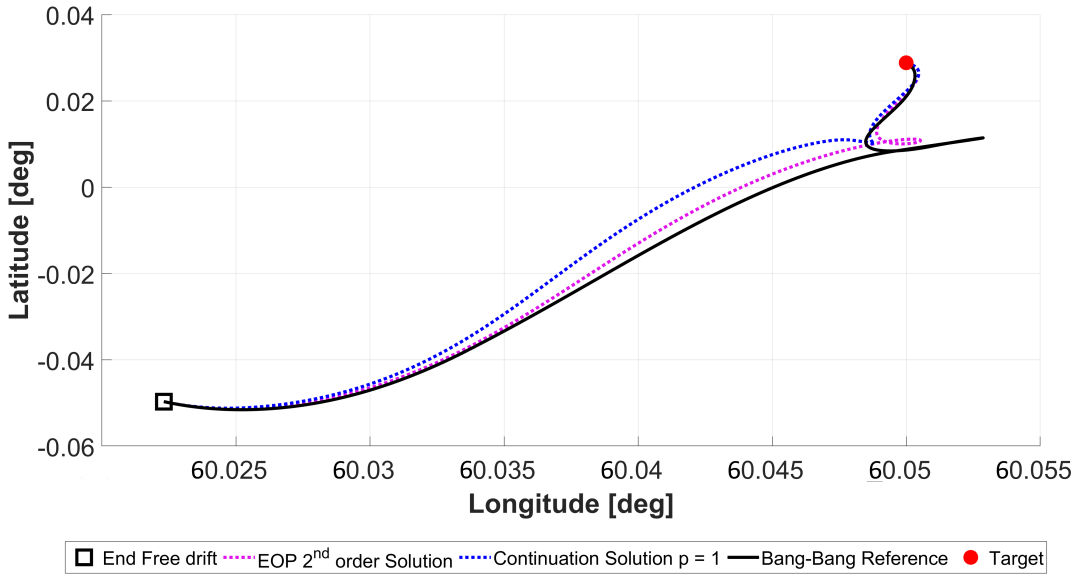

Figure 4.6: Control Tracks Comparison

As a component of the state, the mass consumption follows the switching sequence of the engines. Sketched out in Figure 4.7, the fuel is burnt during the 'ON' modes and drops linearly as described by the Equation 4.1.

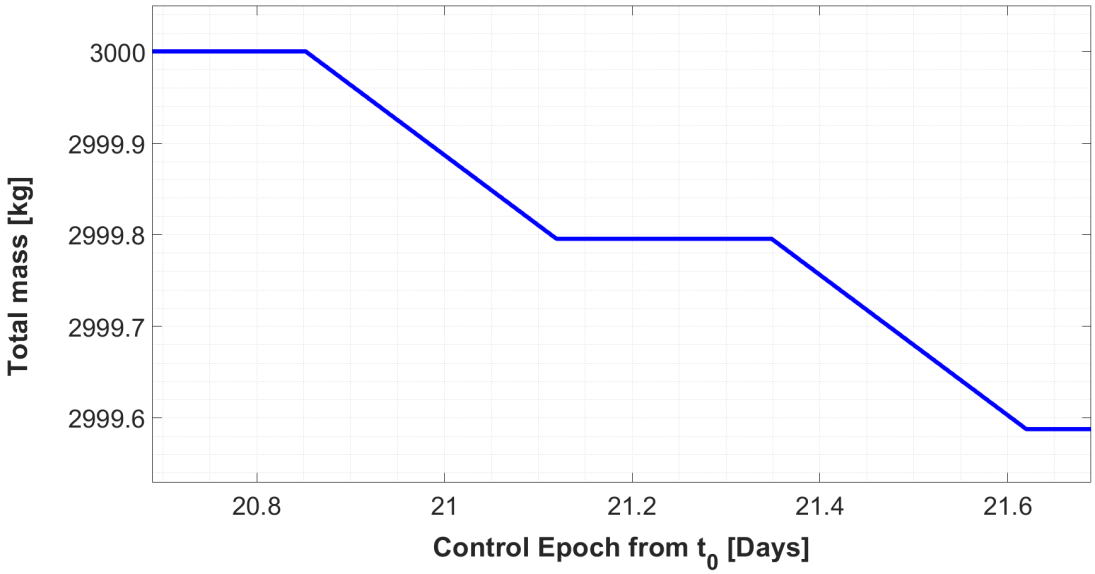

Figure 4.7: Fuel Consumption

With the Tsiolkovsky equation 3.27, it is possible to turn the amount of burnt gas M_b into a velocity variation Δv transmitted to the test satellite.

The thrust arc of the first SK cycle requires a total Δv of $5.158481\,m/s$ powered by $0.415107\,kg$ of propellant and partitioned among the 'ON' phases, as described by Table 4.3.

Phase	**Duration**$[Minutes]$	**Fuel Burnt**$[kg]$	**Δv** $[m/s]$
$t_{Ci} - t_{s1}$	234.82420728	0	0
$t_{s1} - t_{s2}$	384.78206166	0.205981	2.559610
$t_{s2} - t_{s3}$	330.13120183	0	0
$t_{s3} - t_{s4}$	390.91075794	0.209126	2.598871
$t_{s4} - t_{Cf}$	99.35177129	0	0

Table 4.3: FOP Consumption

Then, the analysis is extended over one year, as done for the EOP. The same numerical targets are used and each control cycle is turned into a FOP like the first one.

Due to the high precision granted by the shooting technique, the results of the SK fuel optimal problem can be overlapped to the ones of the numerical EOP, as proven by the analogy between Figure 4.8 and 3.7.

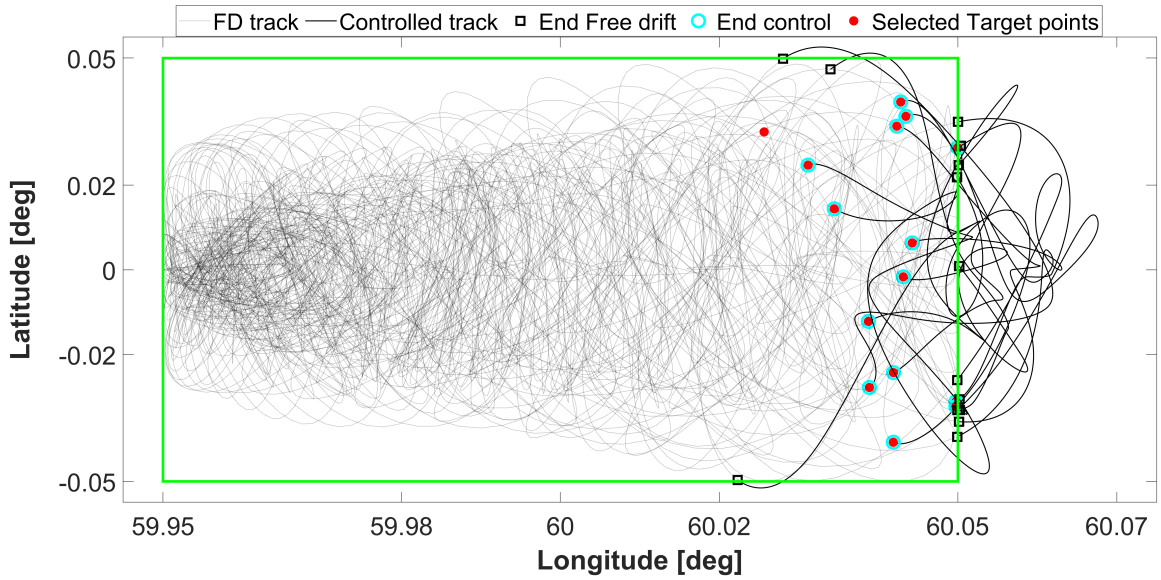

Figure 4.8: SK Box in a Year. FOP Reference Solution

Despite the complexity required by the FOP numerical solution, the final consumption is lower than the EOP one obtained with a shooting method. The fuel burnt in a year can be visualized in Figure 4.10, where it is clear that it drops linearly during each control phase and according to the actual bang-bang shape.

Every cycle has its own switching sequence with different number of commutations and thrust duration, as can be seen in Figure 4.9, which can be compared with the EOP profile in Figure 3.21.

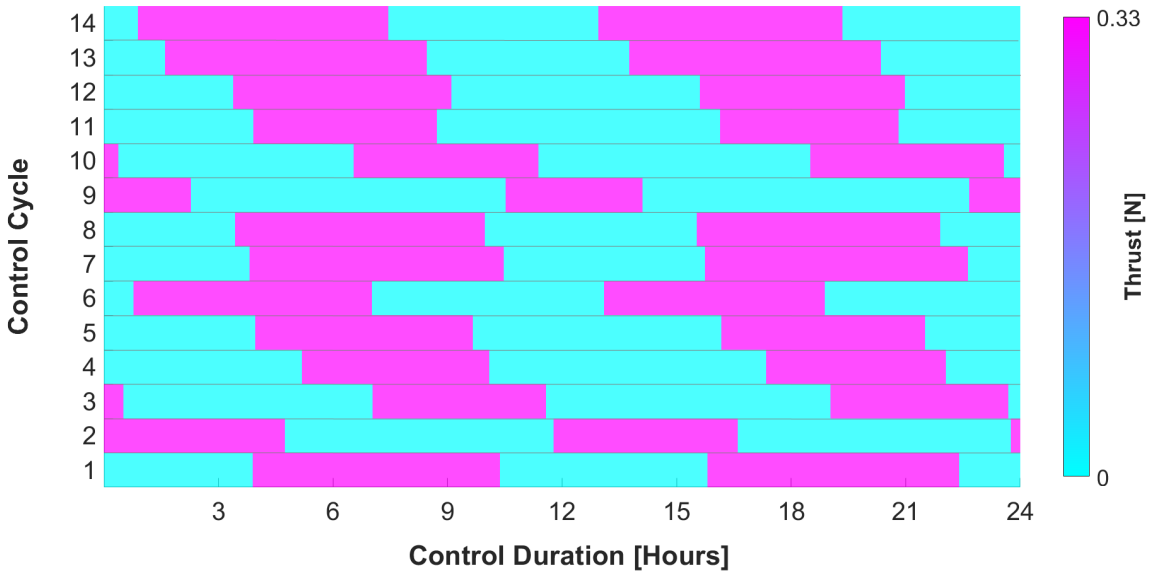

Figure 4.9: Bang-Bang Thrust in a Year SK. One-day control duration. FOP

The advantage of the FOP is enhanced in Table 4.4, in which a comparison with the EOP is presented in terms of cyclic spent propellant and Δv. Since the FOP reference is computed numerically, it does not make sense to compare its performances with previous DA solutions. Thus, only the shooting EOP results are taken into account in this analogy. The overall cost sums up all the contributions.

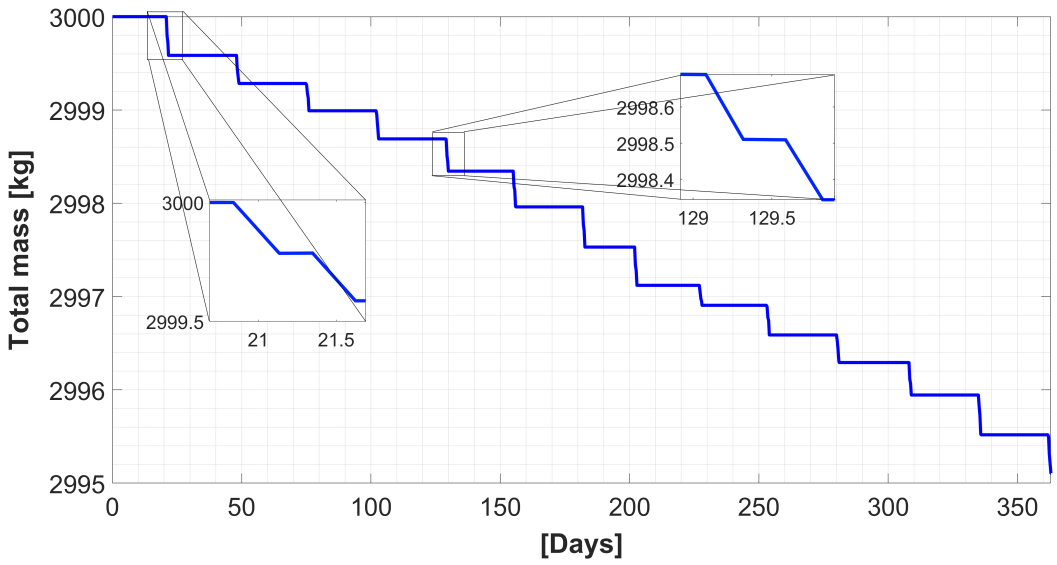

Figure 4.10: Fuel Consumption in a Year. FOP

Cycle	$\mathbf{M_b}$ **FOP**$[kg]$	$\mathbf{M_b}$ **EOP**$[kg]$	$\mathbf{\Delta v_{FOP}}$ $[m/s]$	$\mathbf{\Delta v_{EOP}}$ $[m/s]$
1	0.415107	0.464950	5.158481	5.772032
2	0.301439	0.354253	3.746392	4.398402
3	0.292156	0.342140	3.631371	4.248502
4	0.301490	0.350255	3.747758	4.349765
5	0.345811	0.398811	4.299167	4.953402
6	0.383252	0.434500	4.765222	5.397423
7	0.430700	0.477724	5.355906	5.935256
8	0.409835	0.459910	5.097150	5.714835
9	0.214277	0.256037	2.665254	3.181894
10	0.317866	0.369165	3.954088	4.588266
11	0.295379	0.341943	3.674735	4.250432
12	0.348031	0.400933	4.330237	4.984308
13	0.426673	0.474308	5.309388	5.897354
14	0.410658	0.460914	5.110826	5.731710
TOTAL	**4.892674**	**5.585843**	**60.845975**	**69.403582**

Table 4.4: FOP vs EOP Consumption in a Year. Numerical Solutions

4.3. DA Expansion about Reference Solution

If, due to additional perturbations or uncertainties, a displacement occurs from the expected reference computed in the previous section, it shall be counteracted in order to take the satellite to the desired objective position and velocity $\mathbf{x_{Cf}}$.

When the natural drift comes to an end, the vehicle is located in a neighbourhood of the expected $\mathbf{x_{Ci}}$. If the numerical control law is loaded onboard, the spacecraft shall be able to measure its state and determine an enaugh robust, precise and optimal correction with the purpose of matching the final target starting from a set of points around the nominal $\mathbf{x_{Ci}}$.

With this aim, a DA approach is here developed, recalling the control strategy in Figure 4.11 and referring to [13].

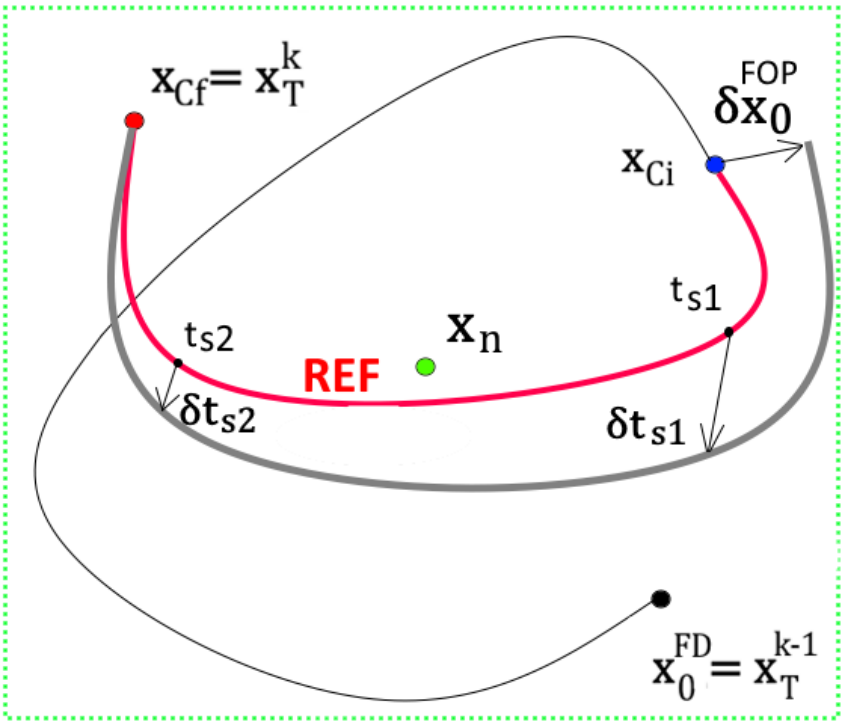

Figure 4.11: FOP control description

As stated above, the corrective operation for this FOP acts with respect to the numerical baseline ($\tilde{\cdot}$) and not to the nominal point $\mathbf{x_n}$ as in the EOP case.

Once the reference solution is found, differential algebraic techniques can be applied in order to obtain the control path characterized by a costate and a switching sequence

variation caused by the initial deviation.

For this intent, the next steps have to be followed.

1. Initialize the state composed by DA variables about $\tilde{\mathbf{x}}_\mathbf{0} = \mathbf{x_{Ci}}$ and $[\tilde{\mathbf{l}}_\mathbf{0}, \tilde{l}_{m0}]$:

$$\begin{cases} [\mathbf{r_0}] = \tilde{\mathbf{r}}_\mathbf{0} + \delta\mathbf{r_0} \\ [\mathbf{v_0}] = \tilde{\mathbf{v}}_\mathbf{0} + \delta\mathbf{v_0} \\ [m_0] = \tilde{m}_0 + \delta m_0 \\ [\mathbf{l_{r0}}] = \tilde{\mathbf{l}}_\mathbf{r0} + \delta\mathbf{l_{r0}} \\ [\mathbf{l_{v0}}] = \tilde{\mathbf{l}}_\mathbf{v0} + \delta\mathbf{l_{v0}} \\ [l_{m0}] = \tilde{l}_{m0} + \delta l_{m0} \end{cases} \tag{4.14}$$

2. A further DA variable is the first switching time t_{s1}:

$$[t_{s1}] = \tilde{t}_{s1} + \delta t_{s1} \tag{4.15}$$

3. Propagate the initial polynomial map 4.14 in a DA environment thanks to the DACE propagator $RK78$ from t_{Ci} to $[t_{s1}]$. This step is not immediate since the integrator has to be modified in order to be able to accept both DA differentials and DA time spans. According to [1], the new $RK78$ takes a coefficient τ ranging from 0 to 1, defines a new time variable

$$t^* = t_{Ci} + \tau([t_{s1}] - t_{Ci}) \tag{4.16}$$

   where t_{Ci} and t_{s1} can be defined as DA elements, and rescales the dynamics as

$$\frac{d\mathbf{z}}{d\tau} = ([t_{s1}] - t_{Ci}) f(\mathbf{x}, \mathbf{l}, \tau([t_{s1}] - t_{Ci})) \tag{4.17}$$

   t^* is also used to compute the non-autonomous perturbations that consequently become DA objects. The ephemeris of the Sun and the Moon shall be updated with the dependence on δt_{s1}.

4. At the end of this expansion, the polynomial map regarding the state at the first switch is available:

$$\begin{pmatrix} [\mathbf{x_1}] \\ [m_1] \\ [\mathbf{l_1}] \\ [l_{m_1}] \end{pmatrix} = \begin{pmatrix} \mathbf{x_1} \\ m_1 \\ \mathbf{l_1} \\ l_{m_1} \end{pmatrix} + \begin{pmatrix} M_{\mathbf{x_1}} \\ M_{m_1} \\ M_{\mathbf{l_1}} \\ M_{l_{m_1}} \end{pmatrix} \begin{pmatrix} \delta\mathbf{x_0} \\ \delta\mathbf{l_0} \\ \delta l_{m_0} \\ \delta t_{s1} \end{pmatrix} \tag{4.18}$$

It is possible to express δt_{s1} as a function of $\delta\mathbf{x_0}, \delta\mathbf{l_0}$ and δl_{m0} by computing the switching function map (see Appendix B) at $[t_{s1}]$, considering that its constant unperturbed part is null at every commutation of the reference:

$$[\rho_1] = 0 + \delta\rho_1 = 1 - \frac{I_{sp} g_0}{[m_1]} \left|[\mathbf{l_{v_1}}]\right| - [l_{m_1}] \tag{4.19}$$

Then, the following map is built and inverted imposing the switching condition $\delta\rho_1 = 0$:

$$\begin{pmatrix} \delta\rho_1 \\ \delta\mathbf{x_0} \\ \delta\mathbf{l_0} \\ \delta l_{m_0} \end{pmatrix} = \begin{pmatrix} M_{\rho_1} \\ I_{\mathbf{x_0}} \\ I_{\mathbf{l_0}} \\ I_{l_{m_0}} \end{pmatrix} \begin{pmatrix} \delta\mathbf{x_0} \\ \delta\mathbf{l_0} \\ \delta l_{m_0} \\ \delta t_{s1} \end{pmatrix} \tag{4.20}$$

$$\begin{pmatrix} \delta\mathbf{x_0} \\ \delta\mathbf{l_0} \\ \delta l_{m_0} \\ \delta t_{s1} \end{pmatrix} = \begin{pmatrix} M_{\rho_1} \\ I_{\mathbf{x_0}} \\ I_{\mathbf{l_0}} \\ I_{l_{m_0}} \end{pmatrix}^{-1} \begin{pmatrix} \delta\rho_1 = 0 \\ \delta\mathbf{x_0} \\ \delta\mathbf{l_0} \\ \delta l_{m_0} \end{pmatrix} \tag{4.21}$$

so

$$\delta t_{s1} = M_{\rho_1=0}(\delta\mathbf{x_0}, \delta\mathbf{l_0}, \delta l_{m_0}) \tag{4.22}$$

and

$$[t_{s1}] = \tilde{t}_{s1} + M_{\rho_1=0}(\delta\mathbf{x_0}, \delta\mathbf{l_0}, \delta l_{m_0}) \tag{4.23}$$

5. Initialize the second commutation time as a DA variable

$$[t_{s2}] = \tilde{t}_{s2} + \delta t_{s2} \tag{4.24}$$

and propagate the state at the previous switch, function of $\delta\mathbf{x_0}, \delta\mathbf{l_0}$ and δl_{m0} from $[t_{s1}]$ to $[t_{s2}]$.

6. Repeat the process for the whole bang-bang sequence until the conditions at the final mode change ($[t_{sf}]$) are expressed depending on the initial displacement $\delta\mathbf{x_0}, \delta\mathbf{l_0}$ and δl_{m0}.

7. Expand the last segment of the trajectory from $[t_{sf}]$ to t_{Cf} and find the final polynomial map:

$$\begin{pmatrix} [\mathbf{x_f}] \\ [m_f] \\ [\mathbf{l_f}] \\ [l_{m_f}] \end{pmatrix} = \begin{pmatrix} \mathbf{x_f} \\ m_f \\ \mathbf{l_f} \\ l_{m_f} \end{pmatrix} + \begin{pmatrix} M_{\mathbf{x_f}} \\ M_{m_f} \\ M_{\mathbf{l_f}} \\ M_{l_{m_f}} \end{pmatrix} \begin{pmatrix} \delta\mathbf{x_0} \\ \delta\mathbf{l_0} \\ \delta l_{m_0} \end{pmatrix} \tag{4.25}$$

8. Extract $M_{\mathbf{x_f}}$ and $M_{l_{m_f}}$, define the final constraint map as in Equation 3.14

$$C = [\mathbf{x_f}] - \mathbf{x_T} \tag{4.26}$$

and build up the following polynomial:

$$\begin{pmatrix} \delta\mathbf{x_0} \\ \delta\mathbf{x_f} \\ \delta l_{m_f} \end{pmatrix} = \begin{pmatrix} I_{\delta\mathbf{x_0}} \\ M_{\mathbf{x_f}} \\ M_{l_{m_f}} \end{pmatrix} \begin{pmatrix} \delta\mathbf{x_0} \\ \delta\mathbf{l_0} \\ \delta l_{m_0} \end{pmatrix} \tag{4.27}$$

Invert it, evaluate it in $\delta\mathbf{x_0}$, impose $\delta\mathbf{x_f}$ equal to the opposite of the constant part of C to enforce the final target, set the transversality condition $\delta l_{m_f} = 0$ and find the control law $[\delta\mathbf{l_0}, \delta l_{m_0}]$:

$$\begin{pmatrix} \delta\mathbf{x_0} \\ \delta\mathbf{l_0} \\ \delta l_{m_0} \end{pmatrix} = \begin{pmatrix} I_{\delta\mathbf{x_0}} \\ M_{\mathbf{x_f}} \\ M_{l_{m_f}} \end{pmatrix}^{-1} \begin{pmatrix} \delta\mathbf{x_0} \\ \delta\mathbf{x_f} \\ 0 \end{pmatrix} \tag{4.28}$$

9. Find the new optimal switching sequence characterized by i new commutation times as:

$$t_{s,i} = \tilde{t}_{s,i} + M_{\rho_i=0}(\delta\mathbf{x_0}, \delta\mathbf{l_0}, \delta l_{m_0}) \tag{4.29}$$

4.4. Perturbed Initial Control State

In order to test this method, an analysis that includes the variation of the reflection coefficient β is presented in this section. This number indicates the amount of radiation absorbed or reflected by the considered surface. The factor C_r introduced in section 2.1.4 is built from β as:

$$C_r = 1 + \beta \tag{4.30}$$

Starting from the first numerical target in section 3.1.2, 100 free-drift tracks are expanded, each one with a different β. A set of 100 values spanning from 0 (total absorption) to 1 (total reflection) are taken into account. Since the reference trajectory is obtained with $\beta = 0.5$, each FD path is expected to end in a neighbourhood of the nominal $\mathbf{x_{Ci}}$, as shown in Figure 4.12.

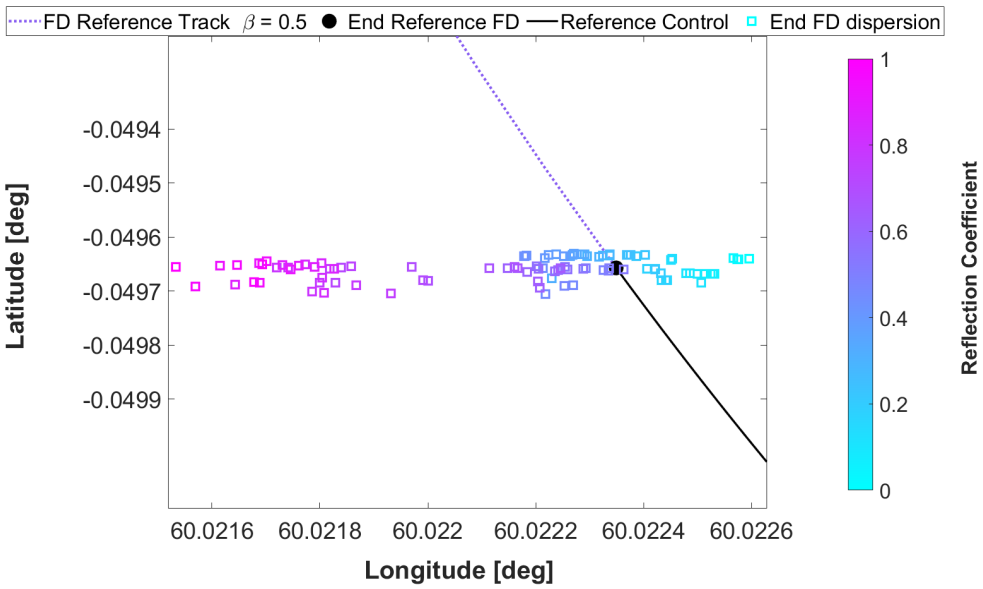

Figure 4.12: End of FD trajectories. Dispersion due to different β

The bang-bang numerical solution can be applied only if the FD phase ends exactly where predicted by the baseline. Otherwise the satellite shall be capable of measuring its actual state and building up a correction to the control law. This is possible by performing another shooting method from the measured conditions or by computing a polynomial high order map about the reference path, as developed above.

The second case is here treated as the best solution to this problem.

By the DA procedure introduced in the previous section, the FOP solution can be expanded up to an arbitrary order. For every possible deviation from the initial nominal point, a new optimal bang-bang profile arises.

4.4.1. DA Maps and Numerical Solution Comparison

A quick analysis is firstly proposed with the purpose of selecting the best fuel optimal control strategy that fits this problem. In the first Figure 4.13, the mean value over the 100 feedback trajectories of the final target matching precision is reported for the numerical reference and for DA 1^{st}, 2^{nd} and 3^{rd} order expansions.

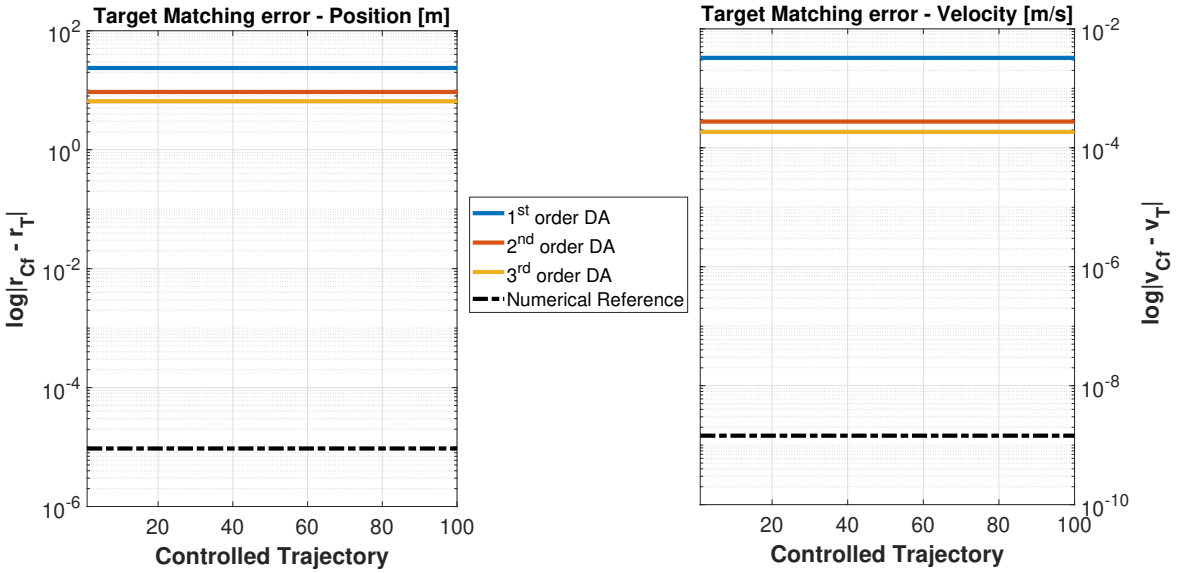

Figure 4.13: Mean State Error on Target matching. Comparison

As already stated in chapter 3, it is not necessary to reach the huge precision granted by the shooting in order to satisfy the SK requirements. The 2^{nd} order solution is already enough for this situation.

The advantage of the DA expansion can be seen in terms of computational burden in Table 4.5. The quickest is the linear control, but, as seen in the EOP, this approach is not sufficiently precise.
The difference between the 2^{nd} and 3^{rd} order final error is very limited, while the computational effort increase a lot. This is why the best choice is the quadratic DA polynomial.

Method	**Effort**$[s]$
1^{st} order DA	9.734
2^{nd} order DA	15.044
3^{rd} order DA	39.285
Shooting	41.178

Table 4.5: Computational Burden. Comparison

Despite the high accuracy of the shooting method, it takes a lot of time to be solved. Moreover, it must be calculated for every additional perturbation, contrarily to the uniqueness of the DA map that can be evaluated in every displacement without the need to recompute it.

4.4.2. Results

A 2^{nd} order map is expanded and then evaluated in each of the 100 final FD deviations in Figure 4.12.

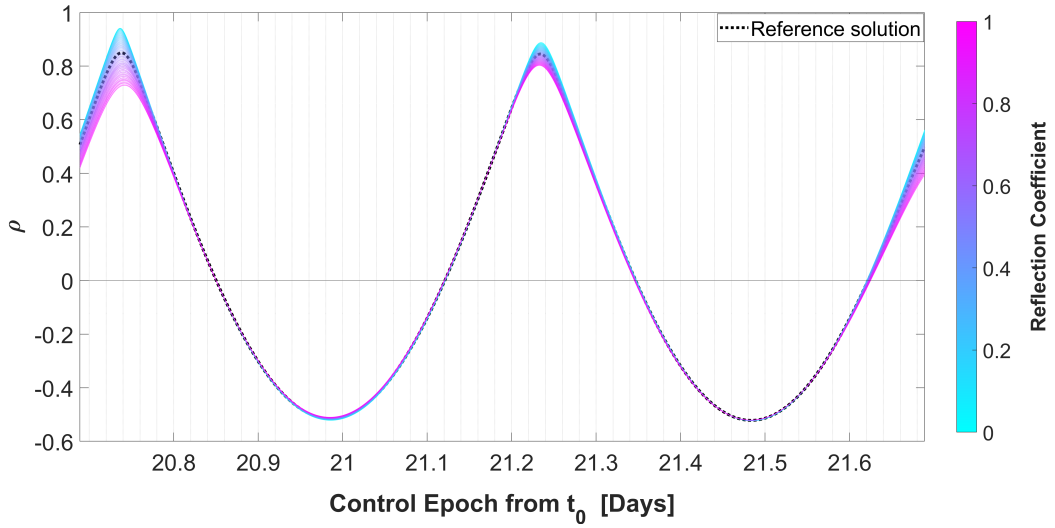

Figure 4.14: Switching Function ρ. Variation

According to this, 100 new switching functions are generated around the reference one, as can be seen in Figure 4.14. Consequently, new commutation sequences appear, depending on the value of the reflection coefficient.

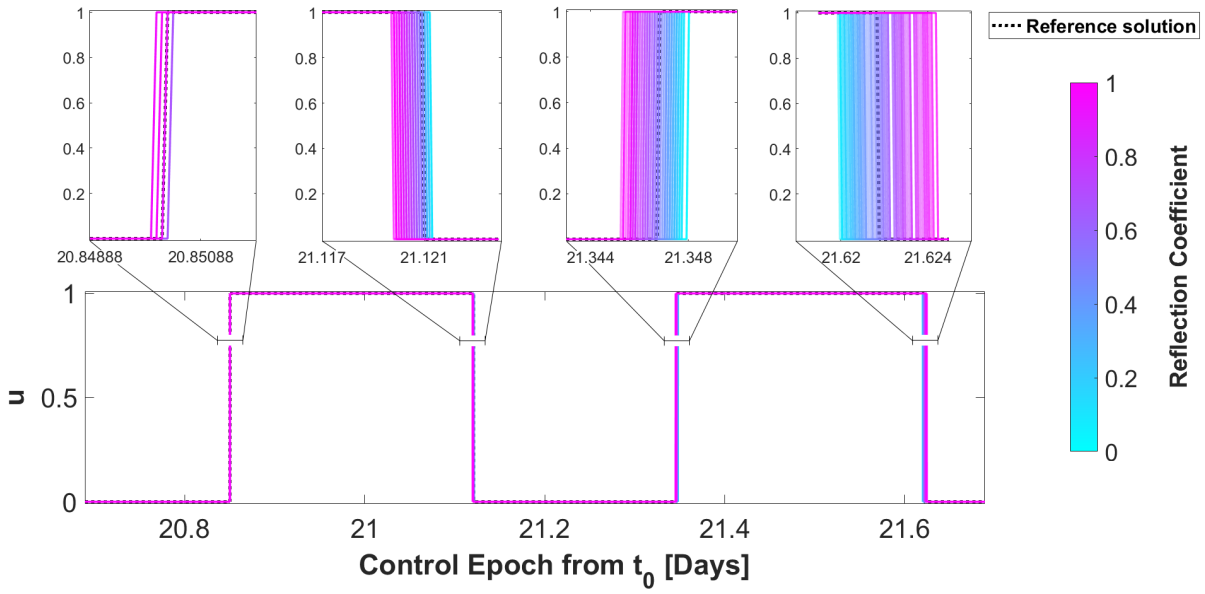

Figure 4.15: u Profile Variation

Figure 4.15 highlights how the throttle u changes between 'ON' and 'OFF' modes compared to the numerical result in Figure 4.4 and with respect to β.

The mass consumption also changes. In particular, the higher the reflection coefficient, the higher the SRP perturbing acceleration and so the more the burnt fuel is, as demonstrated by Figure 4.16.

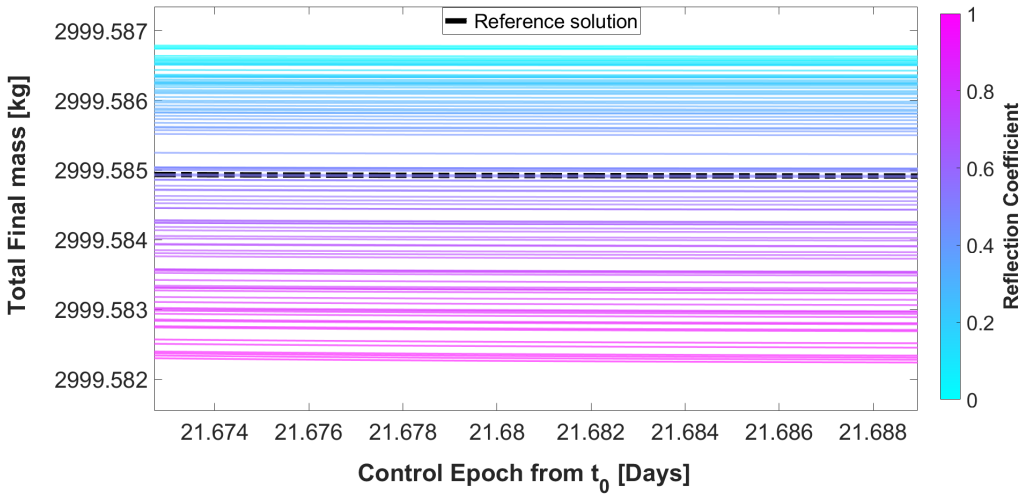

Figure 4.16: Final Mass Variation

The DA 2^{nd} order polynomial is able to reduce the final dispersion a lot and matching the final target with a great accuracy.

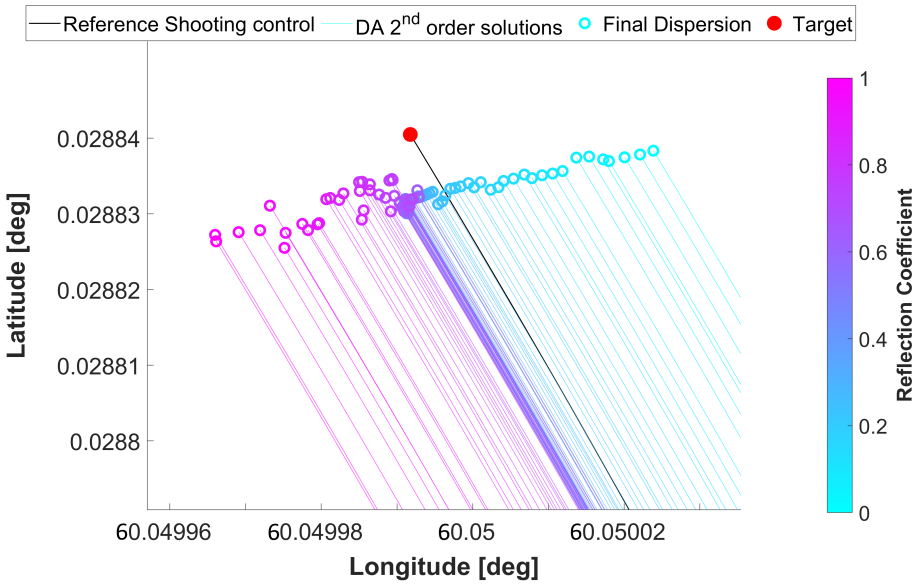

Figure 4.17: End of Controlled trajectories Dispersion due to different β

This is proven by the initial (i) state covariance matrix, expressed in the ECEF frame:

$$C^i_{r,2} = \begin{bmatrix} 4.267 & 71.397 & 1.674 \\ 71.397 & 1493.429 & 20.885 \\ 1.674 & 20.885 & 6.573 \end{bmatrix} 10^{-1} \ km^2$$

$$C^i_{v,2} = \begin{bmatrix} 7.8389 & 0.1687 & -0.3743 \\ 0.1687 & 0.0036 & -0.0081 \\ -0.3743 & -0.0081 & 0.0179 \end{bmatrix} 10^{-3} \ m^2/s^2 \tag{4.31}$$

which, at the end (f) of the control path, is lowered to:

$$C^f_{r,2} = \begin{bmatrix} 7.067 & -12.375 & -2.406 \\ -12.375 & 2171.933 & 41.083 \\ -2.406 & 41.083 & 10.681 \end{bmatrix} 10^{-4} \ km^2$$

$$C^f_{v,2} = \begin{bmatrix} 1.0583 & 0.0199 & 0.0289 \\ 0.0199 & 0.0005 & 0.0006 \\ 0.0289 & 0.0006 & 0.0008 \end{bmatrix} 10^{-8} \ m^2/s^2 \tag{4.32}$$

A better understanding is reached by computing the square root of the trace of the above

matrices. The quadratic polynomial grants:

$$\begin{aligned}\sqrt{Tr(C_{r,2})^i} = 12.2648\ km \Rightarrow \sqrt{Tr(C_{r,2})^f} = 0.4781\ km \\ \sqrt{Tr(C_{v,2})^i} = 0.0887\ m/s \Rightarrow \sqrt{Tr(C_{v,2})^f} = 1.029 \cdot 10^{-4}\ m/s\end{aligned} \tag{4.33}$$

The correctness of the developed feedback control action is established by looking at the following free-drift phase starting from the previous target. Figure 4.18 and Figure 4.19 show the inadequacy of the linear solution and the accuracy of the 2^{nd} order one respectively.

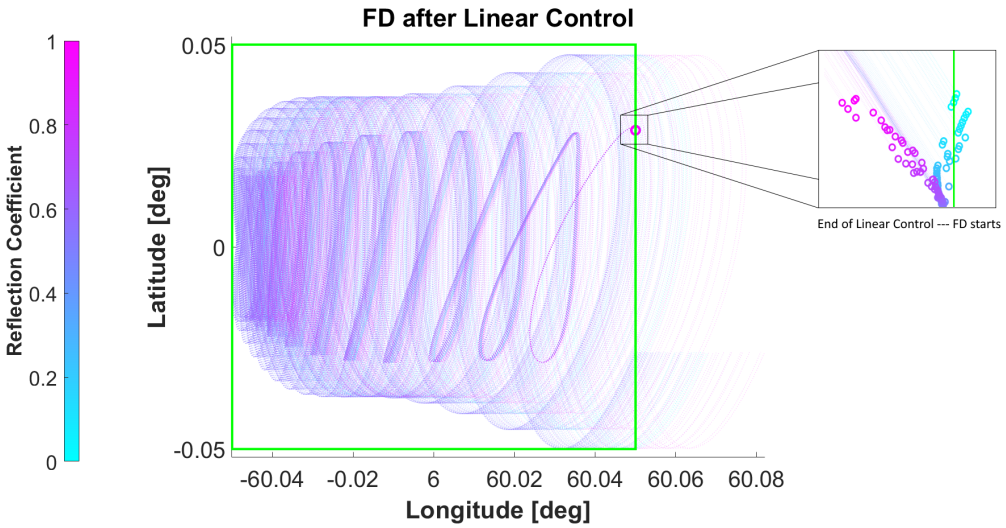

Figure 4.18: Free-Drift tracks after Linear Control

The 1^{st} order solution causes an East violation of the nominal SK box, due to the higher dispersion of the final control states. In fact, the linear case leads to:

$$\begin{aligned}\sqrt{Tr(C_{r,1})^i} = 12.2648\ km \Rightarrow \sqrt{Tr(C_{r,1})^f} = 1.3542\ km \\ \sqrt{Tr(C_{v,1})^i} = 0.0887\ m/s \Rightarrow \sqrt{Tr(C_{v,1})^f} = 8.194 \cdot 10^{-4}\ m/s\end{aligned} \tag{4.34}$$

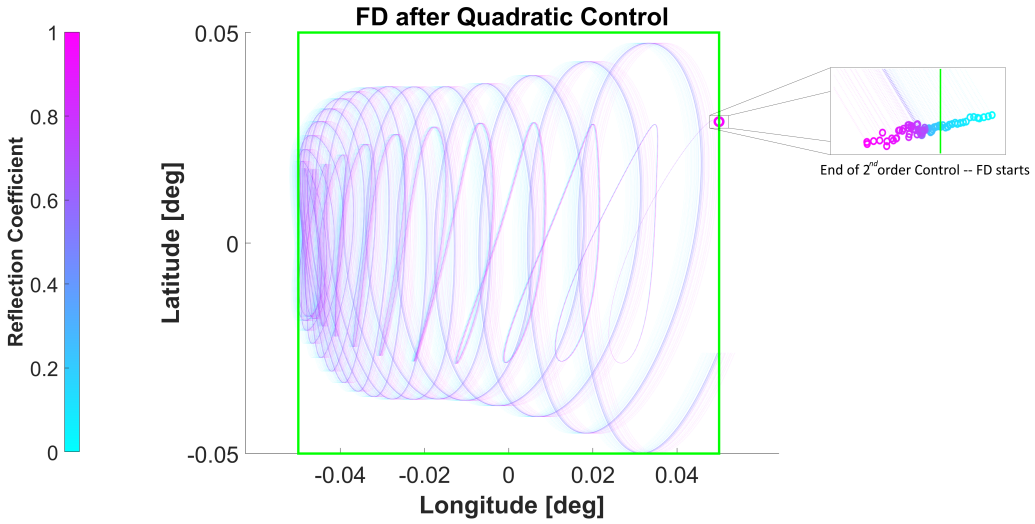

Figure 4.19: Free-Drift tracks after 2^{nd} Order Control

The higher the order, the more similar the natural tracks are. These FD phases are computed with the same reflection coefficient $\beta = 0.5$, but the point from which they begins depends on the β span considered for the previous cycle, and thus on the initial perturbations in Figure 4.12. If these displacements are precisely counteracted, the following free-drifts will collapse into a single *line*.

5 | Conclusions and future developments

The achieved objectives of this work are summarized in this chapter, together with some suggestions for future projects.

5.1. Conclusions

The SK strategy adopted was developed as a perturbed keplerian TBP affected by the geopotential, the Sun and Moon disturbances and the SRP, written in ECEF spherical coordinates. It tried to optimize the overall consumption by reducing the control cycles and maximizing the free-drift duration. It also aimed to lower the onboard computational effort with respect to largely adopted numerical procedures.

The first objective was reached through the computation of optimized targets as shown in section 3.1.2, while the second one has been gained thanks to differential algebra, which seems to be advantageous in this field compared to actual diffuse algorithms.

After the numerical target optimization, the solution of the SK problem was obtained solving an EOP in chapter 3. The application of DA techniques showed that such an optimized approach can not be achieved with linear solutions, as well as that a quadratic control is sufficient to equate the shooting results with great accuracy. A relevant achievement is represented by the 4^{th} order autonomous law linearly corrected by the complete one. This last case permits to find the necessary commands with a very small computational effort end an acceptable value of precision. Performances have been analyzed at the end, highlighting the small amount of Δv required in a year together with an important value of the maximum thrust needed. Variations on control duration have been also introduced, reporting the dependence between this variable and the SK requirements fulfillment.

In chapter 4 the problem was turned into a FOP, starting from previous findings. Bang-bang control actions were considered and compared to the continuous profile of the EOP,

discovering a gain in terms of consumption, despite the higher complexity of the algorithm requested to find the solution. A reference trajectory was demanded to know the baseline of the optimal switching sequence. DA has been applied to build up a robust and quick correction around this nominal path. If the spacecraft is displaced from the desired state, computing a 2^{nd} order map has been demonstrated to be the most convenient way to generate the fixing commands. Linear expansion is very quick but not sufficiently precise, while the shooting method is slow and shall be re-calculated for every eventual displacement.

In the EOP case the SK control can be directly found by the evaluation of onboard loaded polynomials, reducing the effort to a minimum and satisfying the constraints.
In the FOP a robust correction can be obtained around a loaded reference by the onboard expansion of DA quadratic polynomials about it.

5.2. Future Developments

Proven the benefits of DA in this particular environment, future works might develop further enhancements. In particular:

- For all the analyzed cases, the satellite violates the station keeping boundaries due to the lack of path constraints during the controlled stages. One can think to add these bounds along the powered phases.
- A better investigation could be developed regarding the relation between the amplitude of the target searching box and the one of the fulfilled SK region in the case of the most convenient parted autonomous and non-autonomous EOP strategy.
- A further analysis on the disturbances might provide a more global optimization by searching for the best combination of FD and control duration at every cycle.
- The maximum value of the thrust required is quite high for actual electric motors performances. It could be reduced by imposing a bound or by considering longer thrust arcs.
- For a more real and feasible study, specific thrusters configurations can be taken into account, as well as constraints on the direction of their action, on the duration of the firings and on the time needed to recharge the batteries between ON and OFF phases.
- The spacecraft attitude dynamics might be considered together with the SK strategy, e.g. adding pointing requirements.

- The method developed here could be extended to other orbital regimes, such as the aerostationary orbit of Mars, to maintain a satellite above a certain region or to study differences in the gravitational field and in the other disturbances with respect to the Earth case.

Bibliography

[1] R. Armellin, P. D. Lizia, F. Bernelli-Zazzera, and M. Berz. Asteroid close encounters characterization using differential algebra: The case of apophis. *Celestial Mechanics and Dynamical Astronomy 107(4):451-470*, 2011.

[2] E. Bois. First-order accurate theory of perturbed circular motion. *Celestial Mech Dyn Astr 58, 125–138*, 1994.

[3] H. D. Curtis. *Orbital Mechanics for Engineering Students*. Elsevier, 3 edition, 2014. ISBN 9780080977478.

[4] C. Gazzino. Dynamics of a geostationary satellite. HAL science ouverte, 12 2017. Research Report, Rapport LAAS n° 17432, LAAS-CNRS, 2nd Edition.

[5] C. Gazzino, C. Louembet, D. Arzelier, N. Jozefowiez, D. Losa, C. Pittet, and L. Cerri. Integer programming for optimal control of geostationary station keeping of low-thrust satellites. *IFAC PapersOnLine 50-1: 8169–8174*, 2017.

[6] C. Gazzino, D. Arzeliera, L. Cerri, D. Losa, C. Louembet, and C. Pittet. A three-step decomposition method for solving the minimum-fuel geostationary station keeping of satellites equipped with electric propulsion. *Acta Astronautica 158: 12-22*, 2019.

[7] M. M. Guelman. Geostationary satellites autonomous closed loop station keeping. *Acta Astronautica 97: 9–15*, 2013.

[8] L. Hengnian. *Geostationary Satellites Collocation*. Springer, 1 edition, 2014. ISBN 9783642407994.

[9] E. Johnston. List of satellites in geostationary orbit, 2022. URL `https://www.satsig.net/sslist.htm`.

[10] P. D. Lizia, R. Armellin, and M. Lavagna. Application of high order expansions of two-point boundary value problems to astrodynamics. *Celestial Mechanics Dynamical Astronomy 102: 355–375*, 2008.

[11] P. D. Lizia, R. Armellin, F. Topputo, M. Lavagna, F. Bernelli-Zazzera, and M.Berz.

High-order optimal station keeping of geostationary satellites. In *New Trends in Astrodynamics and Applications VI*, 2011.

[12] P. D. Lizia, R. Armellin, F. Bernelli-Zazzera, and M. Berz. High order optimal control of space trajectories with uncertain boundary conditions. *Acta Astronautica 93: 217–229*, 2014.

[13] P. D. Lizia, R. Armellin, A. Morselli, and F. Bernelli-Zazzera. High order optimal feedback control of space trajectories with bounded control. *Acta Astronautica 94, Issue 1: 383-394*, 2014.

[14] D. Losa, M. Lovera, R. Drai, T. Dargent, and J. Amalric. Electric station keeping of geostationary satellites: a differential inclusion approach. In *44th IEEE Conference on Decision and Control, and the European Control Conference*, Seville, Spain, December 12-15, 2005.

[15] B. Martin. Chapter 2 - differential algebraic techniques. In P. Hawkes, editor, *Modern Map Methods in Particle Beam Physics*, volume 108 of *Advances in Imaging and Electron Physics*, pages 81–117. Elsevier, 1999. doi: https://doi.org/10.1016/S1076-5670(08)70228-3. URL `https://www.sciencedirect.com/science/article/pii/S1076567008702283`.

[16] M. Massari and A. Wittig. The differential algebra computational toolbox, 2018. URL `https://github.com/dacelib/dace`.

[17] D. S. Naidu and R. C. Dorf. *Optimal Control Systems*. CRC press, 1 edition, 2003. ISBN 9781315214429.

[18] C. Park, V. Guibout, and D. J. Scheeres. Solving optimal continuous thrust rendezvous problems with generating functions. *Journal of Guidance, Control and Dynamics, 20, 2*, 2006.

[19] G. M. Pasta. Station keeping di satelliti geostazionari mediante controllo ottimo non lineare. Master's thesis, Politecnico di Milano, 2010.

[20] G. Purpura. Python wrapper of dace, the differential algebra computational toolbox, 2022. URL `https://github.com/giovannipurpura/daceypy/blob/master/docs/index.md`.

[21] A. Sukhanov and A. Prado. On one approach to the optimization of low-thrust station keeping manoeuvres. *Advances in Space Research 50: 1478–1488*, 2012.

[22] F. Topputo and C. Zhang. Survey of direct transcription for low-thrust space tra-

jectory optimization with applications. *Abstract and Applied Analysis, vol. 2014, Article ID 851720, 15 pages*, 2014.

[23] D. Vallado. *Fundamentals of Astrodynamics and Applications*. Springer, 3 edition, 2007.

[24] K. Wakker. *Fundamentals of Astrodynamics*. Institutional Repository Library, Delft University of Technology, 1 edition, 2015. ISBN 9789461864192.

[25] Wikipedia. Spherical coordinate system, 2022. URL `https://en.wikipedia.org/wiki/Spherical_coordinate_system`.

[26] X. Xu and P. Antsaklis. Optimal control of switched systems based on parameterization of the switching instants. *IEEE Transactions on Automatic Control 49: 2-16*, 2004.

A | Appendix A

This appendix is about further details on the environment.

A.1. Longitude Drift due to Zonal Harmonics

Nominal longitude (°)	Tangential acceleration (m/s^2)	Longitude drift acceleration (°/day^2)	Nominal longitude (°)	Tangential acceleration (m/s^2)	Longitude drift acceleration (°/day^2)
−137	−4.50E-08	0.001365855	43	−5.59E-08	0.001697176
−136	−4.40E-08	0.001335613	44	−5.52E-08	0.001674382
−135	−4.30E-08	0.001304062	45	−5.43E-08	0.00164916
−134	−4.19E-08	0.001271248	46	−5.34E-08	0.001621531
−133	−4.08E-08	0.001237216	47	−5.24E-08	0.001591519
−132	−3.96E-08	0.001202013	48	−5.14E-08	0.001559152
−131	−3.84E-08	0.001165687	49	−5.02E-08	0.001524462
−130	−3.72E-08	0.001128285	50	−4.90E-08	0.001487487
−129	−3.59E-08	0.001089857	51	−4.77E-08	0.001448264
−128	−3.46E-08	0.001050452	52	−4.64E-08	0.001406839
−127	−3.33E-08	0.00101012	53	−4.49E-08	0.001363258
−126	−3.19E-08	0.000968912	54	−4.34E-08	0.001317574
−125	−3.05E-08	0.000926878	55	−4.18E-08	0.00126984
−124	−2.91E-08	0.00088407	56	−4.02E-08	0.001220116
−123	−2.77E-08	0.000840539	57	−3.85E-08	0.001168464
−122	−2.62E-08	0.000796336	58	−3.67E-08	0.001114949
−121	−2.48E-08	0.000751514	59	−3.49E-08	0.001059642
−120	−2.33E-08	0.000706123	60	−3.30E-08	0.001002614
−119	−2.18E-08	0.000660215	61	−3.11E-08	0.000943941
−118	−2.02E-08	0.000613842	62	−2.91E-08	0.000883702
−117	−1.87E-08	0.000567056	63	−2.71E-08	0.00082198
−116	−1.71E-08	0.000519906	64	−2.50E-08	0.000758859
−115	−1.56E-08	0.000472445	65	−2.29E-08	0.000694427
−114	−1.40E-08	0.000424722	66	−2.07E-08	0.000628775
−113	−1.24E-08	0.000376787	67	−1.85E-08	0.000561996
−112	−1.08E-08	0.000328691	68	−1.63E-08	0.000494184
−111	−9.24E-09	0.000280482	69	−1.40E-08	0.000425438
−110	−7.65E-09	0.000232208	70	−1.17E-08	0.000355857
−109	−6.06E-09	0.000183918	71	−9.41E-09	0.000285543
−108	−4.47E-09	0.000135659	72	−7.07E-09	0.0002146
−107	−2.88E-09	8.75E-05	73	−4.72E-09	0.000143131
−106	−1.30E-09	3.94E-05	74	−2.35E-09	7.12E-05
−105	2.79E-10	−8.47E-06	75	3.15E-11	−9.55E-07
−104	1.85E-09	−5.61E-05	76	2.42E-09	−7.34E-05
−103	3.41E-09	−0.00010356	77	4.81E-09	−0.00014585
−102	4.96E-09	−0.00015068	78	7.19E-09	−0.00021833
−101	6.51E-09	−0.00019746	79	9.58E-09	−0.00029068
−100	8.03E-09	−0.00024385	80	1.20E-08	−0.0003628
−99	9.55E-09	−0.00028982	81	1.43E-08	−0.00043457

Figure A.1: Longitude Drift by zonal harmonics. Tabulation depending on λ_n [8]

A.2. Perturbing Terms in ECEF Spherical Coordinates

The complete dynamics

$$\begin{cases} \dot{r} = v \\ \dot{\lambda} = \xi \\ \dot{\phi} = \eta \\ \dot{v} = -\dfrac{\mu_E}{r^2} + r\eta^2 + r(\xi + \omega_E)^2 \cos\phi^2 + a_r^p(r, \lambda, \phi) \\ \dot{\xi} = 2\eta(\xi + \omega_E)\tan\phi - 2\dfrac{v}{r}(\xi + \omega_E) + \dfrac{1}{r\cos\phi} a_\lambda^p(r, \lambda, \phi) \\ \dot{\eta} = -2\dfrac{v}{r}\eta - (\xi + \omega_E)^2 \sin\phi\cos\phi + \dfrac{1}{r} a_\phi^p(r, \lambda, \phi) \end{cases} \tag{A.1}$$

involves the accelerations obtained by the gradient of the disturbing potentials

$$\mathbf{a^p}(r, \lambda, \phi) = \mathbf{a^p_{grav}}(r, \lambda, \phi) + \mathbf{a^p_{3B}}(r, \lambda, \phi) + \mathbf{a^p_{SRP}}(r, \lambda, \phi) \tag{A.2}$$

that shall be written as function of the spherical coordinates r, λ, ϕ. They assume the following shape. The derivatives are computed with MATLAB® Symbolic Toolbox.

For the geopotential:

$$\begin{aligned} a_{grav}^{p,r}(r, \lambda, \phi) = & -\frac{\mu_E}{2r^4} 3R_E^2 C_{20}(3\sin^2\phi - 1) + \\ & -\frac{\mu_E}{r^4} 9R_E^2 \cos^2\phi(S_{22}\sin 2l + C_{22}\cos 2l) + \\ & -\frac{\mu_E}{r^5} 60R_E^3 \cos^3\phi(S_{33}\sin 3l + C_{33}\cos 3l) + \\ & -\frac{\mu_E}{r^5} 2R_E^3 C_{30}\sin\phi(5\sin^2\phi - 3) + \\ & -\frac{\mu_E}{r^4} 9R_E^2 \cos\phi\sin\phi(C_{21}\cos l + S_{21}\sin l) + \\ & -\frac{\mu_E}{r^5} 60R_E^3 \cos^2\phi\sin\phi(S32\sin 2l + C_{32}\cos 2l) + \\ & -\frac{\mu_E}{r^5} 2R_E^3 \cos\phi(15\sin^2\phi - 3)(C_{31}\cos l + S_{31}\sin l) \end{aligned} \tag{A.3}$$

$$
\begin{aligned}
a^{p,\lambda}_{grav}(r,\lambda,\phi) = & -\frac{\mu_E}{r^4\cos\phi}\,3R_E^2\cos^2\phi(2C_{22}\sin 2l - 2S_{22}\cos 2l)+\\
& -\frac{\mu_E}{r^5\cos\phi}\,15R_E^3\cos^3\phi(3C_{33}\sin 3l - 3S_{33}\cos 3l)+\\
& -\frac{\mu_E}{r^4\cos\phi}\,3R_E^2\cos\phi\sin\phi(C_{21}\sin l - S_{21}\cos l)+\\
& -\frac{\mu_E}{r^5\cos\phi}\,15R_E^3\cos^2\phi\sin\phi(2C_{32}\sin 2l - 2S_{32}\cos 2l)+\\
& -\frac{\mu_E}{2r^5\cos\phi}\,R_E^3\cos\phi(15\sin^2\phi - 3)(C_{31}\sin l - S_{31}\cos l)
\end{aligned}
$$

$$
\begin{aligned}
a^{p,\phi}_{grav}(r,\lambda,\phi) = & \frac{\mu_E}{r^5}\,15R_E^3\cos^3\phi(S_{32}\sin 2l + C_{32}\cos 2l)+\\
& +\frac{\mu_E}{r^4}\,3R_E^2\cos^2\phi(C_{21}\cos l + S_{21}\sin l)+\\
& -\frac{\mu_E}{r^4}\,3R_E^2\sin^2\phi(C_{21}\cos l + S_{21}\sin l)+\\
& +\frac{\mu_E}{2r^5}\,R_E^3C_{30}\cos\phi(5\sin^2\phi - 3)+\\
& -\frac{\mu_E}{r^5}\,30R_E^3\cos\phi\sin^2\phi(S_{32}\sin 2l + C_{32}\cos 2l)+\\
& -\frac{\mu_E}{r^5}\,45R_E^3\cos^2\phi\sin\phi(S_{33}\sin 3l + C_{33}\cos 3l)+\\
& +\frac{\mu_E}{r^5}\,5R_E^3C_{30}\cos\phi\sin^2\phi+\\
& -\frac{\mu_E}{2r^5}\,R_E^3\sin\phi(15\sin^2\phi - 3)(C_{31}\cos l + S_{31}\sin l)+\\
& +\frac{\mu_E}{r^5}\,15R_E^3\cos^2\phi\sin\phi(C_{31}\cos l + S_{31}\sin l)+\\
& -\frac{\mu_E}{r^4}\,6R_E^2\cos\phi\sin\phi(S_{22}\sin 2l + C_{22}\cos 2l)+\\
& +\frac{\mu_E}{r^4}\,3R_E^2C_{20}\cos\phi\sin\phi
\end{aligned}
\tag{A.4}
$$

For the Sun and Moon gravity influence:

$$
\begin{aligned}
a^{p,r}_{3B}(r,\lambda,\phi) = & \frac{\mu_S}{r_S^3}r(3\cos^2\psi_S - 1)+\\
& +\frac{\mu_M}{r_M^3}r(3\cos^2\psi_M - 1)
\end{aligned}
\tag{A.5}
$$

$$
\begin{aligned}
a^{p,\lambda}_{3B}(r,\lambda,\phi) = & -3\frac{\mu_S}{r_S^3}r\cos\psi_S\cos\delta_S\sin(\alpha-\alpha_S)+\\
& -3\frac{\mu_M}{r_M^3}r\cos\psi_M\cos\delta_M\sin(\alpha-\alpha_M)
\end{aligned}
$$

$$
\begin{aligned}
a_{3B}^{p,\phi}(r,\lambda,\phi) = \; & 3\frac{\mu_S}{r_S^3} r\cos\psi_S(\cos\phi\sin\delta_S - \sin\phi\cos\delta_S\cos(\alpha-\alpha_S)) + \\
& + 3\frac{\mu_M}{r_M^3} r\cos\psi_M(\cos\phi\sin\delta_M - \sin\phi\cos\delta_M\cos(\alpha-\alpha_M))
\end{aligned}
\tag{A.6}
$$

For the SRP:

$$
\begin{aligned}
a_{SRP}^{p,r}(r,\lambda,\phi) &= -P_{sr}\cos\psi_S \\
a_{SRP}^{p,\lambda}(r,\lambda,\phi) &= P_{sr}\cos\delta_S\sin(\alpha-\alpha_S) \\
a_{SRP}^{p,\phi}(r,\lambda,\phi) &= -P_{sr}\sin\delta_S\cos\phi - \cos\delta_S\sin\phi\cos(\alpha-\alpha_S)
\end{aligned}
\tag{A.7}
$$

A.3. Single Perturbations Effects

In the next plots, the disturbances are analysed separately.

- The geopotential causes a longitude drift and oscillations on the semi-major axis r and on the radial velocity v. It does not influence the latitude so much.

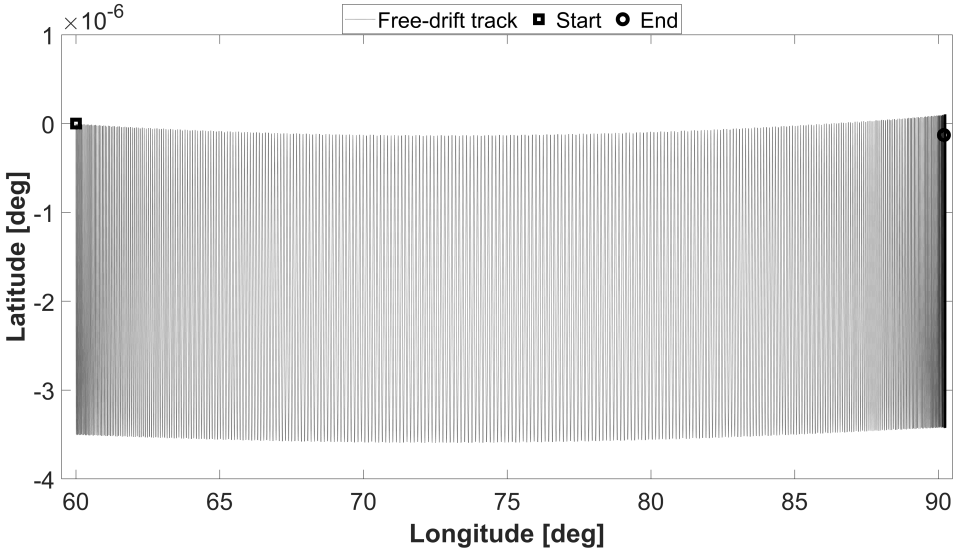

Figure A.2: λ and ϕ evolution due to GG disturbance. 1 Year

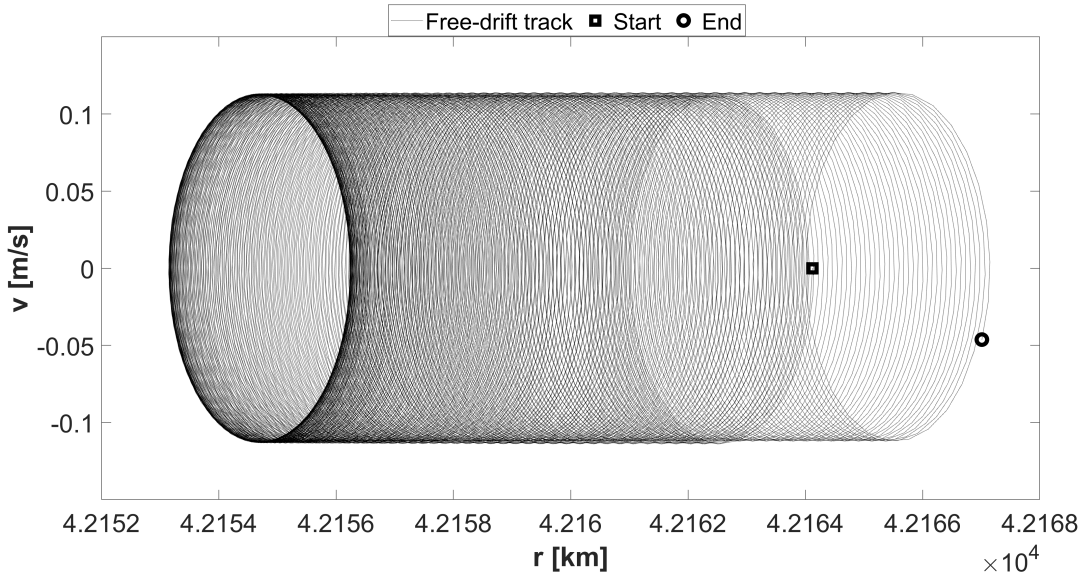

Figure A.3: r and v evolution due to GG disturbance. 1 Year

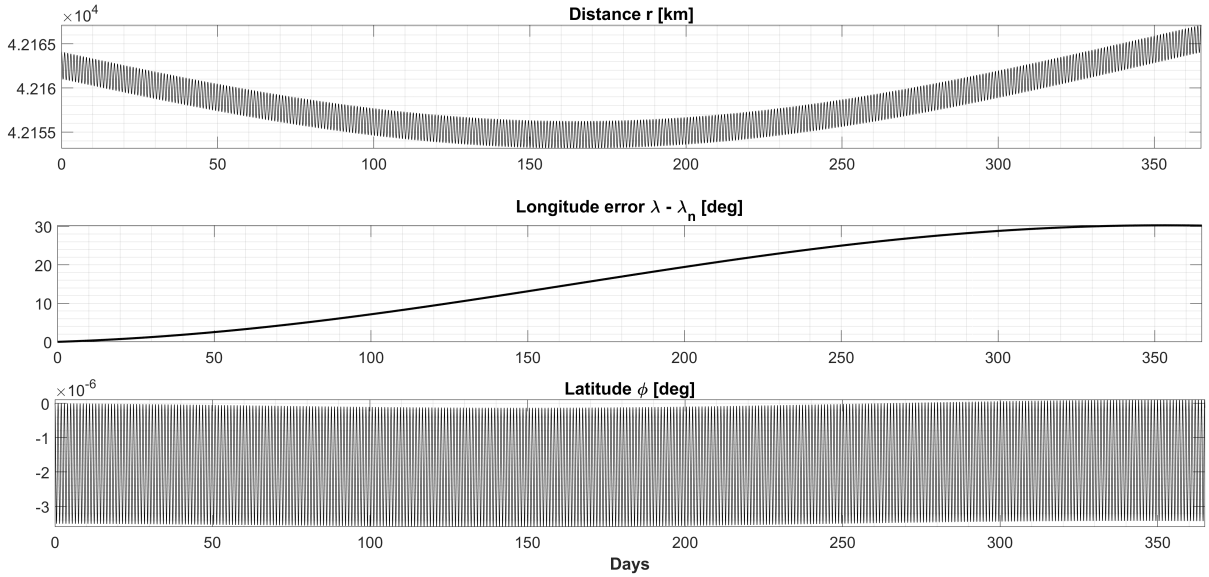

Figure A.4: Position Coordinates evolution due to GG disturbance. 1 Year

- The Moon influences the latitude a lot, with cyclic perturbations of about 28 days. The longitude drift is very contained, while the other coordinates show small variations in the short period.

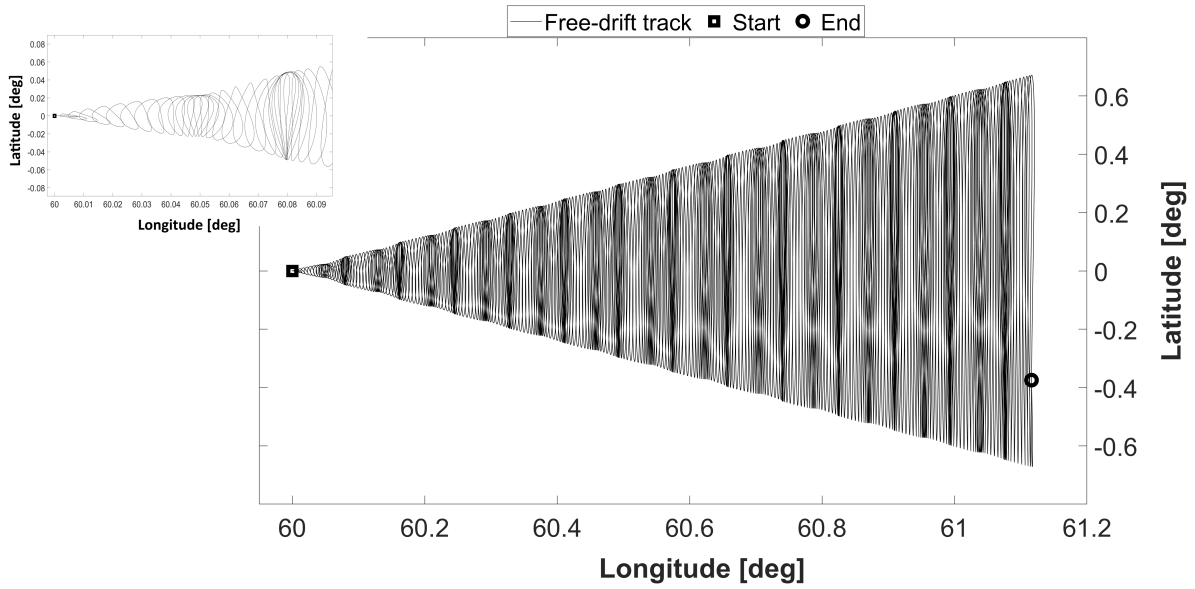

Figure A.5: λ and ϕ evolution due to Moon disturbance. 1 Year

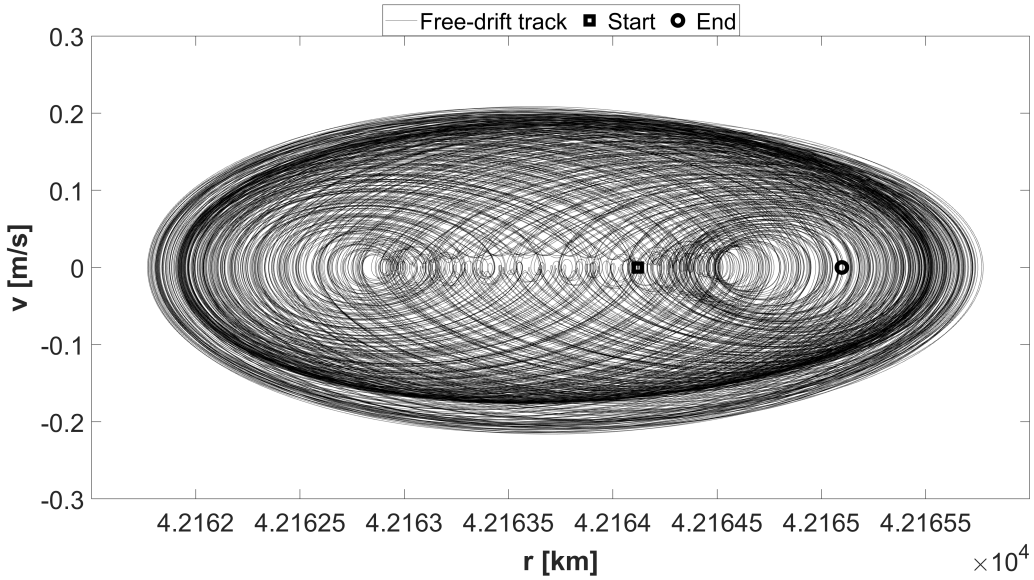

Figure A.6: r and r evolution due to Moon disturbance. 1 Year

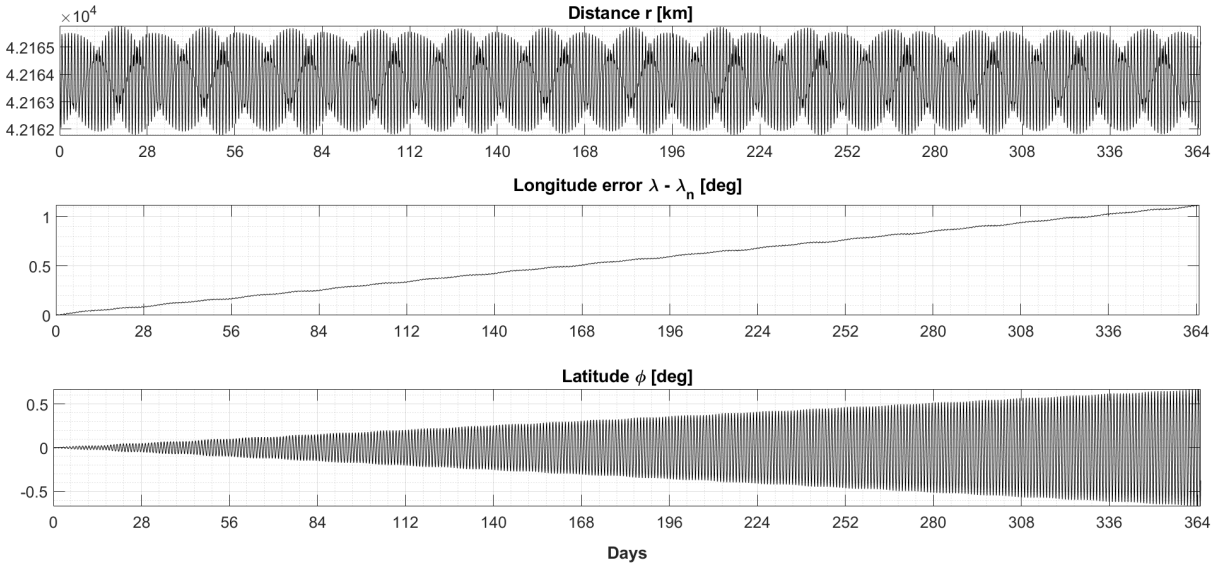

Figure A.7: Position Coordinates evolution due to Moon disturbance. 1 Year

- The Sun acts mainly on the latitude and on the semi-major axis with both short periodicity and one-year secular variation.

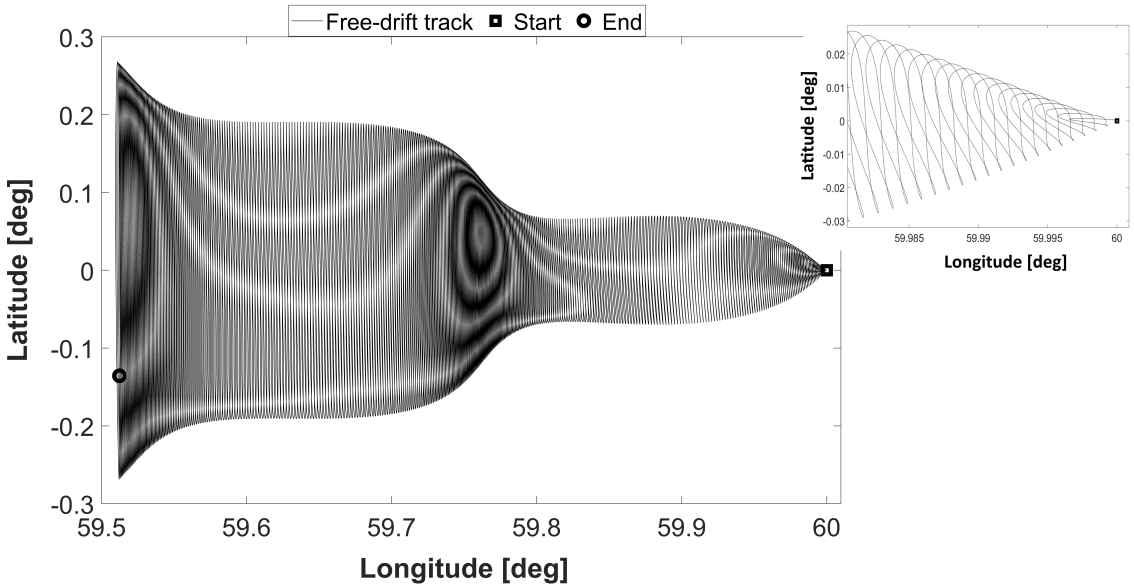

Figure A.8: λ and ϕ evolution due to Sun disturbance. 1 Year

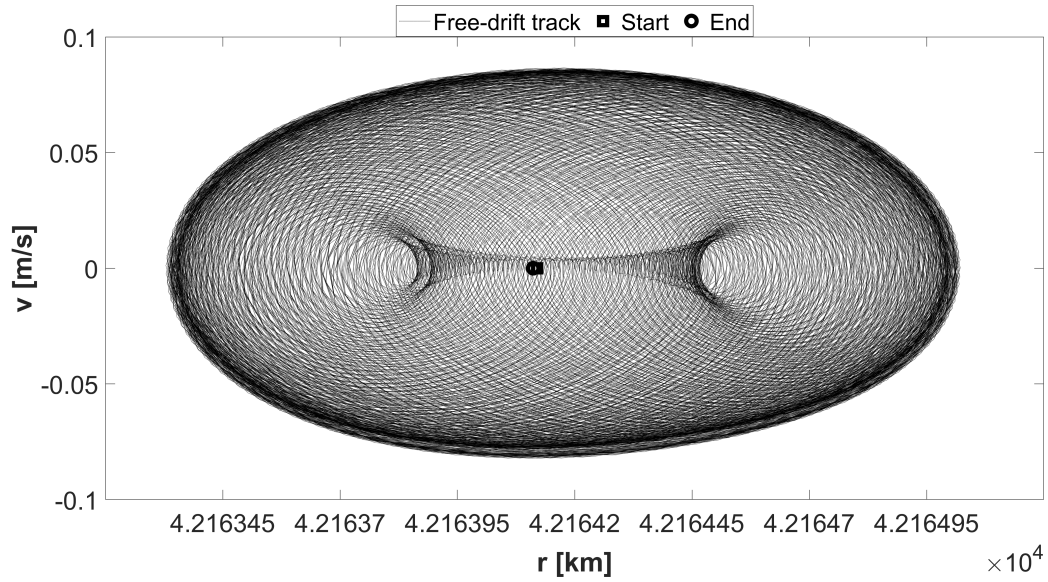

Figure A.9: r and v evolution due to Sun disturbance. 1 Year

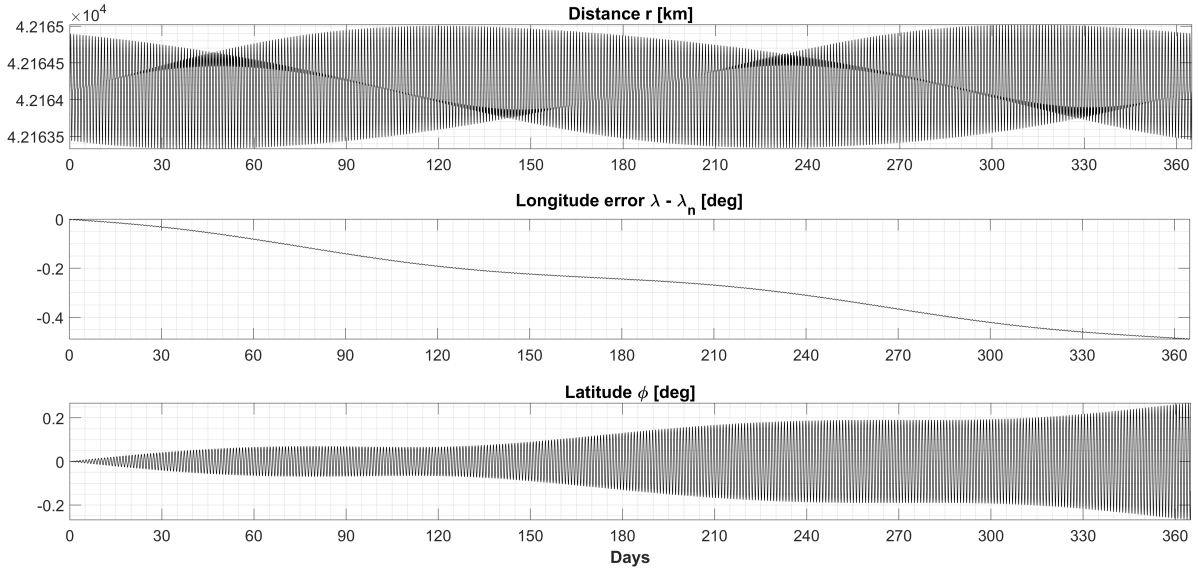

Figure A.10: Position Coordinates evolution due to Sun disturbance. 1 Year

- Finally, the SRP depends on the satellite properties. Its main effect is on the distance and, also, on the longitude drift.

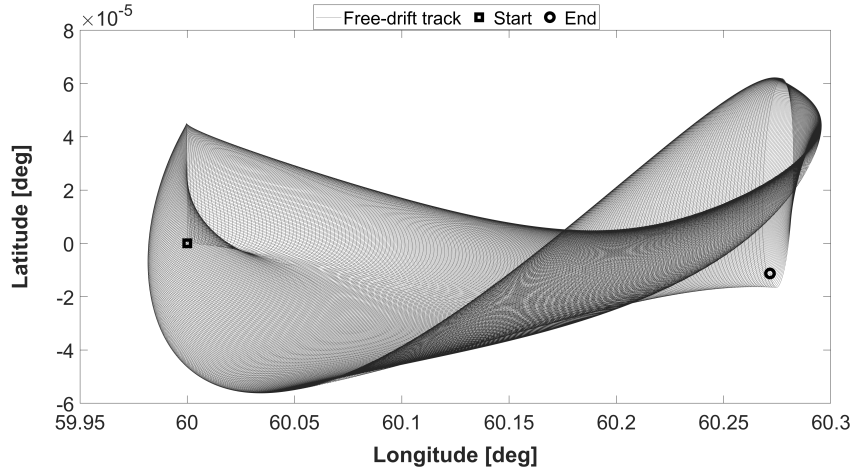

Figure A.11: λ and ϕ evolution due to SRP disturbance. 1 Year

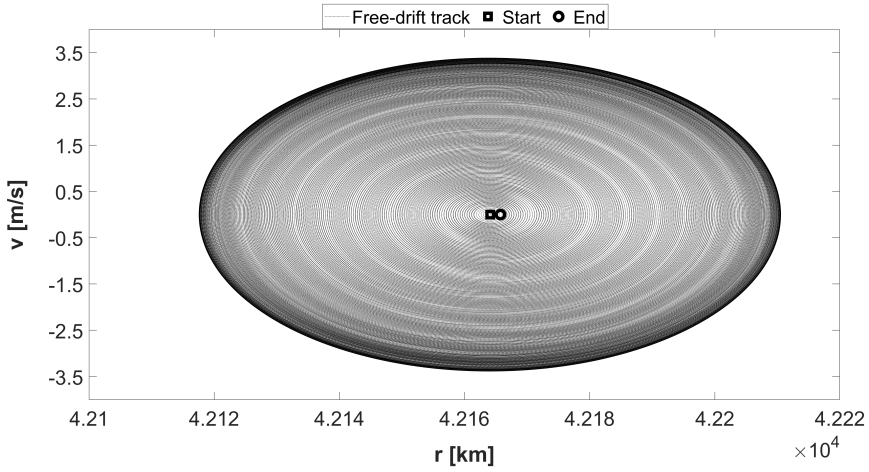

Figure A.12: r and v evolution due to SRP disturbance. 1 Year

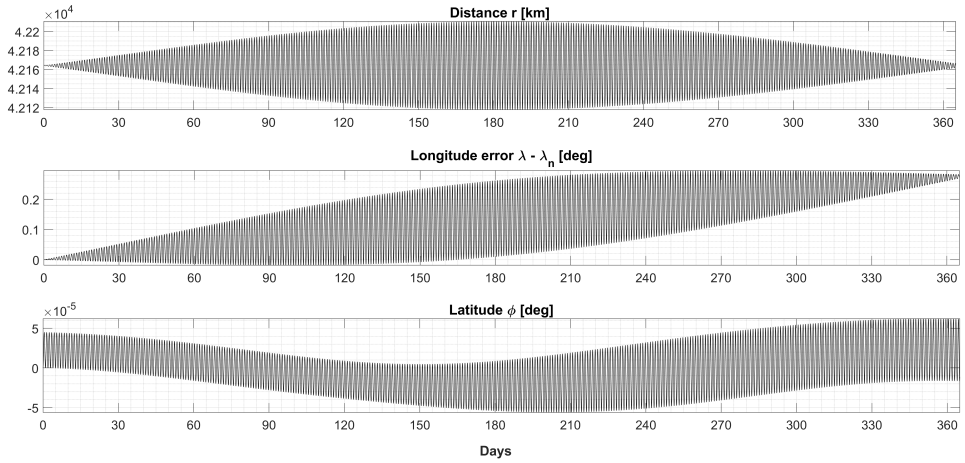

Figure A.13: Position Coordinates evolution due to SRP disturbance. 1 Year

B | Appendix B

This appendix concerns additional insights regarding the control laws.

B.1. EOP STM

The variational approach leading to the TPBVP

$$\begin{cases} \dot{\mathbf{z}}(t) = f(\mathbf{z}, t), & \mathbf{z}(t_0) = \mathbf{z_0} \\ \dot{\mathbf{\Phi}}(t_0, t) = \hat{\mathbf{A}}(t)\mathbf{\Phi}(t_0, t), & \mathbf{\Phi}(t_0, t_0) = \mathbf{I} \end{cases} \tag{B.1}$$

is quickly reported here.

From the definition of the STM and considering a displaced trajectory with respect to a reference, it is known that:

$$\begin{cases} \delta\dot{\mathbf{z}}(t) = \hat{\mathbf{A}}(t)\delta\mathbf{z} & \text{(B.2a)} \\ \delta\mathbf{z}(t) = \mathbf{\Phi}(t_0, t)\delta\mathbf{z_0} & \text{(B.2b)} \end{cases}$$

Deriving the second one and substituting the equation for $\delta\dot{\mathbf{z}}$:

$$\delta\dot{\mathbf{z}}(t) = \dot{\mathbf{\Phi}}(t_0, t)\delta\mathbf{z_0} = \hat{\mathbf{A}}(t)\delta\mathbf{z} \tag{B.3}$$

so

$$\dot{\mathbf{\Phi}}(t_0, t)\delta\mathbf{z_0} = \hat{\mathbf{A}}(t)\delta\mathbf{z} \tag{B.4}$$

Replacing $\delta\mathbf{z}(t) = \mathbf{\Phi}(t_0, t)\delta\mathbf{z_0}$:

$$\dot{\mathbf{\Phi}}(t_0, t)\delta\mathbf{z_0} = \hat{\mathbf{A}}(t)\mathbf{\Phi}(t_0, t)\delta\mathbf{z_0} \tag{B.5}$$

Since this shall be true for any $\delta\mathbf{z_0}$, it follows that:

$$\dot{\mathbf{\Phi}}(t_0,t) = \hat{\mathbf{A}}(t)\mathbf{\Phi}(t_0,t) \tag{B.6}$$

with the initial condition:

$$\dot{\mathbf{\Phi}}(t_0,t_0) = \mathbf{I} \tag{B.7}$$

In order to integrate it, the matrix $\hat{\mathbf{A}}(t)$ must be known. So the best thing is to build and integrate the STM together with the flow $f(\mathbf{z},t)$.

For the controlled dynamical problem

$$\begin{cases} \dot{r} = v \\ \dot{\lambda} = \xi \\ \dot{\phi} = \eta \\ \dot{v} = -\dfrac{\mu_E}{r^2} + r\eta^2 + r(\xi+\omega_E)^2\cos\phi^2 + a_r^p(r,\lambda,\phi) + l_v \\ \dot{\xi} = 2\eta(\xi+\omega_E)\tan\phi - 2\dfrac{v}{r}(\xi+\omega_E) + \dfrac{1}{r\cos\phi}\,a_\lambda^p(r,\lambda,\phi) + \dfrac{1}{(r\cos\phi)^2}\,l_\xi \\ \dot{\eta} = -2\dfrac{v}{r}\eta - (\xi+\omega_E)^2\sin\phi\cos\phi + \dfrac{1}{r^2}\,a_\phi^p(r,\lambda,\phi) + \dfrac{1}{r^2}\,l_\eta(t) \\ \dot{\mathbf{l}} = -\mathbf{A}^T\mathbf{l} \end{cases} \tag{B.8}$$

with $\mathbf{A}$ the Jacobian of the state dynamics. $\hat{\mathbf{A}}$, in this case, represents the Jacobian of the augmented flow $\dot{\mathbf{z}} = [\dot{\mathbf{x}},\dot{\mathbf{l}}] = [\dot{\mathbf{r}},\dot{\mathbf{v}},\dot{\mathbf{l}}_\mathbf{r},\dot{\mathbf{l}}_\mathbf{v}] = f(\mathbf{z},t)$.

$\hat{\mathbf{A}}(t)$ assumes the following, partitioned, $\{12\times 12\}$ shape:

$$\hat{\mathbf{A}}(t) = \begin{bmatrix} \dfrac{\partial f_\mathbf{r}}{\partial \mathbf{r}} & \dfrac{\partial f_\mathbf{r}}{\partial \mathbf{v}} & \dfrac{\partial f_\mathbf{r}}{\partial \mathbf{l_r}} & \dfrac{\partial f_\mathbf{r}}{\partial \mathbf{l_v}} \\ \dfrac{\partial f_\mathbf{v}}{\partial \mathbf{r}} & \dfrac{\partial f_\mathbf{v}}{\partial \mathbf{v}} & \dfrac{\partial f_\mathbf{v}}{\partial \mathbf{l_r}} & \dfrac{\partial f_\mathbf{v}}{\partial \mathbf{l_v}} \\ \dfrac{\partial f_{\mathbf{l_r}}}{\partial \mathbf{r}} & \dfrac{\partial f_{\mathbf{l_r}}}{\partial \mathbf{v}} & \dfrac{\partial f_{\mathbf{l_r}}}{\partial \mathbf{l_r}} & \dfrac{\partial f_{\mathbf{l_r}}}{\partial \mathbf{l_v}} \\ \dfrac{\partial f_{\mathbf{l_v}}}{\partial \mathbf{r}} & \dfrac{\partial f_{\mathbf{l_v}}}{\partial \mathbf{v}} & \dfrac{\partial f_{\mathbf{l_v}}}{\partial \mathbf{l_r}} & \dfrac{\partial f_{\mathbf{l_v}}}{\partial \mathbf{l_v}} \end{bmatrix} = \begin{bmatrix} \hat{\mathbf{A}}_{\mathbf{xx}} & \hat{\mathbf{A}}_{\mathbf{xl}} \\ \hat{\mathbf{A}}_{\mathbf{lx}} & \hat{\mathbf{A}}_{\mathbf{ll}} \end{bmatrix} \tag{B.9}$$

For the EOP:

$$\hat{\mathbf{A}}_{\mathbf{xx}}(t) = \mathbf{A}(t) = \begin{bmatrix} \mathbf{0^{3\times 3}} & \mathbf{I^{3\times 3}} \\ \dfrac{\partial f_{\mathbf{v}}}{\partial \mathbf{r}} & \dfrac{\partial f_{\mathbf{v}}}{\partial \mathbf{v}} \end{bmatrix} \qquad \hat{\mathbf{A}}_{\mathbf{xl}}(t) = \begin{bmatrix} \mathbf{0^{3\times 3}} & \mathbf{0^{3\times 3}} \\ \mathbf{0^{3\times 3}} & \dfrac{\partial f_{\mathbf{v}}}{\partial \mathbf{l_v}} \end{bmatrix}$$

$$\hat{\mathbf{A}}_{\mathbf{lx}}(t) = \begin{bmatrix} \dfrac{\partial f_{\mathbf{l_r}}}{\partial \mathbf{r}} & \dfrac{\partial f_{\mathbf{l_r}}}{\partial \mathbf{v}} \\ \dfrac{\partial f_{\mathbf{l_v}}}{\partial \mathbf{r}} & \dfrac{\partial f_{\mathbf{l_v}}}{\partial \mathbf{v}} \end{bmatrix} \qquad \hat{\mathbf{A}}_{\mathbf{ll}}(t) = \begin{bmatrix} \mathbf{0^{3\times 3}} & \dfrac{\partial f_{\mathbf{l_r}}}{\partial \mathbf{l_v}} \\ -\mathbf{I^{3\times 3}} & \dfrac{\partial f_{\mathbf{l_v}}}{\partial \mathbf{l_v}} \end{bmatrix} \tag{B.10}$$

The derivatives of the flow are very complex expressions due to the shape of the spherical perturbed equations. They are computed using MATLAB® Symbolic Toolbox.

Consequently, the STM is built according to $\hat{\mathbf{A}}(t)$. The process foresees the integration from t_0 to t_f of the system B.1 composed by 156 differential equations: 12 ODEs representing the augmented state plus one ODE for each component of the STM (144).

However, despite the complexity, the expansion is very quick and the final STM can be written similarly to the Jacobian $\hat{\mathbf{A}}$:

$$\mathbf{\Phi}(t_0, t_f) = \begin{bmatrix} \mathbf{\Phi_{xx}} & \mathbf{\Phi_{xl}} \\ \mathbf{\Phi_{lx}} & \mathbf{\Phi_{ll}} \end{bmatrix} \tag{B.11}$$

B.2. DA Polynomials

Autonomous Map EOP

TERM	COEFFICIENT	ORDER	EXPONENTS												
-	-	-	δr	δλ	δϕ	δv	δξ	δη	δl_r	δl_λ	δl_ϕ	δl_v	δl_ξ	δl_η	
1	9.9999815308889484e-01	0	0	0	0	0	0	0	0	0	0	0	0	0	CONSTANT PART
2	-4.0838358283067876e+01	1	0	0	0	0	0	0	1	0	0	0	0	0	
3	-1.1961778213628104e+02	1	0	0	0	0	0	0	0	1	0	0	0	0	
4	-3.3442905489690026e-06	1	0	0	0	0	0	0	0	0	1	0	0	0	
5	-2.6400695857175727e-01	1	0	0	0	0	0	0	0	0	0	1	0	0	
6	6.9111569325639408e+01	1	0	0	0	0	0	0	0	0	0	0	1	0	LINEAR PART
7	4.0216463332688084e-06	1	0	0	0	0	0	0	0	0	0	0	0	1	
8	1.0003402904788674e+00	1	1	0	0	0	0	0	0	0	0	0	0	0	
9	1.0834758070234405e-07	1	0	0	1	0	0	0	0	0	0	0	0	0	
11	1.7054827034948483e-02	1	0	0	0	1	0	0	0	0	0	0	0	0	
12	2.4364910755581004e-04	1	0	0	0	0	1	0	0	0	0	0	0	0	
13	-1.9071809947506525e-07	1	0	0	0	0	0	1	0	0	0	0	0	0	
14	1.6653015043291673e+03	2	0	0	0	0	0	0	2	0	0	0	0	0	
15	1.2323887690326223e+03	2	0	0	0	0	0	0	1	1	0	0	0	0	
16	-2.3263247561903620e+02	2	0	0	0	0	0	0	0	2	0	0	0	0	
17	2.1776909163834820e-04	2	0	0	0	0	0	0	1	0	1	0	0	0	
18	1.1425409709309491e-04	2	0	0	0	0	0	0	0	1	1	0	0	0	
19	-1.0107798652667327e+01	2	0	0	0	0	0	0	0	0	2	0	0	0	
20	-2.1823538737250719e+03	2	0	0	0	0	0	0	1	0	0	1	0	0	
21	-5.2509435448338252e+02	2	0	0	0	0	0	0	0	1	0	1	0	0	
22	-1.3321052699260177e-04	2	0	0	0	0	0	0	0	0	1	1	0	0	
23	8.0651395351408780e+02	2	0	0	0	0	0	0	0	0	0	2	0	0	
24	-5.2681713095867362e+03	2	0	0	0	0	0	0	1	0	0	0	1	0	
25	-2.4193472809701416e+03	2	0	0	0	0	0	0	0	1	0	0	1	0	
26	-3.6059783602079972e-04	2	0	0	0	0	0	0	0	0	1	0	1	0	
27	3.3703364705242780e+03	2	0	0	0	0	0	0	0	0	0	1	1	0	
28	4.1926594047611507e+03	2	0	0	0	0	0	0	0	0	0	0	2	0	
29	-2.6673238000646086e-04	2	0	0	0	0	0	0	1	0	0	0	0	1	
30	-8.5681153576005437e-05	2	0	0	0	0	0	0	0	1	0	0	0	1	
31	1.3613479040469242e+01	2	0	0	0	0	0	0	0	0	1	0	0	1	
32	1.7745325491989628e-04	2	0	0	0	0	0	0	0	0	0	1	0	1	
33	4.1949770866435773e-04	2	0	0	0	0	0	0	0	0	0	0	1	1	
34	4.9791018179846667e+01	2	0	0	0	0	0	0	0	0	0	0	0	2	
35	-5.8813854947376535e+02	2	1	0	0	0	0	0	1	0	0	0	0	0	
36	5.8225231709847151e+02	2	1	0	0	0	0	0	0	1	0	0	0	0	

Figure B.1: Autonomous Polynomial Map. 2^{nd}-order. EOP

The above figure shows the shape of the autonomous polynomial map related to the final controlled state $[\mathbf{x_{Cf}}, \mathbf{l_{Cf}}]$. This is only a section of the first component (r_{Cf}) of the whole series. The final distance r_{Cf} is written as a polynomial where the dependence on the initial perturbation $\delta\mathbf{z_0} = [\delta\mathbf{x_0}, \delta\mathbf{l_0}]$ is represented by a set of coefficients multiplying each displacement elevated to a certain exponent. This particular map regards the dynamics affected by the geopotential only, thus it is constant in time.

FOP Time Dependent Map

TERM	COEFFICIENT	ORDER	EXPONENTS															
-	-	-	δr	$\delta\lambda$	$\delta\phi$	δv	$\delta\xi$	$\delta\eta$	δm	δl_r	δl_λ	δl_ϕ	δl_v	δl_ξ	δl_η	δl_m	δt_{s1}	
1	-2.0604443475508779e-09	0	0	0	0	0	0	0	0	0	0	0	0	0	0	0	0	CONSTANT PART ≃ 0
2	-5.1937254552751644e-01	1	0	0	0	0	0	0	0	0	1	0	0	0	0	0	0	
3	1.0335064739925397e+01	1	0	0	0	0	0	0	0	0	0	1	0	0	0	0	0	
4	1.3681840684988515e+00	1	0	0	0	0	0	0	0	0	0	0	1	0	0	0	0	
5	1.7980941684332994e+00	1	0	0	0	0	0	0	0	0	0	0	0	1	0	0	0	
6	-6.2420268315405014e+00	1	0	0	0	0	0	0	0	0	0	0	0	0	1	0	0	
7	-1.0000021513561839e+00	1	0	0	0	0	0	0	0	0	0	0	0	0	0	1	0	
8	-1.1111666318729472e+00	1	0	0	0	0	0	0	0	0	0	0	0	0	0	0	1	LINEAR PART
9	-1.6801372362219271e+00	1	1	0	0	0	0	0	0	0	0	0	0	0	0	0	0	
10	3.7412265461189760e-05	1	0	1	0	0	0	0	0	0	0	0	0	0	0	0	0	
11	-1.5084419096088439e-01	1	0	0	1	0	0	0	0	0	0	0	0	0	0	0	0	
12	-6.2580875739768094e-01	1	0	0	0	1	0	0	0	0	0	0	0	0	0	0	0	
13	-1.0880643152273577e+00	1	0	0	0	0	1	0	0	0	0	0	0	0	0	0	0	
14	-1.0024522120938432e-01	1	0	0	0	0	0	1	0	0	0	0	0	0	0	0	0	
15	9.9982090639978105e-01	1	0	0	0	0	0	0	1	0	0	0	0	0	0	0	0	
16	-1.1913864374910377e+00	1	0	0	0	0	0	0	0	1	0	0	0	0	0	0	0	
17	-7.6887605732633233e+01	2	0	0	0	0	0	0	0	0	2	0	0	0	0	0	0	
18	-5.3566480004353005e+00	2	0	0	0	0	0	0	0	0	1	1	0	0	0	0	0	
19	-3.2312310811097822e-01	2	0	0	0	0	0	0	0	0	0	2	0	0	0	0	0	
20	-1.3200060983374753e+01	2	0	0	0	0	0	0	0	0	1	0	1	0	0	0	0	
21	1.4145550070199105e+01	2	0	0	0	0	0	0	0	0	0	1	1	0	0	0	0	
22	-2.3366808435924986e+02	2	0	0	0	0	0	0	0	0	0	0	2	0	0	0	0	
23	1.9505790749079534e+02	2	0	0	0	0	0	0	0	0	1	0	0	1	0	0	0	
24	1.8646670104571268e+01	2	0	0	0	0	0	0	0	0	0	1	0	1	0	0	0	
25	-3.6157614382002242e+02	2	0	0	0	0	0	0	0	0	0	0	1	1	0	0	0	
26	-2.7721346848878756e+02	2	0	0	0	0	0	0	0	0	0	0	0	2	0	0	0	
27	3.0762586804874759e+00	2	0	0	0	0	0	0	0	0	1	0	0	0	1	0	0	
28	3.8210225461544578e-01	2	0	0	0	0	0	0	0	0	0	1	0	0	1	0	0	
29	-8.4636408093355673e+00	2	0	0	0	0	0	0	0	0	0	0	1	0	1	0	0	
30	-1.0984456322836008e+01	2	0	0	0	0	0	0	0	0	0	0	0	1	1	0	0	
31	-1.1308835389607699e-01	2	0	0	0	0	0	0	0	0	0	0	0	0	2	0	0	
32	-5.3180592167802562e-05	2	0	0	0	0	0	0	0	0	1	0	0	0	0	1	0	
33	2.1664433195728002e-04	2	0	0	0	0	0	0	0	0	0	1	0	0	0	1	0	
34	2.2899252950134877e-05	2	0	0	0	0	0	0	0	0	0	0	1	0	0	1	0	
35	1.1127401639210086e-04	2	0	0	0	0	0	0	0	0	0	0	0	1	0	1	0	
36	-1.4845179584485157e-04	2	0	0	0	0	0	0	0	0	0	0	0	0	1	1	0	
37	-1.2291223572066860e-05	2	0	0	0	0	0	0	0	0	0	0	0	0	0	2	0	

Figure B.2: Switching Function Polynomial Map. 2^{nd}-order. FOP

In Figure B.2 the map of the switching function ρ_1 is presented after the first integration $[t_{Ci}, t_{s1}]$, highlighting the dependence on the first commutation time t_{s1}. 15 DA variables are needed in the FOP high order expansion about the numerical reference. Here a portion of the 2^{nd} order map is reported. As expected, the constant part of ρ is negligible, since this map represents a displacement with respect to the baseline, which, at the nominal switching time, is 0. By inverting this map and imposing it to be null, the variation of the first switching time δt_{s1} is found with respect to the initial perturbation $\delta\mathbf{z} = [\delta\mathbf{x_0}, \delta m_0, \delta\mathbf{l_0}, \delta l_{m_0}]$

List of Figures

List of Tables

Acronyms

ASRE Approximating Sequence of Riccati Equations

DA Differential Algebra

DACE Differential Algebra Computational Toolbox

ECEF Earth Centered Earth Fixed

EOP Energy Optimal Problem

E-W East-West

FD Free Drift

FOP Fuel Optimal Problem

FP Floating Point

GECS Geocentric Equatorial Coordinate System

GEO Geostationary Earth Orbit

GHA Greenwich Hour Angle

IVP Initial Value Problem

N-S North-South

OCP Optimal Control Problem

ODE Ordinary Differential Equation

SRP Solar Radiation Pressure

STM State Transition Matrix

SK Station Keeping

TBP Two Body Problem

TPBVP Two-Point Boundary Value Problem

List of Symbols

Variable	Description	SI unit
$\mathbf{A}$	State matrix	$[-]$
$\hat{\mathbf{A}}$	Augmented state matrix	$[-]$
$\mathbf{a}^p$	Perturbing acceleration	$[m/s^2]$
a_{GEO}	Geostationary semi-major axis	$[km]$
α	Right ascension	$[deg]$
$\hat{\alpha}$	Thrust direction	$[-]$
$\mathbf{B}$	Input matrix	$[-]$
β	Reflection coefficient	$[-]$
Δt	Time variation	$[s]$
Δv	Velocity variation	$[km/s]$
δ	Declination	$[deg]$
$\delta\mathbf{x}$	Position perturbation	$[-]$
$\delta\mathbf{v}$	Velocity perturbation	$[-]$
$\delta\mathbf{l}$	Costate variation	$[-]$
δt	Time variation	$[s]$
ϕ	Latitude	$[deg]$
Φ	State transition matrix	$[-]$
G	Gravitational constant	$[km^3 \cdot kg^{-1} \cdot s^{-2}]$
g_0	Gravitational acceleration	$[km/s^2]$
H	Hamiltonian	$[-]$
I_{sp}	Specific impulse	$[s]$
J	Perfromance index	$[-]$
k	Iteration index	$[-]$
$\mathbf{l}$	Costate	$[-]$

Variable	Description	SI unit
λ	Longitude	$[deg]$
m	Mass	$[kg]$
M_0	Initial mass	$[kg]$
M_b	Burnt mass	$[kg]$
m_E	Earth's mass	$[kg]$
μ_E	Geocentric gravitational parameter	$[km^3 \cdot s^{-2}]$
μ_M	Moon gravitational parameter	$[km^3 \cdot s^{-2}]$
μ_S	Sun gravitational parameter	$[km^3 \cdot s^{-2}]$
η	Out of plane velocity	$[deg/s]$
ω_E	Earth angular velocity	$[rad/s]$
p	Continuation parameter	$[-]$
R_E	Earth radius	$[km]$
$\mathbf{r}$	Position vector	$[-]$
r	Radial position ECEF	$[km]$
ρ	Radial position GECS	$[km]$
t	Time	$[s]$
$\tilde{\cdot}$	Reference value	$[-]$
T	Thrust	$[N]$
t_{FD}	Free Drift duration	$[s]$
T_E	Earth sidereal period	$[s]$
Θ	Greenwich hour angle	$[deg]$
u	Control acceleration	$[m/s^2]$
$\mathbf{v}$	Velocity vector	$[-]$
v	Radial velocity	$[m/s]$
$\mathbf{x}$	State	$[-]$
$\mathbf{x_n}$	Nominal state	$[-]$
$\mathbf{x_T}$	Target state	$[-]$
ξ	Transversal velocity	$[deg/s]$
$\mathbf{z}$	Augmented state	$[-]$

Acknowledgements

First of all a special thank goes to my advisor Professor Pierluigi Di Lizia for inspiring me during his courses with his passion and knowledge. Thanks to you and Michele Maestrini for giving me the opportunity to participate, in some small way, to your researches and to conclude my studies with this thesis, constantly encouraging me to express my best. Your helpfulness and collaboration can not be taken for granted and have been crucial to reach the most relevant possible outcome.

Then, I would like to thank all the people that directly or indirectly participated to this journey.
Thank you Luca, you have been my mad mate during these years together with one of my best friends Lorenzo. You alleviated every day at university and during the lockdown period. You made me laugh even during bad times. An important thought goes to Niccolò, Jacopo, Luca, Simone, Jorge, Luca, Eleonora, Lorenzo, Francesco and Silvia. Thank you all, we shared great and unforgettable moments during the last two years.
Thank you to my great friend of a lifetime Riccardo and to Martina for always being genuinely near me, as well as Francesca, Greta, Tommaso, Virginia, and Gabriele. Thank you for every hour we spent together and for your true and constant support.
A sincere thank to my close and essential friend Carolina, I am lucky I can count on you and on every word and advice you are able and you always want to give me to make me feel better.
A special thought to athletics to be a life teacher and a big outlet, to my coach Adolfo, to Maurizio and to all my training partners and friends, in particular Matteo and Leonardo. Thank you for every talk and for every second and effort we put on the track, you really taught me to be determined and focused on my goals and dreams while never giving up. Thank you Vinc, I will never forget your humanity and your dedication.

Thank you Marinella, you are beyond any definition, you are part of me and part of this. Thank you for the joy you can bring in my life, thank you for knowing me better than anyone else and for being the person I grew up with. Wherever we are, you will always be my guiding star.

Finally I really want to thank my whole family.
Thank you to my grandparents Maria, Anna and Ivo, who certainly need someone to translate these words, for taking care of me and for giving me your example. Thank you for always being by my side, for your wisdom and for teaching me your simple and humble values. I will always carry you in my heart.
Thank you to my aunts Cristina and Miriam and my uncles Valter, Eugenio and Giovanni for your constant and sincere interest. Thank you to my cousin Federico for all the adventures we had together, you are like my little brother.
The most important thanks goes to my parents Cinzia and Silvano. Thank you for your love, your presence and your support in every moment of my life. Thank you for putting up with me, for every sacrifice you did and for helping me to find the strength that sometimes I need. Without you I would have never reached this goal and I hope I made you proud of me.

Thank you all.